Institut für Erd- und Umweltwissenschaften, Universität Potsdam
DFG Graduiertenkolleg 1364
und
Helmholtz-Zentrum Potsdam – Deutsches GeoForschungsZentrum GFZ
Sektion 5.2 – Klimadynamik und Landschaftsentwicklung

LAKE SEDIMENTS AS CLIMATE AND TECTONIC ARCHIVES IN THE INDIAN SUMMER MONSOON DOMAIN

Kumulative Dissertation
zur Erlangung des akademischen Grades
"doctorrerumnaturalium"(Dr. rer. nat.)
in der Wissenschaftsdisziplin Geologie – "Paläoklimatologie"

eingereicht an der
Mathematisch-Naturwissenschaftlichen Fakultät
der Universität Potsdam

von
AnoopAmbili

Potsdam, June 2012

Published online at the
Institutional Repository of the University of Potsdam:
URL http://opus.kobv.de/ubp/volltexte/2013/6479/
URN urn:nbn:de:kobv:517-opus-64799
http://nbn-resolving.de/urn:nbn:de:kobv:517-opus-64799

Dedicated to

My

Teachers, Wife & Mother

Abstract

The Indian summer monsoon (ISM) is one of the largest climate systems on earth and impacts the livelihood of nearly 40% of the world's population. Despite dedicated efforts, a comprehensive picture of monsoon variability has proved elusive largely due to the absence of long term high resolution records, spatial inhomogeneity of the monsoon precipitation, and the complex forcing mechanisms (solar insolation, internal teleconnections for e.g., El Niño-Southern Oscillation, tropical-midlatitude interactions). My work aims to improve the understanding of monsoon variability through generation of long term high resolution palaeoclimate data from climatically sensitive regions in the ISM and westerlies domain. To achieve this aim I have (i) identified proxies (sedimentological, geochemical, isotopic, and mineralogical) that are sensitive to environmental changes; (ii) used the identified proxies to generate long term palaeoclimate data from two climatically sensitive regions, one in NW Himalayas (transitional westerlies and ISM domain in the Spiti valley and one in the core monsoon zone (Lonar lake) in central India); (iii) undertaken a regional overview to generate "snapshots" of selected time slices; and (iv) interpreted the spatial precipitation anomalies in terms of those caused by modern teleconnections. This approach must be considered only as the first step towards identifying the past teleconnections as the boundary conditions in the past were significantly different from today and would have impacted the precipitation anomalies.

As the Spiti valley is located in the in the active tectonic orogen of Himalayas, it was essential to understand the role of regional tectonics to make valid interpretations of catchment erosion and detrital influx into the lake. My approach of using integrated structural/morphometric and geomorphic signatures provided clear evidence for active tectonics in this area and demonstrated the suitability of these lacustrine sediments as palaleoseismic archives. The investigations on the lacustrine outcrops in Spiti valley also provided information on changes in seasonality of precipitation and occurrence of frequent and intense periods (ca. 6.8-6.1 cal ka BP) of detrital influx indicating extreme hydrological events in the past. Regional comparison for this time slice indicates a possible extended "break-monsoon like" mode for the monsoon that favors enhanced precipitation over the Tibetan plateau, Himalayas and their foothills.

My studies on surface sediments from Lonar lake helped to identify environmentally sensitive proxies which could also be used to interpret palaeodata obtained from a ca. 10m long core raised from the lake in 2008. The core encompasses the entire Holocene and is the first well dated (by ^{14}C) archive from the core monsoon zone of central India. My identification of authigenic evaporite gaylussite crystals within the core sediments provided evidence of exceptionally drier conditions during 4.7-3.9 and 2.0-0.5 cal ka BP. Additionally, isotopic investigations on these crystals provided information on eutrophication, stratification, and carbon cycling processes in the lake.

Kurzfassung

Der Indische Sommer Monsun (ISM) ist eines der bedeutendsten Klimaphänomene auf der Erde und hat großen Einfluss auf die Lebensbedingungen und -grundlagen von nahezu 40% der Weltbevölkerung. Trotz großer Bemühungen ist es bisher nicht gelungen ein genaues und umfassendes Verständnis der Monsun-Variabilität zu gewinnen. Hauptgründe dafür sind das Fehlen von langjährigen und hochaufgelösten Klimazeitreihen, räumlichen Inhomogenitäten in den Niederschlagsverteilungen und die Komplexität der treibenden klimatischen Mechanismen (Sonneneinstrahlung, interne Wechselwirkungen des Klimasystems, wie z.B. zwischen Tropen und mittleren Breiten oder die Auswirkungen der El Niño Oszillation).

Die Zielsetzung der hier vorgestellten Arbeit ist ein verbessertes Verständnis der Monsun-Variabilität zu entwickeln, auf Basis von hochaufgelösten und weit reichenden Paläoklimazeitreihen aus klimasensitiven Regionen des ISM und der Westwindzone. Um die Zielsetzung umzusetzen habe ich: (i) Proxys identifiziert (sedimentologische, geochemische, isotopische, und mineralogische), die empfindlich auf Umweltveränderungen reagieren; (ii) die identifizierten Proxys zur Erzeugung von langjährigen Paläoklima-Daten für zwei klimasensible Regionen verwendet, eine im NW des Himalaja (Übergangs-Westwindzone und ISM Gebiet von Spity Valley) und eine in der Kernzone des Monsun (Lonar-See) in Zentralindien; (iii) Übersichts-"Momentaufnahmen" der regionalen klimatischen Bedingungen für ausgewählte Zeitpunkte der Vergangenheit erzeugt; und (iv) räumliche Niederschlagsanomalien in Hinblick auf heutige Wechselbeziehungen im Klimasystem interpretiert. Dieser Ansatz stellt allerdings nur einen ersten Schritt zur Identifizierung von paläoklimatischen Wechselbeziehungen im Monsunsystem dar, da sich die Randbedingungen in der Vergangenheit deutlich von den heutigen unterscheiden und diese einen signifikanten Einfluss auf die Niederschlagsanomalien haben.

Da das Spity Valley im tektonisch aktiven Himalaja-Orogen lokalisiert ist, ist es von entscheidender Bedeutung die regionalen tektonischen Prozesse zu verstehen, um Erosionsvorgänge des Einzugsgebiets und die Einfuhr von Detritus in den See korrekt interpretieren zu können. Mein Ansatz der Nutzung kombinierter strukturell/morphometrischer und geomorphologischer Charakteristiken lieferte klare Beweise für aktive Tektonik im untersuchten Gebiet und demonstrierte damit die Eignung dieser lakustrinen Sedimente als paläoseismisches Archiv. Die Untersuchung lakustriner Aufschlüsse in Spity Valley lieferte auch Informationen saisonale Änderung der

Niederschlagsverteilung sowie das Auftreten von häufigen und intensiven Perioden (ca. 6,8-6,1 cal ka BP) detritischer Einfuhr, welche auf extreme hydrologische Ereignisse in der Vergangenheit schließen lässt. Ein regionaler Vergleich dieser Periode deutet auf einen möglicherweise erweiterten „break-monsoon-like" Modus für den Monsun hin, welcher hohe Niederschläge über dem Tibetischen Plateau, dem Himalaja und seinen Gebirgsausläufern begünstigt.

Meine Studien an den Oberflächensedimenten des Lonar-Sees haben dazu beigetragen umweltsensitive Proxys zu identifizieren, die auch zur Interpretation von Paläodaten von einem ca. 10 m langen Sedimentkern genutzt wurden, der 2008 erbohrt wurde. Der Kern umfasst das gesamte Holozän und stellt das erste gut ^{14}C-datierte Archiv aus der Kernmonsunzone Zentralindiens dar. Die Identifizierung von authigenen Evaporit-Kristallen (Gaylussite) innerhalb der Sedimente liefert einen Beweis für ungewöhnlich trockene Bedingungen in den Perioden zwischen 4,7-3,9 und 2,0-0,5 cal ka BP. Darüber hinaus lieferten Isotopen-Untersuchungen dieser Kristalle Informationen zur Eutrophierung, Stratifikation und zum Kohlenstoff-Kreislauf des Sees.

Contents

Acknowledgement

My sincere thanks to my supervisors PD Dr. Sushma Prasad and Prof. Achim Brauer for their continuous support and stimulating discussions during my research.

I would like to acknowledge the financial support I received from the DFG funded Graduate School (GK -1364), Universität Potsdam. I would like to give my special thanks to Prof. Dr. Manfred Strecker for giving me this opportunity and also for supporting my field visits, workshops and conferences. Also, I am grateful to the coordinators of the graduate school Dr. Andreas Bergner, Dr. Rasmus Thiede, and Dr. Henry Wichura for their help in dealing with the administration. I would also like to thank PhD students from the Graduate School for their friendship and providing a stimulating academic environment.

Besides my advisors, my sincere thanks also go my colleagues from the Deutsches GeoForschungsZentrum Potsdam especially Dr. B. Plessen, P. Dulski and R. Naumann for training me in their laboratories. I would also like to extend my warmest thanks to my scientific colleagues from the Indian Institute of Geomagnetism, Universität Potsdam, Universität Hamburg, and Indian Institute of Tropical Meteorology for their encouragement, insightful comments and stimulating discussions. In particular, I am grateful to Dr. Nathani Basavaiah and Dr. R. Krishnan for their timely advice and encouragement.

Finally I owe my loving thanks to my wife Rimjhim Singh and my mother Ambili Omana. Without their constant support and encouragement it would have been impossible for me to finish this work. My special gratitude is due to my brother in law, sister, and friends in Potsdam for their loving support.

1. Introduction

The word Monsoon is derived from Arabic word `Mausam` which means reversal of seasonal winds. The seasonal migration of the intertropical convergence zone (ITCZ) over the latitude of maximum insolation regulates the monsoon circulation (Charney, 1969; Gadgil, 2003). During summer (June to September) ITCZ shifts towards the low pressure area and surface winds bring large amounts of precipitation from the Arabian Sea and Bay of Bengal to continental India (Fig. 1.1a). This pattern is reversed during winter when north easterly (NE) winds bring cold and relatively dry air into large parts of the Indian subcontinent (Fig. 1.1b) (Gadgil, 2007). Only in southern India the NE winds bring in precipitation after picking up moisture over the Bay of Bengal.

An apparent increase in the frequency and magnitude of extreme events (floods and droughts) in recent years, over the Asian region, has drawn attention to the strong socio-economic impact of such natural disasters on ca. 40% of the world's population. Analyses of meteorological data (Goswami et al., 2006; Malik et al., 2011) not only confirms this general observation but also indicates an increase in spatial variability of rainfall extremes (Ghosh et al., 2011) against the backdrop of rising global surface temperatures. Model simulations also indicate spatially heterogeneous increase in monsoon rainfall by the end of this century (Rajendran and Kitoh, 2008). However, all such studies are based on instrumental records covering only a few decades. Longer, high resolution palaeoclimate records are essential for understanding the monsoon variability on societal and longer time scales. This is important as similarities have been found between the pattern of interannual variability and intraseasonal variability over longer time scales (Webster et al., 1998; Ummenhofer et al., 2011), suggesting that the monsoon oscillates between several basic states under the influence of remote forcing induced by sea surface temperatures (SST), orbital changes, solar variability, and/or land surface conditions. Interestingly, corals and stalagmites also indicate that the intensity, duration, and nature of ISM (Indian Summer Monsoon) teleconnections (e.g., El Niño-Southern Oscillation (ENSO), tropical mid-latitude interactions) have also varied significantly in the past (Cobb et al., 2003; Sinha et al., 2011).

1.1. Climate over the Indian subcontinent

1.1.1. Modern ISM: spatial and interannual variability

While it has been proven that the modern climate in India is dominated by the ISM that brings in over 80% of the total annual rainfall during the summer monsoon season (Gadgil, 2003), the northern parts of India also receive some winter precipitation associated with eastward propagating high level westerly synoptic scale waves known as 'Western Disturbances' originating mostly from Mediterranean. Though the wintertime disturbances bring limited precipitation over northern India, the complex links between the summer monsoon and wintertime circulation regimes and the variations in the forcing mechanisms can result in spatially inhomogenous changes in the monsoon rainfall (Bookhagen and Burbank, 2010). Several studies have highlighted the regional inhomogeneities in precipitation patterns (Krishna Kumar et al., 1999; Krishnan et al., 2009) resulting from remote forcings – a detailed overview of the most prominent of these and factors and teleconnections that influence the modern ISM is presented in Pant and Rupa Kumar (1997), Prasad et al., (in review) and is summarised below:

1. **Snow cover** has an important effect on the regulation of the thermal contrast because of its ability to alter the surface albedo and to regulate moisture content which in turn cools the land surface (Cohen and Entekhabi, 2001; Dash et al., 2005). Studies have noted an inverse relationship between the ISM and the wintertime snow cover over Eurasia and the Himalayan region. These studies suggest that excess (deficit) winter seasons over the Eurasian and Himalayan region tend to be followed by below (above) normal summer monsoon rainfall over India (e.g., Dickson, 1984; Bamzai and Shukla, 1999; Mamgain et al., 2010). The spatial variability of ISM during the El Niño years is shown in Fig. 1.1c.

2. The interannual variability of the Indian monsoon rainfall (IMR) is strongly correlated with various indices of the **ENSO** phenomenon in the tropical Pacific (e.g., Sikka, 1980; Ropelewski and Halpert, 1987; Krishna Kumar et al., 1999). The time-series of year-to-year variations in the summer monsoon rainfall over India for the period 1871-2009 indicates that El Niño events are frequently accompanied by a significantly reduced Indian monsoon and widespread drought conditions due to anomalous subsidence associated with a shift in the descending branch of the zonal Walker circulation; while several wet monsoons have accompanied La Niña episodes (i.e., the

cold phase of ENSO) (e.g., Goswami, 2005; Ummenhofer et al., 2011). However, recent studies also suggest that this link might not be permanent but could itself be modulated on e.g., decadal timescales (e.g., Krishna Kumar et al., 1999; Kucharski et al., 2007). Krishna Kumar et al., 1999 attributed this weakening of the ENSO-Monsoon relationship to the possible Eurasian warming in recent decades that helps to sustain the monsoon rainfall at a normal level despite strong ENSO events.

3. Sub seasonal or intraseasonal variations of the monsoon on time scales longer than synoptic variability (1-10 days) can arise in "normal" monsoon pattern (Goswami, 2005). These synoptic disturbances are referred to as **active/break cycles** (Krishnamurti and Bhalme 1976; Sikka, 1980). During the active cycle, monsoonal rainfall intensifies whereas during break cycles weak rainfall is observed even during peak monsoon period (Blanford, 1886). Several studies have reported persistent intrusion of cold and dry north-westerly winds from the mid-latitude and subtropical regions of west-central Asia into the Indo-Pak region during intense monsoon breaks (e.g., Ramaswamy, 1962; Kripalani et al., 1997; Joseph and Srinivasan, 1999; Krishnan and Sugi, 2001). This advection of cold and dry northwesterly winds into the monsoon region produces anomalous tropospheric cooling, reduces the meridional temperature gradient and can weaken the monsoon convective activity (Fig. 1.1d). The final result of the break cycle is a shifting of the monsoon trough to the foothills of Himalayas resulting in large amount of rainfall over Indo-Gangetic plains but with a corresponding decrease in rainfall (break cycles) reported in central India.

4. Studies during the last decade have shown an interannual mode of variability in Indian Ocean SSTs that has an east–west structure and can produce its own El Niño-like phenomenon which is now referred to in the literature as the **Indian Ocean Dipole** (IOD, 1961, 1983, 1994) (Saji et al., 1999; Webster et al., 1999; Behera et al., 1999; Abram et al., 2007; Overpeck and Cole, 2007). Rainfall is enhanced over the eastern equatorial Indian Ocean and suppressed over the western Indian Ocean during positive IOD episode. The configurations of the SST, wind and rainfall anomalies are reversed for the negative phase of IOD. Studies have shown that positive IOD events are generally associated with anomalous wet conditions (Fig. 1.1e) over South Asia (e.g., Yamagata et al., 2004; Sundaram et al., 2010; Krishnan et al., 2011).

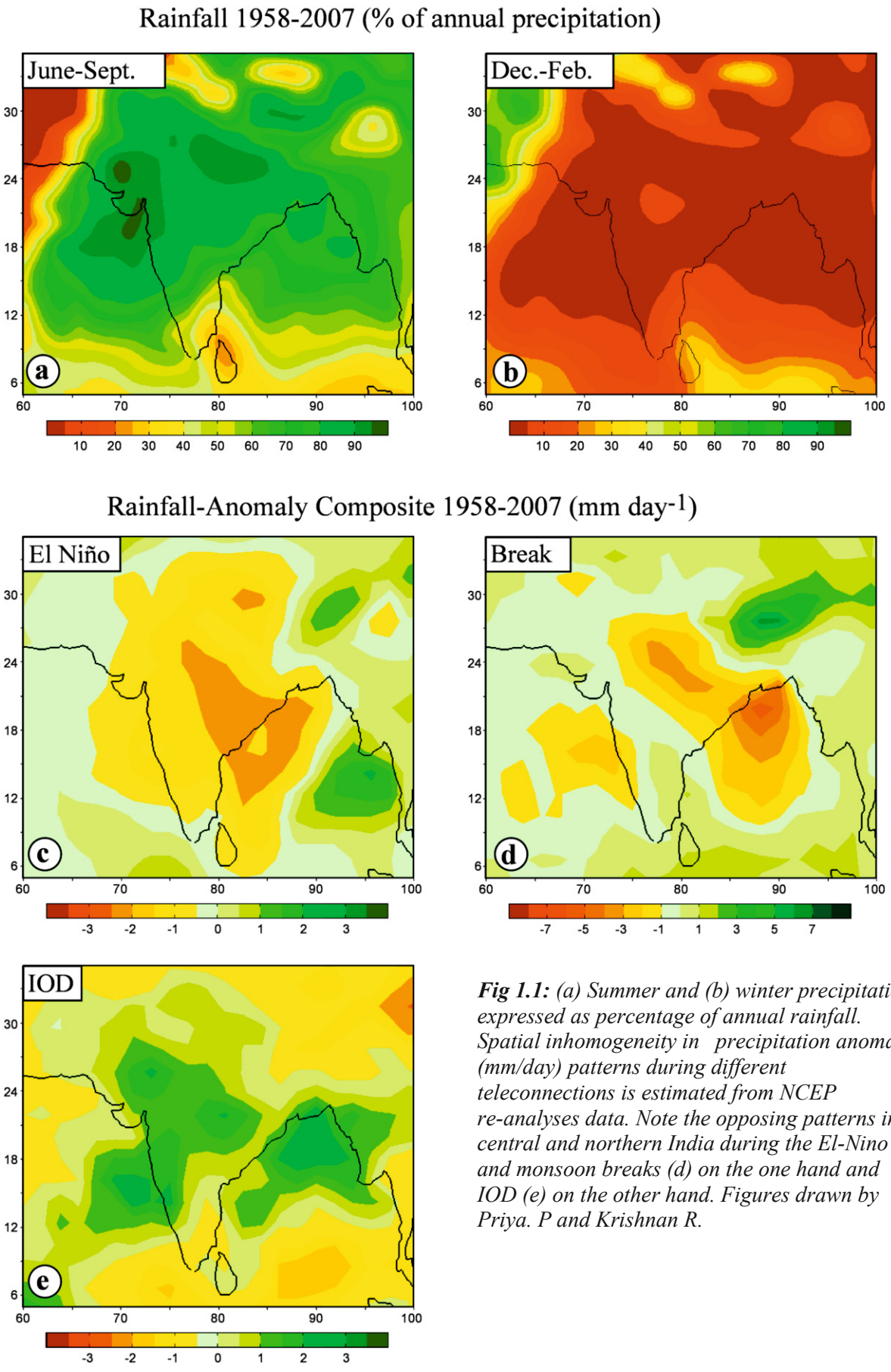

Fig 1.1: *(a) Summer and (b) winter precipitation expressed as percentage of annual rainfall. Spatial inhomogeneity in precipitation anomaly (mm/day) patterns during different teleconnections is estimated from NCEP re-analyses data. Note the opposing patterns in central and northern India during the El-Nino (c) and monsoon breaks (d) on the one hand and IOD (e) on the other hand. Figures drawn by Priya. P and Krishnan R.*

1.2. Holocene ISM Variability

The meteorological data on monsoon rainfall extends back to ca. 150 years. Additionally, historical records extending to 900 AD are also available (Pant and Rupa Kumar, 1997). Marine reconstructions of palaeomonsoon variability (e.g., Van Campo et al., 1982; Sirocko et al., 1993; Overpeck et al., 1996; Gupta et al., 2003; Ponton et al., 2011) indicate changes in monsoon wind strength over centennial time scales that have been linked to northern hemispheric temperature fluctuations (e.g., Schulz et al., 1998), solar variability (e.g., Gupta et al., 2005), and changes in orbital parameters (Clemens et al., 1991). Interestingly, periods of increased monsoon wind strength inferred from these records do not always coincide with increased precipitation over nearby continental regions (Fleitmann et al., 2004; Prasad and Enzel, 2006) suggesting either a proxy limitation, decoupling of proxies of marine upwelling and the position of ITCZ (Burns., et al., 2002), and/or a complex process of moisture transport by the two branches of the ISM (Arabian Sea and the Bay of Bengal).

The majority of palaeoclimate research on terrestrial sediments (Singh et al., 1974; Bryson and Swain, 1981; Swain et al., 1983; Wasson et. al., 1984; Prasad et al., 1997; Enzel et al., 1999) was carried out in NW India. In addition to the summer monsoon rainfall this region also receives some amount of winter rainfall (≤20%) from cyclones steered by the mid-latitude westerlies. Centennial scale reconstructions of Holocene palaeoclimate clearly indicate wetter climate during the early and mid-Holocene in this presently arid region. Highest lake levels were reached ~7.2-6.0 cal ka, when increased summer rains were supplemented by high winter rains brought in by the mid-latitude westerlies. There were also multiple century-scale spells of drought during the Holocene. Recent efforts to obtain high resolution data have focussed on tree rings (e.g., Borgaonkar et. al., 1996), ice cores (Thompson et al., 2000) and stalagmites (e.g., Yadava et al., 2004; Neff et al., 2001; Fleitmann et al., 2003; Sinha et al., 2005). These have yielded information about monsoon variability on decadal time scales and indicated the past sensitivity of the monsoon to solar variability (Neff et al., 2001), North Atlantic Oscillation (Neff et al., 2001), ice rafted debris in the N. Atlantic (e.g., Fleitmann et al., 2003) and ENSO (Thompson et al., 2000). Unfortunately, the temporal and spatial availability of such high-quality records is so far limited.

Only recently has more palaeoclimate data become available (Sharma, 1992; Chauhan et al., 1997; Chauhan et al., 2000; Phadtare, 2000; Kar et al., 2002; Chakraborty et al., 2006; Bhattacharayya et al., 2006; Bhattacharayya et al., 2011) from the Himalayan region and NE

India (Dixit and Bera, 2012). Pollen reconstructions (Phadtare, 2000; Chauhan et al., 2000; Kar et al., 2002) though qualitative, indicate several warm and cold events during the Holocene in the Himalayan region. Chauhan et al., (2000) documented warm/moist and cold/dry periods in the Spiti region coincident with the Medieval Warm period (MWP) and the Little Ice Age (LIA) in Europe. Periods of intensified monsoon have been associated with the formation of landslide dammed lakes in the Sutlej valley region (Bookhagen et al., 2005) and monsoonal variability has been associated with fluvial terraces formation (Bookhagen et al., 2006). Enhanced monsoon rainfall during early Holocene from lake sediments in Tibet and Leh (Gasse et al., 1996; Trivedi and Chauhan, 2009; Demske et al., 2009; Wünnemann et al., 2010) and late glacial glacier oscillations (Owen et al., 2001) resulting from the northward migration of the ITCZ have been reported from the presently dry regions of the Himalayas. Short-term arid events coeval with the Younger Dryas (YD) period and the 8.2 ka event have been reported from Tibet (e.g., Gasse and Van Campo, 1994) and the Indian Himalayas (Juyal et al., 2004; Scherler et al., 2010). However, recent studies especially in the Himalayas and Tibetan plateau indicate a rather complex regional pattern of early Holocene climate change and resulting environmental response (Herzschuh, 2006; Mischke and Zhang, 2010). A number of palaeo-records suggest that the warmest and wettest period in the Holocene occurred in the middle Holocene rather than the early Holocene (Herzschuh, 2006; Wang et al., 2010) and reasons for this asynchronous behavior are still debated. The long term pollen record (Dixit and Bera, 2012) from eastern Indian state of Assam, influenced by the Bay of Bengal branch of the ISM, indicates cooler and drier conditions during the YD period followed by relatively warmer and wetter conditions until 8.3 cal ka. The warm and humid climate regime reported between 7.1-1.5 cal ka from Assam is longer than that reported from the NW Indian lakes (Prasad et al., 1997; Enzel et al., 1999; Prasad and Enzel, 2006).

Central India has not yet received sufficient attention barring some limited paleoclimatic reconstructions (Ely et al., 1996; Quamar and Chauhan, 2012). Palaeoflood reconstructions from the Narmada valley in central India indicate that the cluster of extreme floods in the past few decades represents an anomalous increase in both the magnitude and frequency of large floods when compared with the >1700 yr record of palaeoflood deposits on this river (Ely et al., 1996). Pollen based centennial scale reconstructions (Quamar and Chauhan, 2012) from a central Indian Nitaya lake indicate cooler and drier conditions 12.7-7.1 cal yr BP. Intensified monsoon and warmer condition were noticed only between 7.1-4.6 cal yr BP followed by weakening monsoon.

Summarising,

(i) Although reconstructions differ depending on geographical location and/or proxy and archives, there is unambiguous evidence that the intensity of the ISM has varied significantly in the geological past with regional reports of short-term climate fluctuations (temperature and/or hydrology) possibly correlatable with the YD period, the Medieval Warming Period (MWP), the 4.2 cal ka event, and the Little Ice Age (LIA).

(ii) There is a significant regional variability in Holocene ISM continental reconstructions, as well as differences between marine and continental records. While this could be partly attributed to regional differences, the possibility of chronological problems and/or proxy (in) sensitivity cannot be excluded.

(iii) Modern and palaeodata suggest that reconstructions from the Himalayan region could possibly indicate atypical, rather than representative monsoon rainfall (Staubwasser and Weiss, 2006).

1.3. Scope of this study

My research focusses on palaeolake sediments from two regions: one from the Himalayan region (Spiti valley) that lies in transitional westerlies and ISM domain; and the second one from the Lonar lake in central India that completely lies in the ISM domain. The focus of my work was the following:

(i) Identify suitable proxies for palaeoclimate reconstruction. In the Spiti palaeolake sediment no organic proxies (organic matter, pollen, microfauna) were found and the reconstructions are based on lithological and sedimentological characterisation of lacustrine sediments. The Lonar sediments however showed several geochemical, isotopic, and mineralogical climate proxies (Chapters 3 and 4).

(ii) Explore the role of tectonism and climate variability in landscape evolution in the Spiti valley (Chapter 2).

(iii) Reconstruct palaeoclimate for the time interval covered by the sediments. This was 8.7-6.1 cal yr BP (Spiti valley) and Holocene (Lonar lake) (Chapters 4, 5 and 6).

(iv) Identify spatial inhomogeneities in palaeo-precipitation patterns that could provide clues to existence of past teleconnections (Chapter 3).

Below, a short summary of the various publications and manuscripts (in review) that form my thesis is presented.

Chapter 2 "**Tectonic versus climate influence on landscape evolution: a case study from the upper Spiti valley, NW Himalaya"** investigates the role of interplay of climate and tectonics in landform evolution in the upper Spiti valley. We have undertaken structural, geomorphological, and morphometric analyses to infer Holocene tectonism in the region and evaluated the possible climate-landslide link in light of the recent literature from this region.

Chapter 3 **"Extreme events and spatiotemporal changes in precipitation patterns in NW Himalayas during the early-mid Holocene**" provides results from the palaeoclimate investigation of 41m thick radiocarbon dated lacustrine outcrops from the upper Spiti valley. Field investigations coupled with petrographical, geochemical and mineralogical studies were undertaken for high resolution palaeoclimate reconstruction. This reconstruction was then compared with available literature from the monsoon domain to obtain information on spatial precipitation variability during selected time slices.

Chapter 4 "**Environmental implications of surface sediments from the monsoonal Lonar Lake, Central India"** deals with the geochemical, magnetic, and sedimentological investigations into the catchment and surface lake sediments from the Lonar lake, central India. Our study evaluates the potential of measured parameters for palaeoenvironmental reconstruction i.e. proxy identification, and is also the first of this kind on Indian lakes. This data lays the framework for palaeoclimate interpretation from a 10m long core that has been raised from this lake.

Chapter 5 **"Holocene climate variability: first results from Lonar lake, Central India"** describes my contribution to the coring process in the Lonar lake, development of composite lithology, and chronology of the entire 10m core long core. Results of additional analyses on this core are presented in Chapter 6.

Chapter 6 "**Palaeoenvironmental implications of evaporative gaylussite crystals from Lonar lake, Central India**" reports results from petrographic, mineralogical, geochemical and isotopic investigations on carbonate minerals found within the Lonar sediment cores, with the aim of evaluating their potential as palaeoenvironmental proxies. Isotopic ($\delta^{18}O$ and $\delta^{13}C$)

studies on the evaporative gaylussite crystals and residual bulk carbonates (calcite) from the long core show that evaporation is the major control on $\delta^{18}O$ enrichment in both minerals. However, $\delta^{13}C$ enrichment mechanisms are different with significant contribution from organic cycling processes in gaylussite, and biological productivity triggered enriched carbon in bulk carbonates.

Chapter 7 provides a synthesis of the conclusions drawn in this study and perspectives on future research in this region.

Tectonic versus climate influence on landscape evolution: a case study from the upper Spiti valley, NW Himalaya

***A. Anoop*[ab]**, *S. Prasad*[a], *N. Basavaiah*[c], *A. Brauer*[a], *F. Shahzad*[d], *K. Deenadayalan*[c]

[a] German Research Center for Geosciences (GFZ), Telegrafenberg, Potsdam, Germany
[b] DFG Graduate School 1364, University of Potsdam, Germany
[c] Indian Institute of Geomagnetism, Colaba, Mumbai, India
[d] Earth System Dynamics Group, Institute of Geology, University of Tuebingen, Germany

Published in Geomorphology 145–146, 32–44

Abstract

We have undertaken structural, geomorphological, and morphometric analyses to investigate the role of tectonism and climate in the landscape evolution in the upper Spiti valley, NW Himalayas. Geomorphometric analyses coupled with field investigations reveal active tectonic deformation in the Spiti region. The calculated geomorphic indices (steepness, concavity and Hack) demonstrate uplift/subsidence along the Kaurik-Chango fault, whereas transverse topographic index (T- index) reveals basin tilting associated with active faulting near Hansa and Lingti valley. Investigation of well-dated Mane palaeo-lake sediments also provides evidence of regional tectonic instability. Four episodes (ca. 7.8, 7.4, 6.5 and 6.1 cal ka) of neotectonic activity have been identified during the period of the lake's existence. We have also compiled data on the regional climate variability and compared it with the age of the Mane palaeo-landslide. Our results indicate that the landslide occurred towards the end of the early Holocene intensified monsoon phase and is located near an active fault. Our data on regional tectonic instability and the coincidences of modern and palaeo-landslides with zones of active deformation suggest that tectonism is an important factor governing landscape stability in the Spiti region.

Keywords

Geomorphic indices, Holocene, Palaeo-lake sediments, Palaeo-landslides, Monsoon

2.1. Introduction

Tectonism (Barnard et al., 2001) and intensified monsoon (Bookhagen et al., 2005) are considered to be the dominant factors governing landscape evolution in the Himalayan region. Recent studies have drawn attention to the increased frequency of occurrence of landslides during phases of intensified monsoon (e.g., Bookhagen et al., 2005; Dortch et al., 2009), and highlighted the link between terrace formation in NW Himalaya and monsoon dynamics (Bookhagen et al., 2006). In particular, large-scale mass movements (landslides) in the Spiti valley (Mane and Hansa, Fig. 2.1) have been attributed to intensified monsoon (Bookhagen et al., 2005; Phartiyal et al., 2009). However, the role of regional tectonic instability in triggering landslides has not been sufficiently explored in the Himalayan region. This lacunae needs to be addressed as numerous conceptual models and field investigations suggest that deformation and large scale mass movements triggered by tectonic activity can have a direct control in shaping the landscape and drainage evolution (Delcaillau et al., 1998; Burbank and Anderson, 2000). We propose that an understanding of the long-term regional tectonic history that can provide information about the stability of the region, against the background of climate change, is essential for deciphering the relative influence of both factors in initiating mass movements. Morphometric analyses, in combination with the investigation of Quaternary landforms (e.g., river terraces, lake sediments etc) can provide information about regional tectonic stability. Lake sediments in particular can be used as excellent archives (Sims, 1973, 1975; Upadhyay, 2003; Perucca et al., 2009; Wang et al., 2011) that can potentially provide a long-term chronologically constrained palaeoseismic record.

In the present study we focus on the Spiti region (northwestern Himalayas, India) that lies in the transitional zone between the westerlies and the Indian summer monsoon – the modern-day precipitation is, however, dominated by the westerlies (Singh and Kumar, 1997; Wulf et al., 2010). Most of the studies in this region have focused on large landforms (e.g., landslide debris, Bhargava and Bassi, 1998; Bookhagen et al., 2005) and few lacustrine outcrops in the Lingti valley and Hansa palaeolake sediments (e.g., Phartiyal et al., 2009). The Spiti valley shows extensive lake outcrops that were deposited due to the landslide damming of the Spiti River during the geologic past; however, not all the deposits are chronologically constrained. In the present work, we have investigated only the early Holocene palaeolake sediments formed by the landslide damming near Mane village (hereafter referred to as Mane palaeolake) in the upper Spiti valley. Previous dating on the

Mane palaeolake sediments indicates an early Holocene age: ^{14}C dates show lake existence between 8.7-6.1 cal ka (Bookhagen et al., 2005), while Optically Stimulated Luminescence (OSL) dating indicates age boundaries between 13±2 ka to 8 ± 1 ka (Phartiyal et al., 2009). Based on the inferred age of the Mane landslide in the Spiti valley, and its comparison with the monsoon proxy records, Bookhagen et al. (2005) and Phartiyal et al. (2009) have suggested that this landslide occurred during the early Holocene intensified monsoon period. However, the continuously deposited Mane palaeolake sediments have a high potential of recording tectonic perturbations and providing data on the long-term stability of the region. Our objective is to explore the relative importance of tectonics and climate in shaping the Holocene landscape in this region. For this we have (i) undertaken field mapping of geomorphic features and palaeolake sediments in the upper Spiti valley; (ii) analysed digital elevation models to evaluate geomorphic parameters for active deformation in the region; (iii) for the first time, compiled a detailed tectonic map of the upper Spiti valley based on previously published and new data from our study; (iv) examined the Mane palaeolake sediments for evidence of neo-tectonic activity; and (v) compared the timing of the Holocene (Mane) landslide with the newly available data on regional Holocene climate variability, to investigate the possible trigger for the landslide.

2.2. Study region

2.2.1. Regional geological setting

Spiti valley forms part of the Tethyan Himalayan, known for its complete record of sedimentation from upper Proterozoic to Eocene sediments (Sinha, 1989; Bhargava and Bassi, 1998). High grade metamorphosed sediments (Vaikrita group) of High Himalayan Crystalline Sequence (HHCS) bordering the southern part of Spiti valley form the base of the Tethyan sediments (Khatri et al., 1978; Myrow et al., 2006) (Fig. 2.1). The early Miocene extensional structures referred to as South Tibetan Detachment System (STDS) separate the HHCS from the low grade sedimentary rocks of Tethyan Himalaya (Vannay et al., 1999). Our study area lies in the upper Spiti valley, with lithologies dominated by rocks from Paleozoic and Mesozoic successions (Bhargava and Bassi, 1998). The Paleozoic (Permo-Carboniferous) rocks comprise friable and splintery shale, quartzite and meta-sediments, whereas the Mesozoic successions are dominated by black limestone with intercalations of shale, dolomite and sandstone (Lilang group), shales (Spiti formation) and sandstones (Guimal formation) (Fig. 2.1).

Structural investigation revealed that Spiti valley forms part of a large syncline (Spiti-Zanskar Syncline) with a NW-SE-striking fold axis (Fuchs, 1982; Hornung et al., 2007). The valley encompasses several active and inactive faults affecting the Precambrian–Quaternary successions (Hayden, 1904; Bhargava, 1990; Steck, 2003; Thiede et al., 2006) (Fig. 2.1). The termination of the Spiti syncline in the lower Spiti valley gives rise to N-S-trending Kaurik-Chango (K-C) fault and nearby NNE-trending west-dipping fault of the Leo-Pargil Horst fault systems (Singh and Jain, 2007). These fault systems largely control the active tectonics in the region (Khatri et al., 1978; Singh and Jain, 2007). Continued exhumations of high-grade metamorphic rocks are reported along these fault zones (Theide et al., 2006). Additionally, neotectonic activity along the NW-SE Spiti fault has also been reported by Bhargava (1990).

2.2.2. Previous evidence of neotectonic activity from Spiti valley

Modern seismic data for the last five decades shows the region is seismically active (Singh et al., 1975; Khatri et al., 1978). The earthquake in 1975 (Singh et al., 1975) with a recorded magnitude of 6.8 M_s is the best example of the recent seismic activity in this region. Massive landslides and slope failures also followed the earthquake in which debris from one of the major rock slides in the Parachu valley (Fig. 2.1) attained a height of 60 m and blocked the Parachu River – a modern analogue to the early Holocene damming of the Spiti River. Intense damage was noted along the N-S-trending Kaurik-Chango fault indicating its genetic relationship with the earthquake (Singh et al., 1975). The fault plane solution of the earthquake provides evidence for the east-west extension of normal faults in Spiti valley (Hintersberger et al., 2010).

The investigation of late Quaternary fluvial-lacustrine sediments from Spiti valley also yielded evidence of tectonic uplift and palaeoseismicity (Mohindra and Bagati, 1996; Singh and Jain, 2007; Phartiyal et al., 2009; Hintersberger et al., 2010). Thermoluminescence (TL) dating of the deformation structures in lake sediments near Sumdo village (Fig. 2.1) demonstrates seismic activity between 90,000 years to 26,000 years ago with a recurrence interval of approximately 10,000 years (Singh and Jain, 2007). In the Lingti valley, Hintersberger et al. (2010) identified NW-SE and N-S striking normal faults in lake sediments with a possible seismogenic origin due to its termination in layers with soft sediment deformation structures. Based on the OSL dating of these deformation structures, Hintersberger et al. (2010) proposed commencement of seismogenic activity in the upper Spiti (Lingti) valley from 39.9 ± 2.2 ka. However, the Holocene data in the Spiti region is

based on OSL dates on limited outcrops investigations (two outcrops at Lingti and Hansa with one seismite each) that yielded ages of 12 ka and 7.1 ± 1 ka, respectively (Phartiyal et al., 2009).

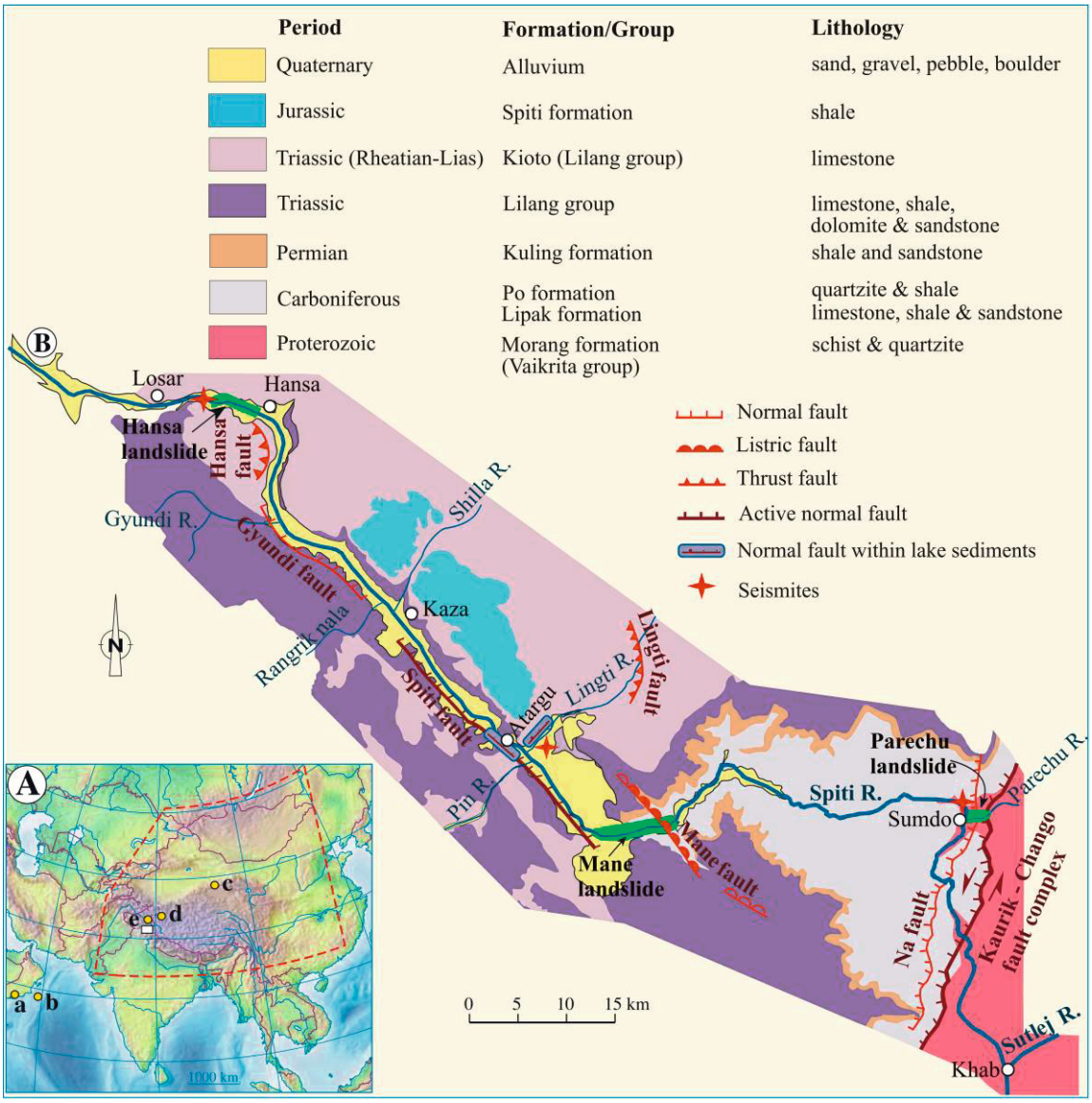

Fig. 2.1: *(A) The map showing investigated region (white rectangle) and sites referred to in the text (a) Qunf cave, Oman (Fleitmann et al., 2003), (b) Arabian sea core (Gupta et al., 2003), (c) paleoclimate records from central Asia (the area shown in red dotted line), (Herzschuh, 2006), (d) Western Tibetan lakes (Van Campo and Gasse, 1993), (e) Tsokar lake (Demske et al., 2009). (B) The geologic succession and tectonic map of the Spiti valley (compiled after Mohindra and Bagati, 1996; Bhargava and Bassi, 1998; Steck, 2003; Phartiyal et al., 2009; Hintersberger et al., 2010). The seismites and landslides reported from the region are also shown.*

2.3. Methodology

2.3.1. Drainage network analysis of Spiti Valley

Drainage network analysis can be used as a powerful tool for identifying active and recent tectonic deformation. The use of digital elevation models (DEM) in this kind of study permits characterisation and comparison of landscapes with high resolution and accuracy. To decipher the active tectonics of the Spiti valley, we have performed the drainage network analysis of Spiti valley using 30 m ASTER GDEM (ASTER Global Digital Elevation Model) data. Drainage network consisting of 28 major streams (Spiti River and its tributaries) in the Spiti valley was extracted using a matlab based toolbox for tectonic geomorphology, TecDEM (Shahzad and Gloaguen 2011a, 2011b). The longitudinal profile of the Spiti River was analysed from the source (Losar) to the confluence point of the Spiti with the Sutlej River at Khab (Fig. 2.2). Geomorphometric parameterization, i.e. concavity (θ), steepness (ksn), slope-gradient (Hack) index, were calculated to identify morphometric anomalies along the longitudinal profile of the stream and their correlation with controlling factors such as lithology and tectonics (Snyder et al., 2000; Schoenbohm et al., 2004; Shahzad and Gloaguen 2011a). The normalised steepness map of the study area was prepared by applying stream profile analysis on the 28 selected streams. For each stream channel, the contributing drainage area and channel slope was calculated from the DEM using TecDEM. Knick-point distribution was also prepared using slope breaks along the selected streams (Fig. 2.3). In order to get realistic and meaningful results, concavity and steepness indices were normalised with a reference concavity of ($\theta_{ref} = 0.45$) as suggested by Snyder et al. (2000). Hack index was applied to a contour interval of 100 m to calculate the variation in stream gradient (Fig. 2.2).

Additionally, a quantitative morphometric method - topographic symmetry index (T-index), following the basic technique presented in Cox (1994) and Cox et al. (2001), was calculated to infer the basin asymmetry of the region. The T-index provides evidence of tilting influence on drainage pattern (Cox, 1994). T-index is calculated as the ratio of orthogonal distance from the stream channel to the center of its drainage basin and distance from basin margin to the centre of the basin (Garrote et al., 2006). T-index is a dimensionless quantity and can be represented on a scale between 0 to 1.

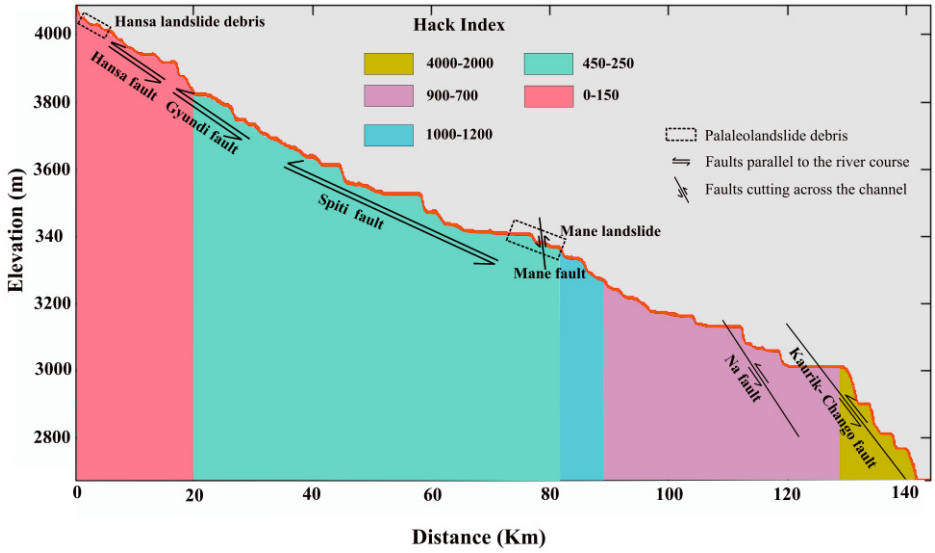

Fig. 2.2: *Longitudinal profile of the Spiti River extracted from Losar to its confluence point with the Sutlej River (Khab). See Fig. 2.1B for location of extracted profile. Hack indices are also calculated at different segments along the Spiti River profile. Changes in gradient and Hack indices demonstrate the response of stream profile to active faults in the region. Refer to Fig. 2.1B for location of faults and landslides.*

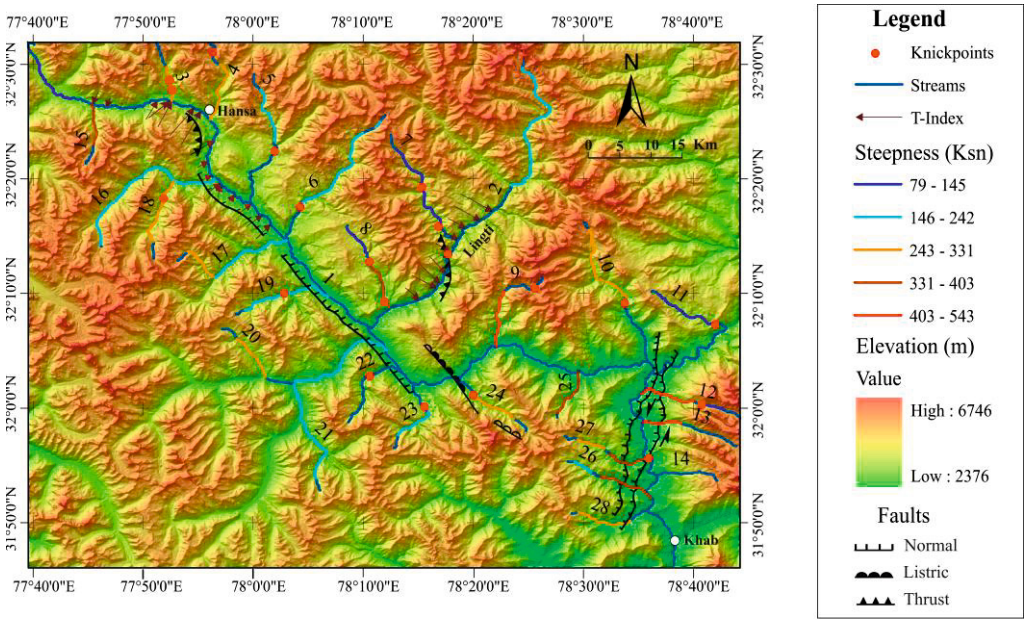

Fig. 2.3: *Distribution of normalised steepness values for channel segments in study area. Knickpoints along the selected streams are also plotted with red circle. T-Index along the selected basins of strahler order 5 was calculated and show evidences of basin tilting.*

2.3.2. Geomorphology of the investigated area

A field study involving identification and mapping of prominent geomorphic features (river terraces, landslides and alluvial fans) was conducted along the course of the river in the upper Spiti valley. The mapping of palaeo-landslide debris and palaeolake sediments (laminated clayey silt alternating with fine sand) was also carried out in the upper Spiti valley. The

height of lake sediments is measured above the basal fluvial unit. Additionally, we have investigated the morphological features of the palaeo-landslides and the lateral extent of the palaeolake deposits.

2.3.3. Chronology of neotectonic activity in the Mane palaeolake sediments

Extensive field investigations of Mane palaeolake sediments (stratigraphic position and lateral extent) were undertaken to identify evidence of neotectonic activity in the upper Spiti valley. A precise chronology for the neotectonic activity (seismites and brittle faults) was ascertained based on radiocarbon dating of unaltered wood samples from the palaeolake sediments. Care has been taken to collect organic samples due to the formation of secondary thick carbonate crust (10-15 cm) on the surface of the lake outcrops. These thick crusts often contain reworked organic material which can give incorrect ages. Therefore, we have collected wood samples from different stratigraphic horizons after a thorough cleaning of the outcrop (removal of ca. 10-15 cm of surface carbonate crust or more until the original sediment surface and structures were visible). We have focussed on samples that were deeply embedded (after outcrop surface cleaning) parallel to the laminations and neglected samples from the events layers (gravel layers). The ^{14}C dating of the wood samples was performed at Poznan radiocarbon laboratory, Poland (Table 2.1). The ^{14}C dates were converted from conventional ^{14}C ages into the calendar ages using OxCal 4.1 software (Bronk Ramsay, 2001, 2009) with the IntCal 09 calibration curve (Reimer et al., 2009). Previous studies reviewed in this paper have also used U/Th dating methods (Fleitmann et al., 2003), OSL (Singh and Jain, 2007; Phartiyal et al., 2009), and cosmogenic radio-nuclide dating (Bookhagen et al., 2006) that yield ages in calendar years. These are referred to in ka.

Table 2.1. *AMS radiocarbon dates from the Atargu lake sediments.*

Height	Material	Lab no.	^{14}C age (y)	^{14}C age cal BP (1σ)
40.9- 41[a]	wood fragment	-	5286 ± 35	6073 ± 66
26.86 -26.88	wood fragment	Poz-33168	5650 ± 60	6436 ±73
24.57-24.59	wood fragment	Poz-33167	5680 ± 40	6465 ± 53
18.54 -18.55	wood fragment	Poz-33165	5870 ± 40	6691 ± 49
6.55-6.57	wood fragment	Poz-33176	6490 ± 80	7397 ± 75
0 - 0.1[a]	wood fragment	-	7926 ± 38	8781 ± 104

[a] organic samples from previous work (Bookhagen et al., 2005)

2.4. Results

2.4.1. Drainage network analysis of Spiti River

River responses to active tectonics can often produce characteristic geomorphic features indicating surface deformation in an area (Jain and Sinha, 2005). The deflection or abrupt change in the river course coincident with deformation indicates the sensitivity of rivers to tectonic movements (uplift /subsidence) (Holbrook and Schumm, 1999). The course of the Spiti River in the upper valley follows the trace of the Spiti fault (Bhargava, 1990) and makes a sharp turn towards the toe end of the fault in W-E direction (Fig. 2.1). In the lower Spiti valley the W-E-flowing river makes an abrupt shift in the course near Sumdo and follows the trace of K-C fault (Fig. 2.1), suggesting that the Spiti river course is mainly controlled by the active faults in the region. We also note that all the three major landslides (Hansa and Mane palaeo-landslides, and the 1975 earthquake-triggered Parachu landslide) in the Spiti valley have occurred along the fault zones (Fig. 2.1).

The extracted longitudinal river profile of the Spiti River provides evidence of active deformation in the region (Fig. 2.2). The rivers that are not affected by tectonic deformation mostly develop a smooth concave longitudinal profile. Departures of the river gradient from this ideal smooth shape reflect variations in the lithology of the river bed or variations in rock uplift rates along the river course (Burbank and Anderson, 2000). The sharp knick-point observed mostly along the active fault zones indicates tectonic influence as the cause for the gradient change (Fig. 2.2). However, smaller change in gradient noticed along the Mane palaeo-landslide debris (dashed box in Fig. 2.2) could be due to the slope changes associated with transition from low gradient lake deposits to rapids associated with landslide deposits. The analysis of geomorphic indices such as slope-gradient (Hack) and steepness index along various segments of Spiti River corroborates the results of river profile analysis (Figs. 2.2, 2.3). Variations in stream gradient (Hack index) along a river typically reveal changes in lithology or tectonic control (zones of differential uplift or subsidence) (Kirby et al., 2003). The very high value of Hack index (2000-4000) observed along the K-C (normal) fault zone indicates differential uplift as the cause for this variation (Fig. 2.2). Similarly high steepness values (Fig. 2.3) related to rapid slope changes were also noted along the K-C fault zone while the rest of the region shows low to medium steepness. Therefore, the extracted longitudinal profile and geomorphic indices (steepness and Hack indices) demonstrate active deformation in the Spiti region along the K-C fault zone. Our result is concordant with the

previous finding showing continued tectonically induced exhumation along this fault zone (Thiede et al., 2006).

The calculated Transverse Topographic Symmetry (T-index) provides evidence for active tilting in the region (Fig. 2.3). In the study area, basin tilting was identified near Hansa and the Lingti valley along the major faults (Fig. 2.3). This concurrence illustrates active faulting as the cause for the tilting. It is noted that in the Hansa region, the drainage pattern is diverted towards the NW-SE direction, following the overall dip of the region. The general mass movement (two palaeo-landslides have been identified from this region, Phartiyal et al., 2009), also occurred along the tilted direction. Hence, the ongoing tectonic activity, shown by our T-index calculations, could be the reason behind the vulnerability of Hansa region to mega-landslides. Therefore, the calculated geomorphic indices (Hack index, steepness and concavity) indicate active deformation along the K-C fault, whereas the T-index demonstrates ongoing activity along the Hansa and Lingti faults. The apparent dissimilarity of the results of the T-index with other geomorphic indices (Hack index, concavity and steepness) is due to the sensitivity of these indices to different types of activity - broad tilting versus differential uplift and subsidence.

2.4.2. Geomorphological investigations

The upper Spiti valley

The Spiti valley is characterised by a U-shaped cross-section in the upper valley (upstream of the Mane village) and deeply cut V-shape in the lower part. The sidewalls of the valley are mostly covered with talus scree, limiting the exposure of bed rocks. Meandering and braiding, that often reflects relative changes in gradient is found within the course of the Spiti River, whereas the section within the landslide debris is deeply incised. We mapped terraces, debris and alluvial fans in the upper Spiti valley (Fig. 2.4a). Debris fans, mostly associated with ephemeral streams have partially blocked the Spiti River at several points (Fig. 2.5a). Terraces identified in the upper Spiti valley are mostly paired aggradational river terraces (correlative terraces preserved on both side of the river) found at the mouth of the tributary streams joining the Spiti River. They comprise poorly sorted boulders and gravels indicative of a steady and fast alluviation event. Three levels (T_1, T_2 and T_3) of terraces were identified (Fig. 2.5b). The T_2 and T_3 terraces attain a height of ~ 0.5-1 m, whereas the T_1 terrace occurs at a height of ~20 m from the river bed. Near Lidang, the palaeolake sediments overlying the basal fluvial gravel (see Fig. 2.4b and the following Section 2.4.3 on lake sediments) are

much thinner than at the investigated sections of Atargu. In the absence of datable material we cannot say whether this feature represents upstream pinching-out or if it is due to partial erosion (mean basin denudation rates six times greater than the present rate of ~0.08 mm/yr were prevalent in the Spiti valley during the intensified monsoon phase, Bookhagen et al., 2005) of the upper part of lake sediments. In any case the stratigraphic correlation of the oldest terrace (T_1) with the top of the lake outcrop (regardless of which part of the lacustrine section) at Lidang (Fig. 2.5c) indicates a Holocene age for the terraces as the lake sediments in the upper Spiti valley were deposited during early to mid Holocene. This Holocene age for the terraces has been confirmed by cosmogenic nuclide dating (B. Bookhagen, personal communication).

In addition to paired terraces, an unpaired terrace (near Lidang village) is also observed in the upper Spiti valley. Tilting of fluvial and lake sediments is also noticed near the junction where the Pin River joins the Spiti River (Fig. 2.5d). The tilting mostly reflects incipient and smaller-scale deformation in an area (Holbrook and Schumm, 1999). Here the fluvial profile is tilted 30° towards the NW, parallel to the active Spiti fault, indicating the influence of active tectonics on geomorphic features.

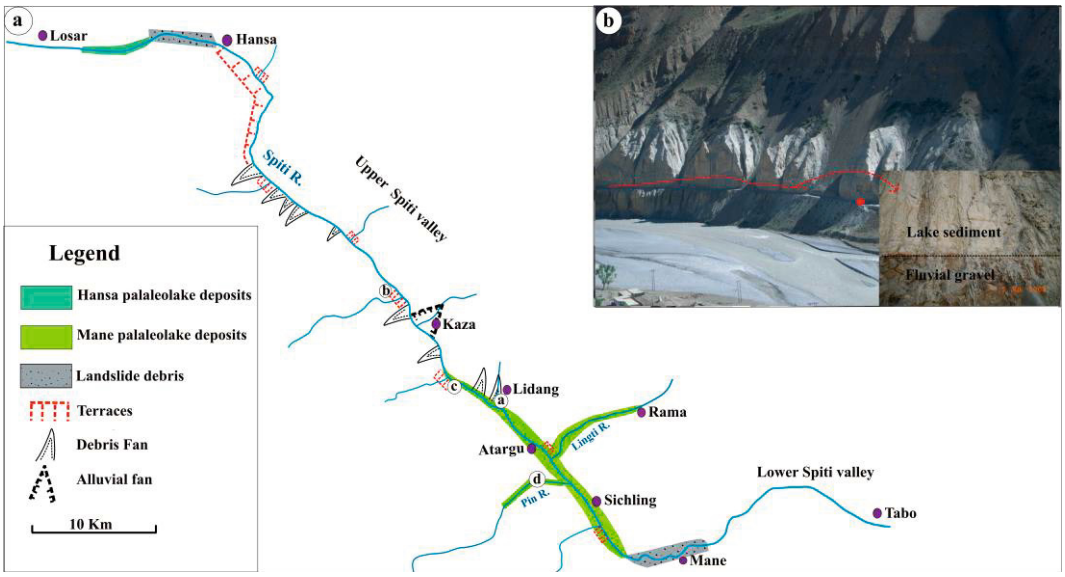

Fig.2.4: *a) Schematic map illustrating prominent geomorphic features of the study area. b) Lake sediments occurring as discrete outcrops along the course of the river (red dot denotes field vehicle for scale).*

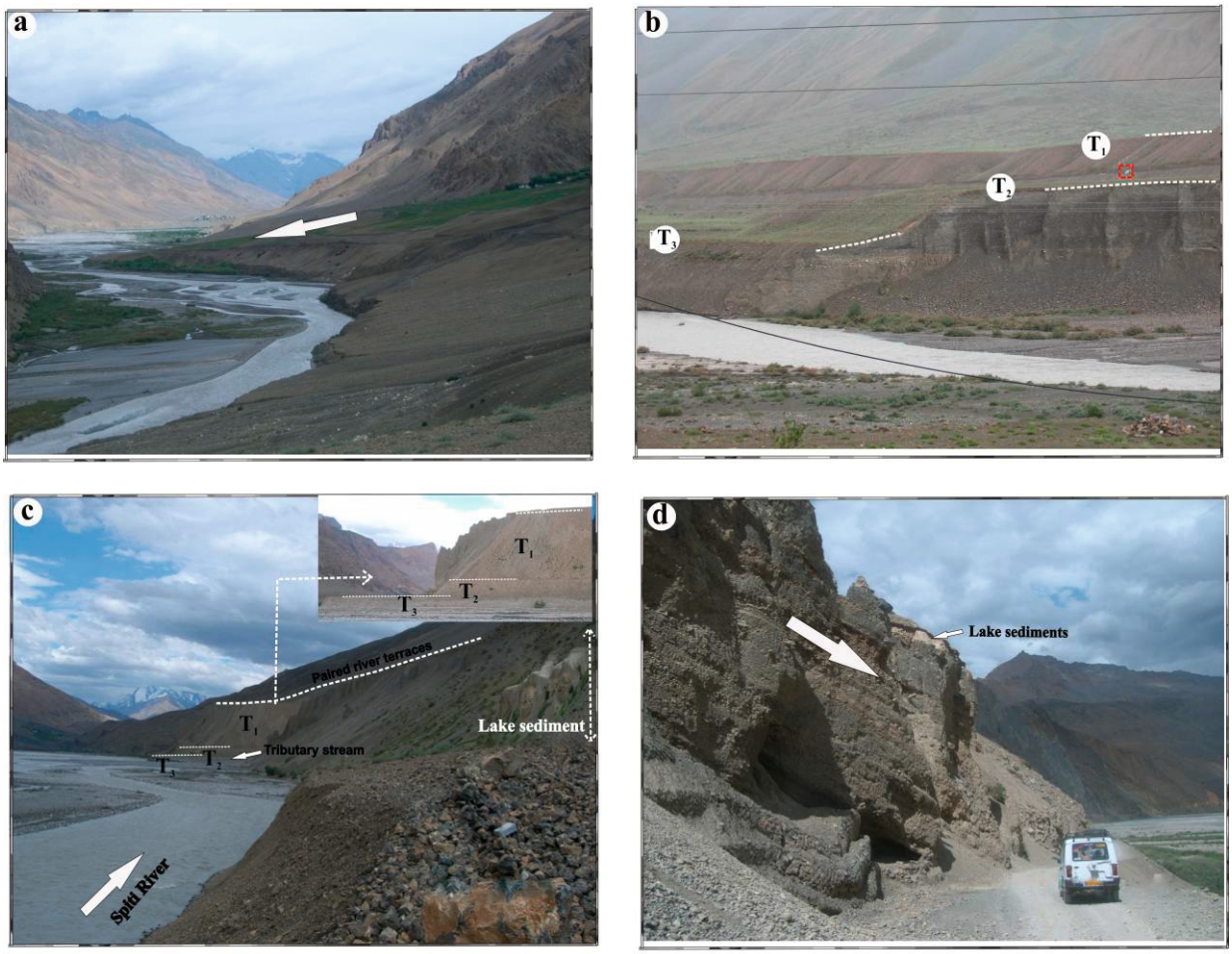

Fig. 2.5: *a) Debris fan identified along the course of the river near Lidang village. b) Different levels of terraces noted near Kaza (Red square denotes field vehicle for scale). c) Stratigraphical correlation between lake sediment and the terraces shows contemporaneous formation of lake sediment and T_1. d) Fluvial gravel tilted in the direction of the Spiti fault. See Figure 2.4a for locations.*

Palaeo-landslides

The palaeo-landslides (Fig. 2.1) in the upper Spiti valley were identified near Hansa (two palaeolandslides, Bhargava and Bassi, 1998) and Mane village (one palaeo-landslide, Bhargava and Bassi, 1998). The landslides are of rock slide type (Weidinger and Korup, 2009) with debris consisting of carbonaceous rocks with fractured and pulverised rock at the bottom of the debris. Our study shows that the Mane and Hansa landslides have some similarities: the top of the debris has angular rocks of even >1 m in diameter (Figs. 2.6a, 2.6b), the movement of both the landslides has taken place mainly along the bedding plane surface (Fig. 2.6a), and the landslide debris climbed up the opposite valley blocking the Spiti river course and resulting in the formation of a lake upstream. Extensive faulting has also been identified in places (Mane and Hansa) where the palaeo-landslides have occurred (Fig.

2.1, Fig. 2.6b). This weakening of rocks through extensive faulting can provide ideal preconditions for mega-landslides. However, the Mane landslide shows one additional feature: the sagging of slope at the head of the major landslide scrap (l_1) (Figs. 2.7a, 2.7b). This sagging of slope creates a depression (l_2) at the head of landslide debris (l_3) (Fig. 2.7c). Secondary depressions, formed due to subsidence within the landslides by dissolution of fractured carbonaceous debris, were also found within the Mane landslide debris. These depressions were subsequently filled with ≥25 m-thick lake sediments (l_4) consisting of indistinctly laminated alternating darkish brown and buff colored clay layers. Finally the erosion of the landslide debris by the Spiti River resulted in the breaking of the dam and dissection of the infilled depressions thereby exposing the fine-grained lacustrine deposits (Fig. 2.7d).

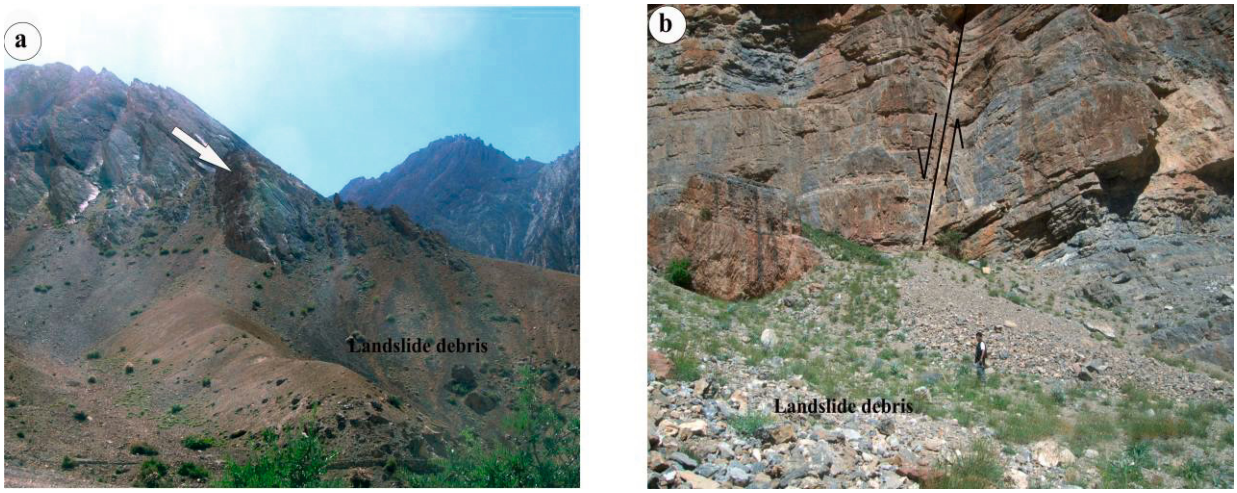

Fig. 2.6: *a) Photograph showing movement of landslides along the bedding plane surface. b) The faulted rocks in the vicinity of Hansa palaeo-landslide.*

Dam Break

We have also investigated the region downstream of the Mane and Hansa palaeo-landslide for evidence (or absence thereof) of the nature of the dam burst. We have not found any evidence (e.g., large volume of unsorted debris) of a catastrophic dam burst and propose a gradual incision through the landslide dam.

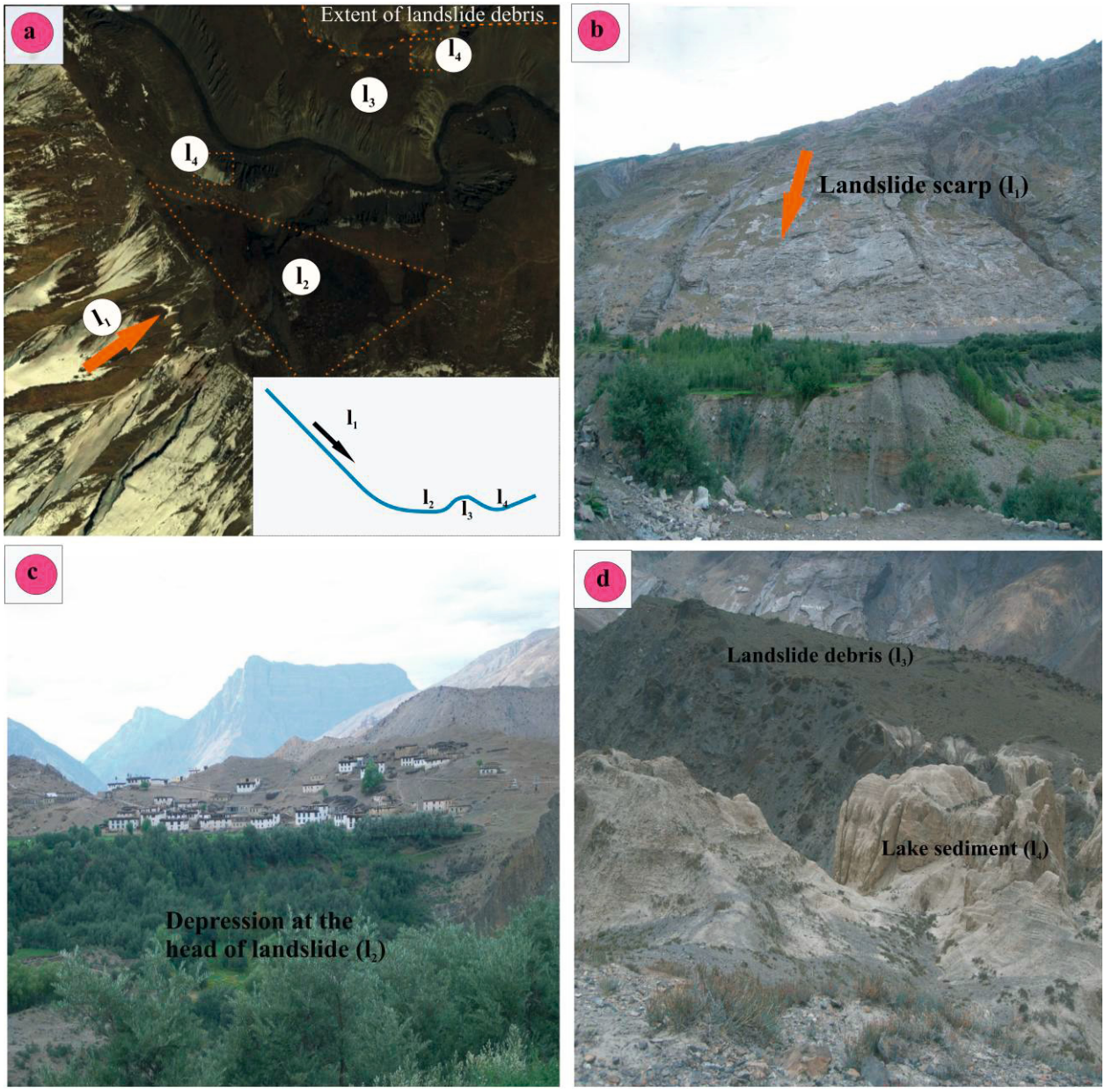

Fig. 2.7: *(a) Google map showing the morphological features of Mane landslide. (b) Major Landslide scarp (l_1), (B. Bookhagen, personal communication, 2007), arrow indicates the direction of landslide advance. (c) Depression (l_2) at the headscrap of the landslides. (d) Landslide debris (l_3) and lake sediments (l_4) within the depressions.*

2.4.3. Mane palaeolake sediments

Chronology

The Mane palaeolake is located within the limestone catchment (Kioto limestone), hence there is a possible hard water effect resulting in spuriously old ages for the dated bulk organic matter or aquatic plants. So the best way for getting reliable radiocarbon dates from the region is to look for organic fragments from terrestrial land plants that draw CO_2 from the atmosphere alone (in equilibrium with the ambient ^{14}C activity) (Phartiyal et al., 2009). Additionally, our careful sampling strategy (Section 2.3.3) is designed to avoid post-depositional contamination. An increase in age with depth for the wood fragments suggests lack of chronological errors arising from the reworking and incorporation of older organic material. The ^{14}C dates derived from our study (Table 2.1) are stratigraphically consistent and fit well with the previous ^{14}C age estimates from the lake sediments (Bookhagen et al., 2005).

However, based on the OSL dating, Phartiyal et al. (2009) indicated older age boundaries of 13±2 and 8±1 ka for the lake sediments. This overestimate might have been caused by insufficient bleaching of sediments in a high energy environment - recent luminescence dating from the region (A. Murray, personal communication) revealed that the modern Spiti river sediments have an unbleached luminescence age of ≥2 ka. Similarly the proposed age assignments (39.9 ± 2.2 ka) for the beginning of seismogenic activity in the upper Spiti valley based on OSL dating of lake sediments by Hintersberger et al. (2010) is also inaccurate as all the studies so far in this region (Bookhagen et al., 2005; Phartiyal et al., 2009; this study) clearly indicate the lake sediments to be of Holocene age. The older OSL ages could be a result of incomplete bleaching of water-borne sediments over short distances (e.g. Prasad and Gupta, 1999; Fuchs and Lang, 2009; Baartmann et al., 2011). We have therefore not considered OSL ages for stratigraphic correlation or intercomparison.

Soft sediment deformation structures within the lake sediments

Due to sparse vegetation, high rate of erosion (Bookhagen et al., 2005), and ongoing tectonic activity (Khatri et al., 1978, Hintersberger et al., 2010), the lake sediments do not occur continuously along the entire valley but form discrete outcrops. They overlie fluvial gravels that were deposited in the river channel prior to damming (Fig. 2.4b). The lake sediments are mostly laminated and include occasional sand and gravel layers. Two deformation zones are identified within the lake sediments separated by undeformed sediments (Fig. 2.8a). The lower zone (LD) attains a thickness of 1.5 m (3 - 4.5 m, ca. 7.8 cal ka) whereas the upper one

(UD) is much thinner (0.5 m thick located between 6.5 -7 m, ca. 7.4 cal ka). We also observed that in the thinner horizon (UD) the deformation disappears laterally and then again reappears further downstream in the same stratigraphic horizon. However, the thicker horizons are generally more continuous and can be traced for more than half a kilometer. The identification of deformation structures at similar height in the lake sediments from the Lingti valley by Bagati and Thakur (1993) shows the wider regional occurrence of these structures. In addition, brittle normal faults (dated to ca. 7.8, 6.5 and 6.1 cal ka) are also identified within the lake sediments (Fig. 2.8b). The deformed zones are discussed in detail below:

Lower Deformed Zone (LD)

Lower deformed zone (LD) includes deformation structures such as injection structure (LD_1), fault grading stratigraphy (LD_2) and flame structures (LD_3). The injection structure has a slightly oblique trend cutting across the laminated sediments (Fig. 2.9a). The structure shows an upward migration of liquefied materials through a fractured zone (l_1). It attains a height of ~15 cm and finally terminates against a deformed zone (l_2). The material within the injection structure is composed of a mixture of sand and clay. The structure implies mobility of sediment at depth to provide a source for the injected material and can be interpreted as partial local liquefaction of sediment (Ringrose, 1989). Fault grading stratigraphy (LD_2) shows a sequence with (a) soupy, (b) rubble, (c) segmented zone, and (d) undeformed zones at the top and bottom of the structure (Fig. 2.9b). The soupy and rubble zone is characterised by completely/partially liquefied sediments whereas the segmented zone comprises faulted sediment. This structure was first described by Seilacher (1969) and interpreted as an effect of strong earthquakes on gradationally compacted beds. The flame structure (LD_3) found within the lake sediment shows evidence of upward migration of liquefied material with the preservation of original laminations. The structure is characterised by broad antiforms and narrow synforms, with antiforms getting truncated at some places (Fig. 2.9c). The deformation is more pronounced in the coarser sand layer rather than the clay layer possibly due to the greater susceptibility of sand layer to liquefaction as compared to the clay layer. The sagging of sand layer into the clay layer is also seen above and below the structure.

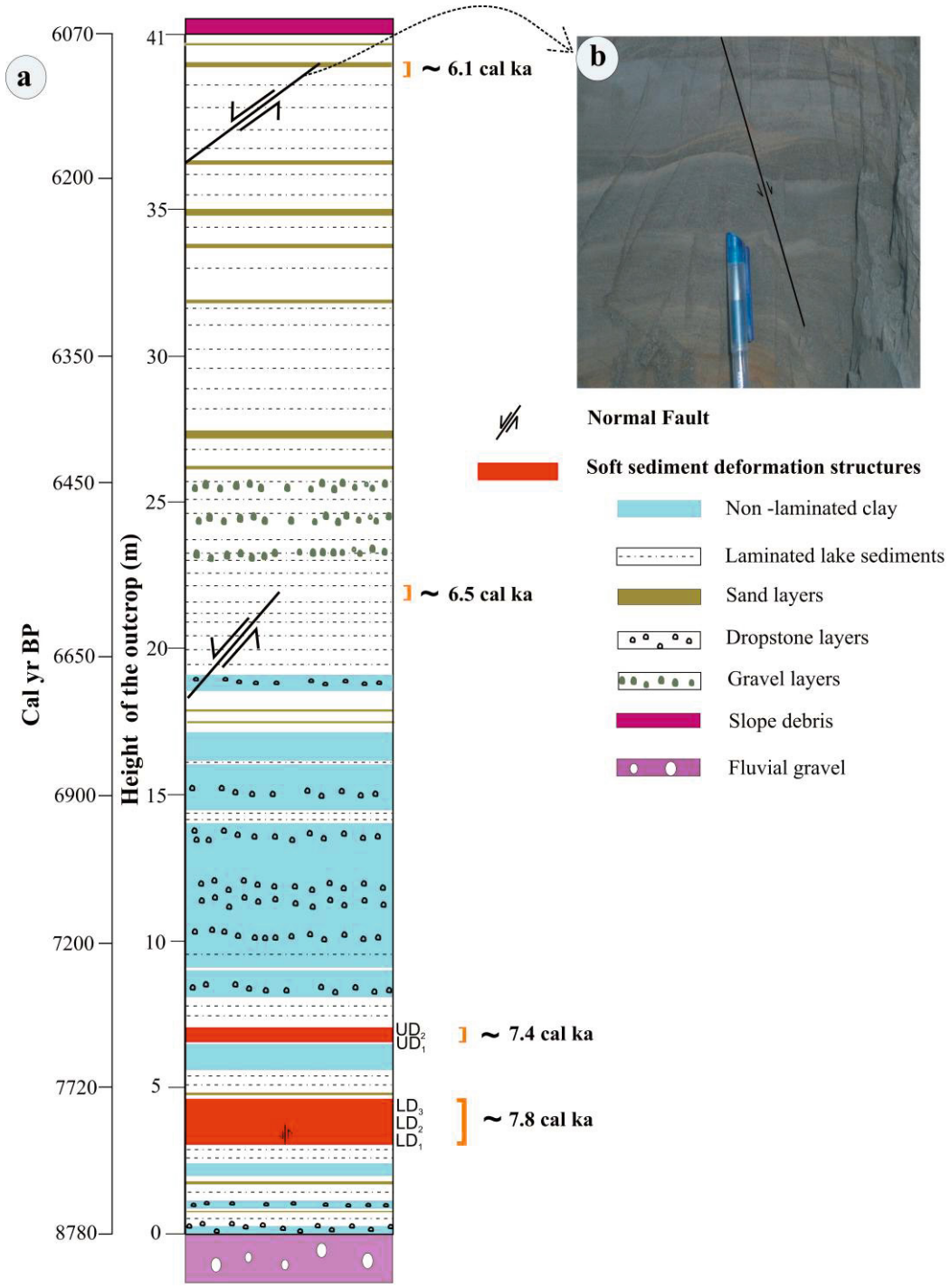

Fig. 2.8: *a) Composite lithological profile of the outcrops showing the deformed zones. (b) Normal faults identified within the lake sediments strikes parallel to the active faults in the Spiti valley.*

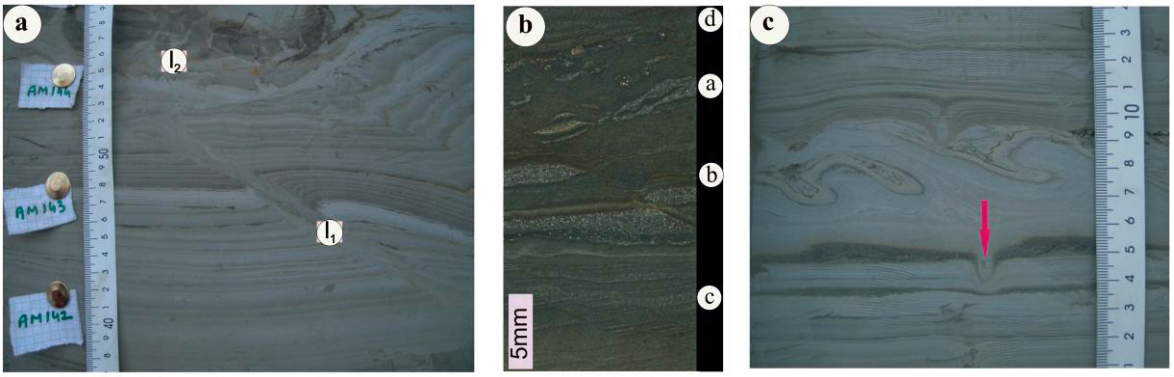

Fig. 2.9: *a) Injection structure (l_1) found at 3.5m above the base. Note that the laminated sediment on the left of injection structure was intensively deformed (l_2). (b) Fault grading stratigraphy a) soupy zone b) rubble zone, c) segmented zone, and d) undeformed zone. (c) Diapiric flame intrusion found within the lake sediment. Sagging of sand layer (arrow) into the clay layer can also be noticed in the figure.*

Upper Deformed Zone (UD)

The structures identified within this zone include Ball and Pillow structures (UD_1) and contorted beds (UD_2). Ball and Pillow structures (UD_1) are formed by the discrepancy in liquefaction capacity of the sand and clay layers (Fig. 2.10a). These structures can be formed by two known processes: (i) by fluidisation processes related to overloading and events of mass sedimentation (Lowe and Lo Piccolo, 1974: Lowe, 1975); and (ii) by seismically-induced liquefaction and selective fluidisation in normal graded bedding. Moretti et al. (1999) have suggested that the sand layer with high susceptibility for liquefaction is prevented from infiltrating below by the clay layer, which acts as barrier to permeability by creating temporary voids filled with water. Subsequently, localised rupture of clay laminae results in the formation of pillow structures. We propose a tectonic origin for this structure as similar sequence of thick (or thicker) sand layers underlain by clay layers are found in different parts of the outcrop (Fig. 2.10b) but the ball and pillow structure is found only in this part of the section.

Contorted beds (UD_2 in Fig. 2.10c) show sand occurring in discrete forms within the clay layers. The structure seems to have been resulted from the thick overlying sand layer sinking downwards into the clay layer. The structure shows a strong resemblance to that experimentally produced by Kuenen (1958) in which the sand layer overlying a clay substrate foundered and broke into discrete forms when shaken by weak vibrations simulating an earthquake.

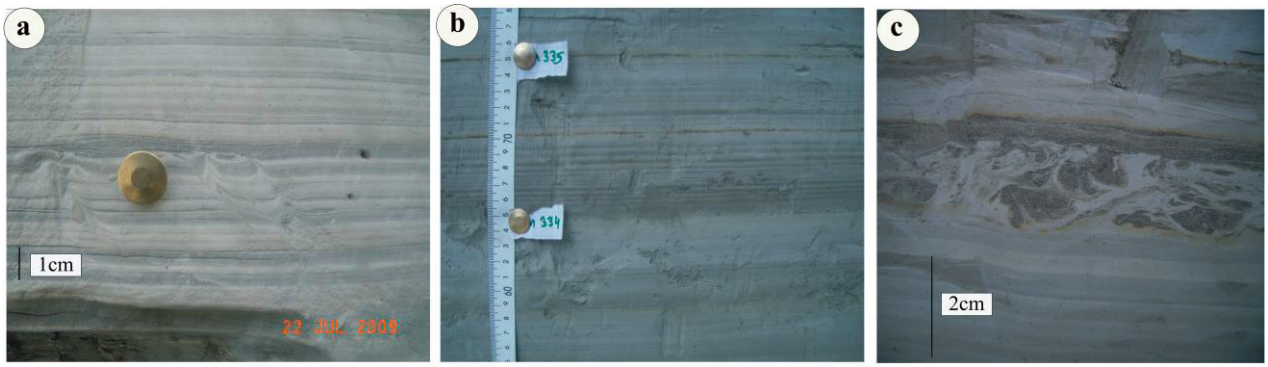

Fig. 2.10: *a) Development of ball and pillow structure within normal graded beds. b) Similar normal graded laminations found in other part of section (10 m from the base of lake sediment) without ball and pillow structure. c) Contortion of layers with sand occurring as discrete forms within clay layer.*

Faults within palaeolake sediments

We also identified brittle normal faults at three different horizons terminating at ca. 3.5m (7.8 cal ka), 22 m (6.5 cal ka), and 40 m (6.1 cal ka) height in the lake sediment. The lower fault (~ 3.5 m) is identified within lower deformation zone (Fig. 2.8a), thereby illustrating a possible seismic origin. The trend of the lower faults (~3.5 m and ~ 22 m) strikes 140° in NW- SE direction whereas the upper one (~ 40 m) strikes 180° in N-S direction (Fig. 2.8b). Therefore, the trends of identified faults are parallel to the active NW-SE trending Spiti fault and the N-S trending K-C fault, indicating activation of these major faults during early to mid Holocene.

2.5. Discussion

2.5.1. Origin of soft sediment deformation structures

Our studies indicate that the deformation structures are formed in noncohesive sediments of Mane paleolake by liquefaction and fluidisation. The possible explanations for the process could be glacial processes, liquefaction resulting from pore pressure changes associated with sudden lake level falls, slope failures, and earthquake-induced liquefaction (Ringrose, 1989). However, in the Spiti valley outcrops, the extensive area of the liquefaction structures, horizontal layering, and absence of any slump structures eliminates the influence of slope failure for their origin. The glacial processes as the cause for deformation structures can be ruled out since deformation structures show wider regional occurrence in comparison to dropstone layers and both occur at different heights within the lake sediments. Density heterogeneities due to increased sedimentation as a cause is also excluded due to the absence of these structures in the upper part (19-40 m) where the sedimentation rate (10 mm/yr in the lower part and 32 mm/yr in the upper part) is three times higher than in the lower part (0-19

m). Thus, soft sediment deformation structures observed within the Mane palaeolake can be associated with seismic events as they fulfill the criteria's put forward by Sims (1973, 1975) and Obermeier (1996) for the identification of palaeo-earthquakes, i.e.: (i) the study area is in a seismically active region (as proved by a recent earthquake (1975 AD) of 6.8 M_s, Singh et al., 1975; Khatri et al., 1978); (ii) potentially liquefiable lacustrine sediments are present; (iii) strong, sudden hydraulic force directed upwards (e.g. injection structure) can be identified; (iv) the structure zones contain internal features that suggest liquefaction and are correlative over large areas within the sedimentary basin; and (v) detectable influences of slopes or slope failures are lacking. We therefore conclude that there are four episodes of tectonic activity (faults and seismites) during the period of lake existence between ca. 8.7-6.1 cal ka. The lower and upper deformation zones (seismites) were dated to ca. 7.8 and 7.4 cal ka, respectively, whereas the two normal faults have an age of ca. 6.5 and 6.1 cal ka. Unfortunately, due to lack of accurate ages on the seismites reported by Phartiyal et al. (2009) and Hintersberger et al. (2010), it is not possible to correlate the events identified in the Mane palaeolake sediments with the previously available data in the Spiti (Lingti) valley.

2.5.2. Tectonic versus climate triggering for the landslides in Spiti valley

We evaluate the evidence for the postulated climatic induced origin (early Holocene monsoon intensification) of the Mane landslide (Bookhagen et al., 2005; Phartiyal et al., 2009). Early Holocene monsoon intensification due to increased solar insolation has been inferred from various proxy records: (i) isotope data from stalagmites in southern Oman (Fig. 2.11a) (Fleitmann et al., 2003) indicate increase in monsoon precipitation between 10.3-8 ka and gradual subsequent decreasing; and (ii) a *G. bulloides* record from an ocean core off the Oman coast, an indicator of upwelling, shows a monsoon wind maxima during the early Holocene, with occurrences of discrete intervals of weak summer monsoon winds (Fig. 2.11b, Gupta et al., 2003). However, recent studies, especially in the Himalayas and Tibetan plateau, indicate a rather complex regional pattern of early Holocene climate change (An et al., 2000; Mischke and Zhang, 2010; Wang et al., 2010). Herzschuh (2006), based on the 75 palaeoclimatic records from central Asia, also pointed out that the regions dominated by the westerlies and East Asian summer monsoon do not uniformly show any early Holocene climate optimum - for this area optimal wet conditions prevailed during the mid-Holocene (Fig. 2.11c). An overview by Prasad and Enzel (2006) indicates regional inhomogenties in Holocene climate change over northern India, related to westerlies versus monsoon interactions. Due to this spatial inhomogeneity of the Indian monsoon and the tropical-

midlatitude interactions that can interrupt the 'normal' monsoon pattern (Gadgil, 2003; Prasad and Enzel, 2006), and the contribution of winter westerlies in the Spiti valley, we have focused on well-dated regional records (e.g., Demske et al., 2009) closer to our study area that have a similar climate regime. Summarising: (i) pollen records from the western Tibetan lakes (Fig. 2.11d) show weaker Indian summer monsoon between 9-8 cal ka (Van Campo and Gasse, 1993, Gasse et al., 1996); (ii) a pollen record from Tsokar lake (Fig. 2.11e) indicates that the Indian summer monsoon reached its maximum between 10.9 and 9.2 cal ka and was followed by a period of enhanced westerly winds and weakened summer monsoon (Demske et al., 2009); and (iii) radionuclide dating of terraces from NW Himalaya revealed an attenuation of the Indian summer monsoon around 8.7 ka, when less moisture reached the internal parts of the orogen (Bookhagen et al., 2006). Based on the available data, we conclude that the Mane landslide occurred (ca. 8.7 cal ka) towards the end or after the early Holocene monsoon intensification. While monsoon intensification as the trigger for the Mane palaeo-landslide can be ruled out, we cannot totally exclude the possibility that one (or a few) extremely high monsoon rainfall event(s) during the weakened monsoon period could have caused the Mane palaeo-landslide. Indeed, such landslides have been observed in Sutlej valley in 2008 and Leh in 2010 – but these latter two landslides were much smaller in size as compared to the early Holocene Mane landslide. Also, considering that the modern seismic data from Himalayas provides ample evidence of earthquakes triggering landslides (Singh et al., 1975; Saraf, 2000; Owen et al., 2008), and the proximity of the Mane landslide to the active K-C fault, a tectonic trigger for the palaeolandslide is a strong possibility. We suggest three possible scenarios that could have triggered the Mane landslide: (i) one (a few) extreme rainfall event(s) during a period of weaker monsoon, (ii) water saturation of sediments and increased pore pressure caused by early Holocene monsoon intensification could have contributed to slope instability, thus increasing the likelihood of occurrence of landslides in this tectonically active region, and (iii) tectonic trigger. While it is not possible to identify the exact triggering mechanism amongst the three proposed above with complete certainty, the occurrence of all three palaeo-landslides in the upper Spiti valley along the active fault zones (Fig. 2.1) would point to a predominant tectonic influence.

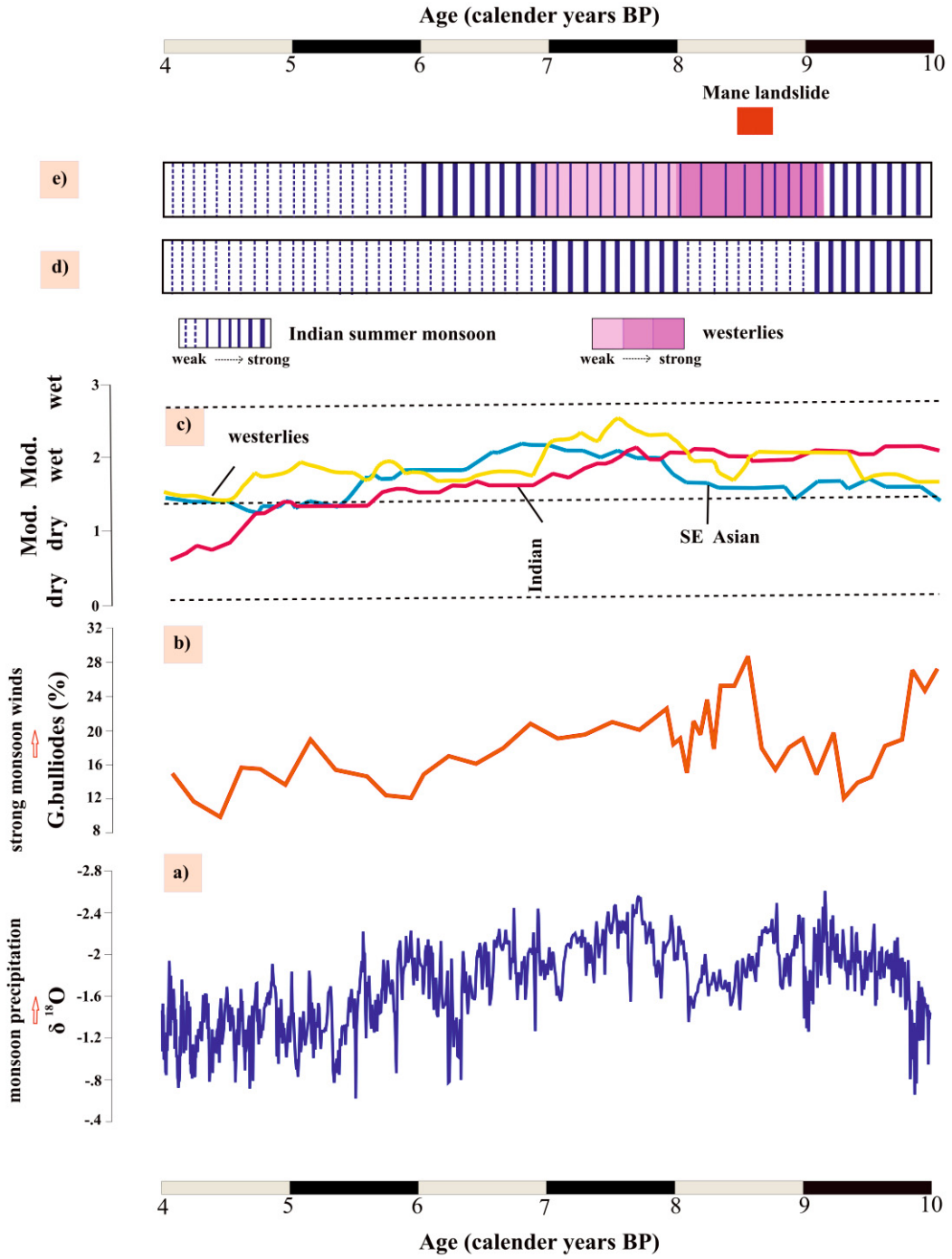

***Fig. 2.11**: Holocene climatic variability from various proxy records a) $\delta^{18}O$ of stalagmite data from southern Oman (Fleitmann et al., 2003), b) G. bulloides (%) from Arabian Sea (Gupta et al., 2003), c) Holocene effective moisture over monsoonal Asia, inferred from the palaeoclimate records (Herzschuh, 2006), (d) Compilation of climate interpretation based on the pollen record from western Tibetan lakes (Van Campo and Gasse, 1993; Gasse et al., 1996), (e) Pollen based climate information from Tso Kar lake, Ladakh, NW Himalayas (Demske et al., 2009). Red box indicate the age of landslide that caused the damming of river in upper Spiti valley (Bookhagen et al., 2005).*

2.6. Conclusions

We have investigated the role of tectonism and climate in the landscape evolution in the upper Spiti valley. In summary:

1. Geomorphology (tilted terraces and fluvio-lacustrine sediments) and abrupt changes in Spiti River course indicate a dominant tectonic influence in this region.
2. Geomorphic parameters (Hack index, steepness indices) indicate large-scale tectonic deformation along the Kaurik-Chango fault zone.
3. The calculated T-index demonstrates active deformation associated with faults in the Hansa and Lingti valley. This ongoing tectonic deformation could be the reason for the susceptibility of the Hansa region to mega-landslides.
4. Investigation of Mane palaeolake sediments reveals evidence for four episodes (ca. 7.8, 7.4, 6.5 and 6.1 cal ka) of neotectonic activity during the period of lake existence. The faults within palaeolake sediments dated to 6.5 cal ka and 6.1 cal ka show parallelism with the K-C and Spiti faults, indicating recent reactivation of these major faults.
5. Based on the combination of modern and palaeoclimate data, and our results on regional tectonic stability, we propose three possible scenarios that could have triggered the landslides in the Spiti valley: (i) extreme monsoon event(s), (ii) water-logging of sediments during the early Holocene monsoon intensification that could have made them susceptible to a tectonic trigger, and (iii) tectonic triggering. At this stage it is not possible to unequivocally state which of these three proposed mechanisms caused the landslide but their location only near active faults, as well as the repeated evidence of neotectonic activity, would clearly suggest some role for tectonism.

2.7. Acknowledgements

The funding for this research was provided by the German Research Council (DFG, Deutsche Forschungs Gemeinschaft) graduate school GK-1364.We are grateful to T. Longpo, B. Lal and T. Cherring for their invaluable help during the field work. We also thank L. Olaka, H. Echtler, B. Bookhagen, D. Scherler, R. Singh, and P. Kunagu for useful discussions, and B.S Kotlia for introducing us to this interesting region. Constructive and thought provoking comments by an anonymous reviewer helped in significantly improving the manuscript. Thanks are also due to A. Hendrich for his help with designing the figures.

Extreme events and spatiotemporal changes in precipitation patterns in NW Himalayas during the early-mid Holocene

***A. Anoop*[ab*]**, *S. Prasad*[a], *R. Krishnan*[c], *R. Naumann*[a], *P. Dulski*[a]

[a]German Research Center for Geosciences (GFZ), Telegrafenberg, Potsdam, Germany
[b]DFG Graduate School 1364, University of Potsdam, Germany
[c]Indian Institute of Tropical Meteorology, Pune, India

In review: Quaternary research

Abstract

We have undertaken high resolution palaeoclimate reconstruction on radiocarbon dated palaeolake sediments from upper Spiti valley, NW Himalayas. This site lies in the climatically sensitive westerlies and Indian summer monsoon (ISM) transitional regime and provides an opportunity to reconstruct the precipitation seasonality and extreme climate events that are characterised by intensified erosion. The investigation of lake sediment reveals distinct lithofacies that provide evidences of changes in depositional environment and climate during early-mid Holocene (8.7-6.1 cal ka). The period (8.7-7.6 cal ka) is marked by lake establishment. A sustained cooler period with weakened summer monsoon is observed during ~7.6-6.8 cal ka. A shift from colder to warmer climate with enhanced ISM is noted during ~6.8-6.1 cal ka. Several short term cooler periods were identified at ca. 8.7, 8.4-8.2 and 7.2-6.9 cal ka. Based on an overview of regional climate records we show that there is an abrupt switch in precipitation seasonality ca. 6.8 ka that is followed by onset of intensified ISM in NW Himalayas and stronger westerlies in NW India, a condition similar to that observed during the "break monsoon" years.

Key words

Extreme events, Lake sediments, Monsoon, Spiti valley

3.1. Introduction

The intergovernmental panel on climate change (IPCC) has reported an increase in the frequency of occurrence of extreme rainfall events in many parts of monsoonal Asia in a globally warm climate (Cruz et al., 2007). The recent extreme rainfall events in Asia in 2010 and 2011 would tend to bear out this conclusion. However, meteorological records that form the basis of such investigations from India are limited to ca. 100 years. Interestingly, similarities have been found between patterns of interannual variability and intraseasonal variability that cause extreme climate events (Webster et al., 1998; Sinha et al., 2011; Ummenhofer et al., 2011), suggesting that the monsoon oscillates between several basic states under the influence of remote forcing induced by SST or land surface conditions (e.g., Indian Ocean Dipole (IOD), ENSO (El Niño/Southern Oscillation). Long term regional palaeoclimate records can provide an understanding of the causal mechanisms that can trigger such climate extremes.

The available long term palaeomonsoon record from India has limited geographical coverage, and at best centennial scale resolution (Prasad et al., 1997; Enzel et al., 1999; Phadtare, 2000; Prasad and Enzel, 2006; Demske et al., 2009; Quamar and Chauhan, 2012) that makes it difficult to identify "extreme climate events". We have therefore investigated laminated palaeolake sediments from the climatically sensitive region of Spiti (NW Himalayas) with the aim of reconstructing past occurrence of such events. An advantage of working in this region is that it lies in the transitional area affected by both the Indian summer monsoon (ISM) and mid latitude westerlies (Fig. 3.1). The purpose of this study is to a) select suitable proxies for palaeoenvironment reconstruction by identifying links between contemporary climate, surficial processes, and sediment proxies in the modern Spiti Valley; b) use the proxies to reconstruct palaeoenvironment during early-mid Holocene from the laminated lacustrine sediments from this region; c) compare the reconstructed palaeoclimate record from Spiti valley with other regional Holocene records in the monsoon and westerly domains, and to obtain "snapshots" of spatiotemporal precipitation changes during the investigated time interval, and finally (d) interpret the reconstructed "snapshots" in terms of teleconnections governing long term regional climate variability.

3.2. Study area

3.2.1. Modern climate

The Spiti Valley is located in the northwest Himalayas above the tree line (3600 m asl), between 77–79° E, 31–33° N (Fig. 3.1). The valley lies in a rain shadow region with cold arid to semi arid climate and an annual maximum temperature fluctuating between +30°C and –30°C (Kumar et al., 1994). The modern climate data from the Spiti valley shows that the moisture in the region is mostly derived during winter in the form of snow from mid latitude westerlies (Sharma et al., 1991; Singh and Kumar, 1997; Wulf et al., 2010).The region over the high-mountain ridges of the NW Himalaya also witnesses occasional rains due to intensification of the summer monsoons (Bookhagen et al., 2005; Bookhagen and Burbank, 2010).While increases in the rainfall activity over the southern slopes of the Himalayas are known to be typically associated with "breaks" in the Indian summer monsoon (Dhar et al. 1984; Krishnan et al., 2000, 2009; Gadgil, 2003), the physical mechanism behind extended abnormal monsoonal rains over NW Himalaya (extreme events) is still poorly understood due to the lack of sufficient long term data.

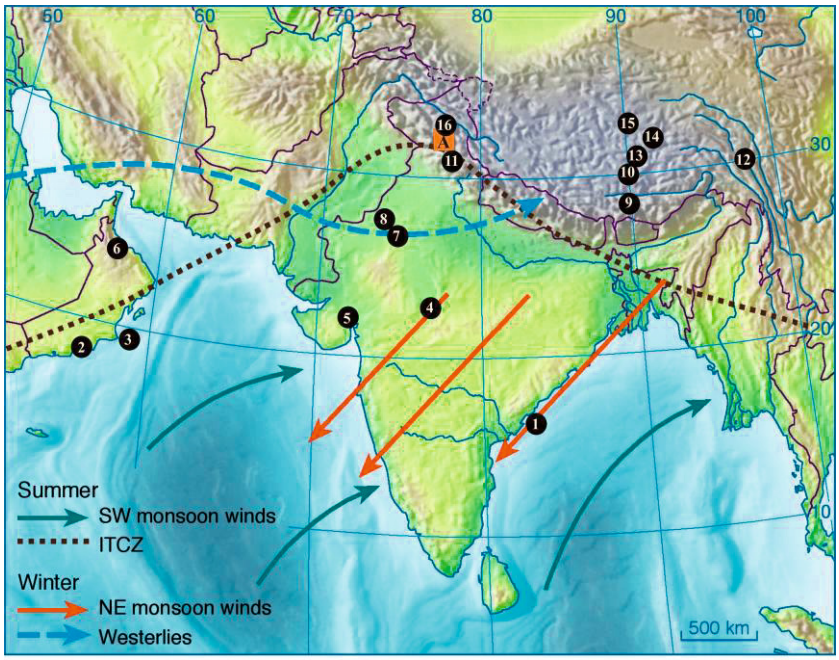

Fig.3.1: *Map of South Asia showing major features of the winds in SW Asia (modified after Prasad and Enzel, 2006).The location of the investigated site (A) in Spiti valley is also shown. The number (1-16) is used to indicate the palaeorecords discussed in the text (for details refer to Table 3.1).*

Table 3.1: *Paleoclimate records discussed in the text arranged from North to East.*

No	Location	N (°)	E (°)	Elevation	Archive	Wind system	Reference
1	**16A**	16.35	82.41	n.d	Marine core	a*	Ponton et al., 2012
2	**Qunf cave**	17.10	54.18	650	Stalagmite	a	Fleitmann et al., 2003
3	**Site 723 A**	18.03	57.36	n.d	Marine core	a	Gupta et al., 2003
4	**Nitaya**	22. 40	77. 42	250 m	Lake	a	Quamar and Chauhan, 2012
5	**Nal Sarovar**	22.48	72	n.d	Lake	a & b*	Prasad et al., 1997
6	**Hoti cave**	23.05	57.21	n.d	Stalagmite	a & b	Burns et al., 1998
7	**Didwana**	27.33	74.55	n.d	Lake	a	Singh et al., 1990
8	**Lukransar**	28.50	73.55	n.d	Lake	a & b	Enzel et al., 1999
9	**Chen co**	28.53	90.33	4420	Lake	a	Zhu et al., 2009
10	**Nam co**	30.30	90. 16	4718	Lake	a	Herrmann et al., 2010
11	**Gujjar Hut**	30.50	78.47	3500	Peat	a	Phadtare, 2000
12	**Lake Naleng**	31.10	99.75	4200	lake	a	Kramer et al., 2009
13	**Cueo lake**	31.50	91.50	4532	Lake	a	Wu et al., 2006
14	**Ahung Co**	31.62	92.06	4575	Lake	a	Morill et al., 2006
15	**Zigetang**	32.0	90.9	4560	Lake	a	Herzschuh et al., 2006
16	**Tsokar**	33.10	78.00	4527	Lake	a & b	Demske et al., 2009

*a Indian summer monsoon; *b Westerlies

3.2.2. Modern discharge and erosion

The discharge data from the Spiti River shows that about 80 percent of the annual flow occurs between May and September, mainly from snowmelt (Sharma et al., 1991). During winter the river remains partially frozen (personal communication with local population) resulting in reduced sediment load. Monitoring data in the region for past several decades (Sharma et al., 1991; Bookhagen et al., 2005; Wulf et al., 2010) shows that during abnormal monsoon years the discharge increases and is accompanied by increased erosion and enhanced mean basin denudation rates resulting in higher contribution of coarser sediments to the river load. Observations show that mean basin denudation rates are six times greater than the present rate of ~0.08 mm/yr in the Spiti valley during intensified monsoon years (Bookhagen et al., 2005). Our own observations in this region in 2008 also indicated that high energy debris flows are common during strong monsoon years. Therefore, coarser grain size

in discharge load resulting from intensified surficial erosion is generally a reliable indicator of extreme events in the region.

3.2.3. Geology

The Spiti valley forms the part of Tethyan Himalaya known for its complete record of sedimentation from Proterozoic to Eocene sediments (Bhargava and Bassi, 1998; Sinha, 1989). Our study area lies in the upper Spiti valley with lithologies dominated by rocks from Paleozoic and Mesozoic successions (Bhargava and Bassi, 1998). The Paleozoic (Permo-Carboniferous) rocks comprise friable and splintery shale, quartzite and meta sediments, whereas the Mesozoic successions are dominated by black limestone with intercalations of shale, dolomite and sandstone (Lilang group), shales (Spiti formation) and sandstones (Guimal formation). It is also noted that the Lilang group of rocks dominates the right bank of the Spiti River, whereas the left bank consists mostly of limestone (Kioto formation) and shales (Spiti formation) (Fig. 3.4).

3.2.4. Palaeolake sediments

The investigated lake sediments in the Spiti valley were formed as a result of landslide damming of the Spiti River near the Mane village (Fig. 3.2a, henceforth referred to as Mane palaeolake) during early Holocene (8.7-6.1 cal ka, Bookhagen et al., 2005; Anoop et al., 2012). The palaeolake sediments in these high altitude regions are largely clastic with low organic matter. Due to high rate of erosion (Bookhagen et al., 2005) and ongoing tectonic activity (Bhargava, 1990; Anoop et al., 2012; Phartiyal and Kothyari, 2012) lake sediments are not preserved continuously along the entire valley, they occur instead as discrete outcrops. After extensive field studies we have focused our investigations on the most complete and accessible outcrops near Atargu (ca. 41m thick palaeolake sediments) for palaeoclimate investigations. Additionally, lake sediments formed on the top of the Mane landslide debris (Fig. 3.2c) were also investigate as they could provide additional information related on overflow and lake level changes.

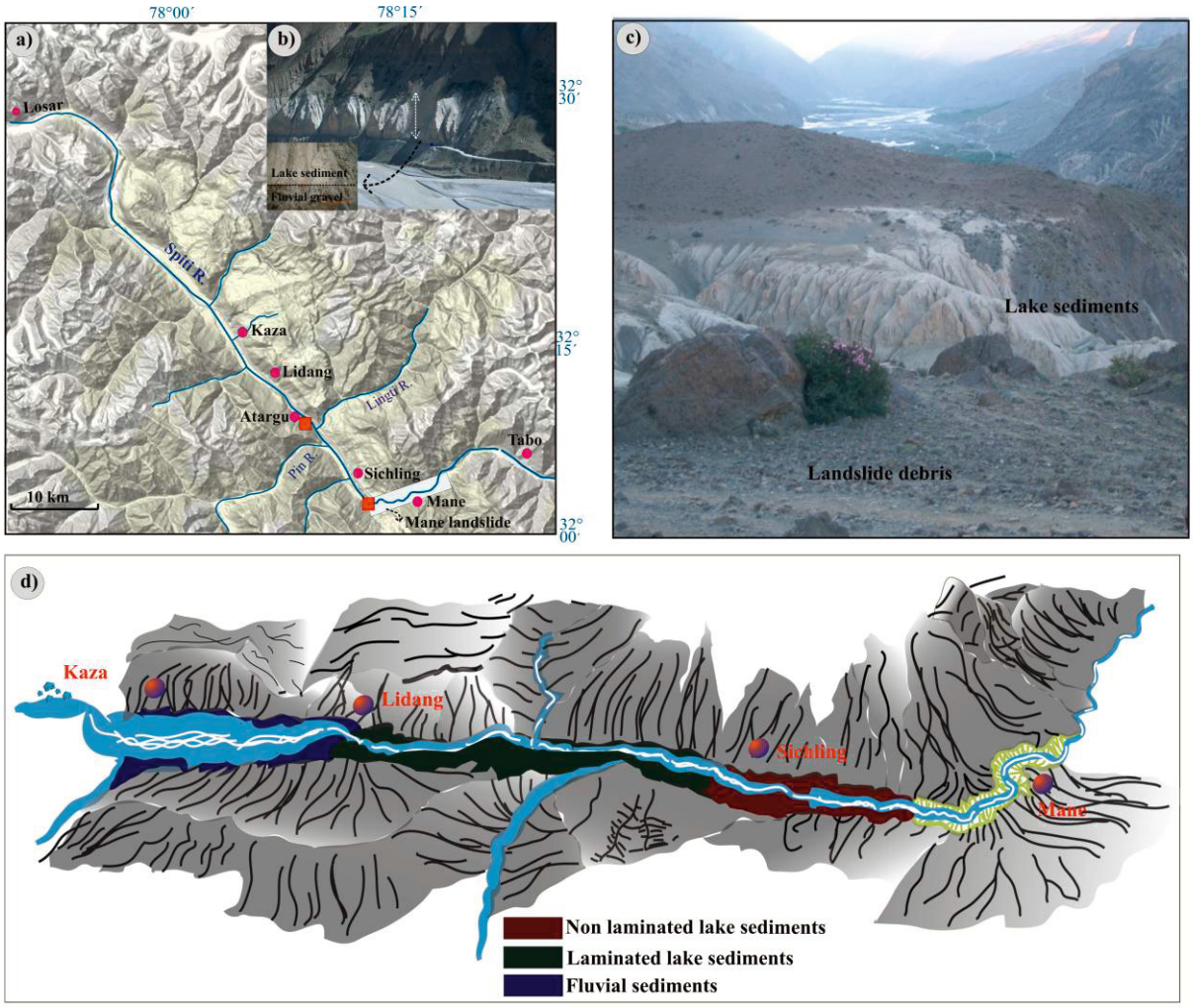

Fig. 3.2: *a) Satellite image of the upper Spiti valley showing the location of investigated outcrop (red square) near Atargu and Mane, b) photograph of the 41m thick lacustrine outcrops for palaeoclimate reconstruction, c) lake sediments within the Mane landslide debris, d)distribution and characteristics of the palaeolake sediments within the Mane palaeolake*

3.3. Methods

3.3.1. Modern sediments

The catchment area samples were collected from the Spiti River, its tributaries, and surface samples from characteristic rock types. In all tributaries, samples were collected just before they joined the Spiti River as this gave an overview of the stream catchment area geology. We undertook (i) semi-quantitative XRD and quantitative XRF analysis for detailed mineralogical and geochemical characterisation of bulk, sand, and clay sized fractions; (ii) tests for the presence of pollens (A. Bhattacharya, M. Stebich, per comm.) and microfossils.

3.3.2. Palaeolake sediments

Field investigations and sampling

Detailed field mapping of the Mane palaeolake deposits was conducted along the course of the upper Spiti river, upstream of the palaeolandslide. The height of lake sediments is measured above the basal fluvial unit. The investigated outcrops are partly laminated but also include seismites and sedimentary structures, event layers (coarse sand and dropstones), unlaminated clay, and gravel layers which were documented in a detailed lithostratigraphic record. Nearly all of the event layers could be traced for several tens of meters after outcrop cleaning.

For microfacies investigations, block samples were collected in stainless steel boxes (34 cm X 6 cm) with a vertical overlap of at least 5cm. Additional samples were also collected from event layers.

Laboratory methods

Microfacies: Overlapping thin sections were prepared after saturating the sediment blocks with epoxy. Thin-section images were obtained with a digital camera (Carl Zeiss Axiocam) and the software Carl Zeiss Axiovision 2.0.

XRF: The abundances of major elements within the block of palaeolake sediments were measured on 10cm long, epoxy impregnated sediment blocks using scanning X-ray fluorescence. The analytical system is an EAGLE III XL μ-XRF spectrometer with a low power Rh xray tube. All measurements were performed with X-ray tube voltage adjusted to 40 kV and spot and step size of 250 and 200 μm respectively. The resulting data are semi-quantitative, but produce relative down-core fluctuations in element composition reported in counts per second (cps). Additionally, quantitative abundance of major elements was also determined using X-ray fluorescence spectroscopy (XRF). For this, 1 g powdered sample material was mixed together with 6 g Fluxama and 0.5 g nitrate ammonium and gradually heated and melted on 5 different burners. The resulting glass discs were analysed for quantitative chemical composition using PANalytical AXIOS Advanced analytical system. The water and CO_2 content were also calculated in order to determine the elemental percentages.

XRD: These investigations were carried out for event layers and distinct facies by selective sub sampling in the field and laboratory. The analyses were performed using Siemens D-500 X-ray diffractometer (Cu kα radiation, 40 kV, 30 mA and graphite

monochromator). Quantitative mineral contents of these samples have been calculated using BGMN/AUTOQUAN software.

3.3.3 Chronology

^{14}C dating

The chronology of Atargu lake sediments is based on ^{14}C dates on wood fragments (Bookhagen et al., 2005; Anoop et al., 2012).Additionally, organic fragments for radiocarbon dating were also collected from lake sediments located within the Mane landslide debris (samples MA-1, MA-2 and MA-3 in Table 3.2).Care was taken to ensure that the dated organic samples represented *in situ*, and not the post-depositionally emplaced samples, as our field observations (in years 2007, 2008 and 2009) indicate rapid secondary thick carbonate crust (10-15 cm) formation on the surface of the lake outcrops. These thick crusts often contain reworked organic material that can give incorrect ages. Therefore, we have collected wood samples from different stratigraphic horizons after a thorough cleaning of the outcrop (removal of ca. 10-15 cm of surface carbonate crust). We have focussed on samples that were deeply embedded (after outcrop surface cleaning), parallel to the laminations, and avoided samples from the events layers that could possibly represent older reworked material. The ^{14}C measurements of the wood samples were performed in Poznan laboratory, Poland (Table 3.2). The age-depth model for the lake sediments (Fig. 3.3) was constructed using the depositional model technique in OxCal for the determination of outliers in the sequence (Ramsey, 2008, 2009).

All the ^{14}C ages discussed in the text were calibrated using the OxCal 4.1 software (Bronk Ramsey, 2008, 2009) using the IntCal09 calibration data set (Reimer et al., 2009) and are referred to as cal yr BP. The studies reviewed in this paper include U/Th (Fleitmann et al., 2003) and luminescence dating methods that yield ages in calendar years. These are referred to as ka.

Laminae counting

The lamina counting of the lake sediments is hampered by the presence of seismites, event (coarse sand and gravel) layers, and unlaminated clay sequences. However, the counting of couplets (comprising of coarse and fine sublaminae, see also Section 3.4.2) was performed for selected thin sections where the laminations are clearly visible. The counting of laminae and measurement of their thickness were carried out using block sample image scans and Zeiss Axiophot Microscope.

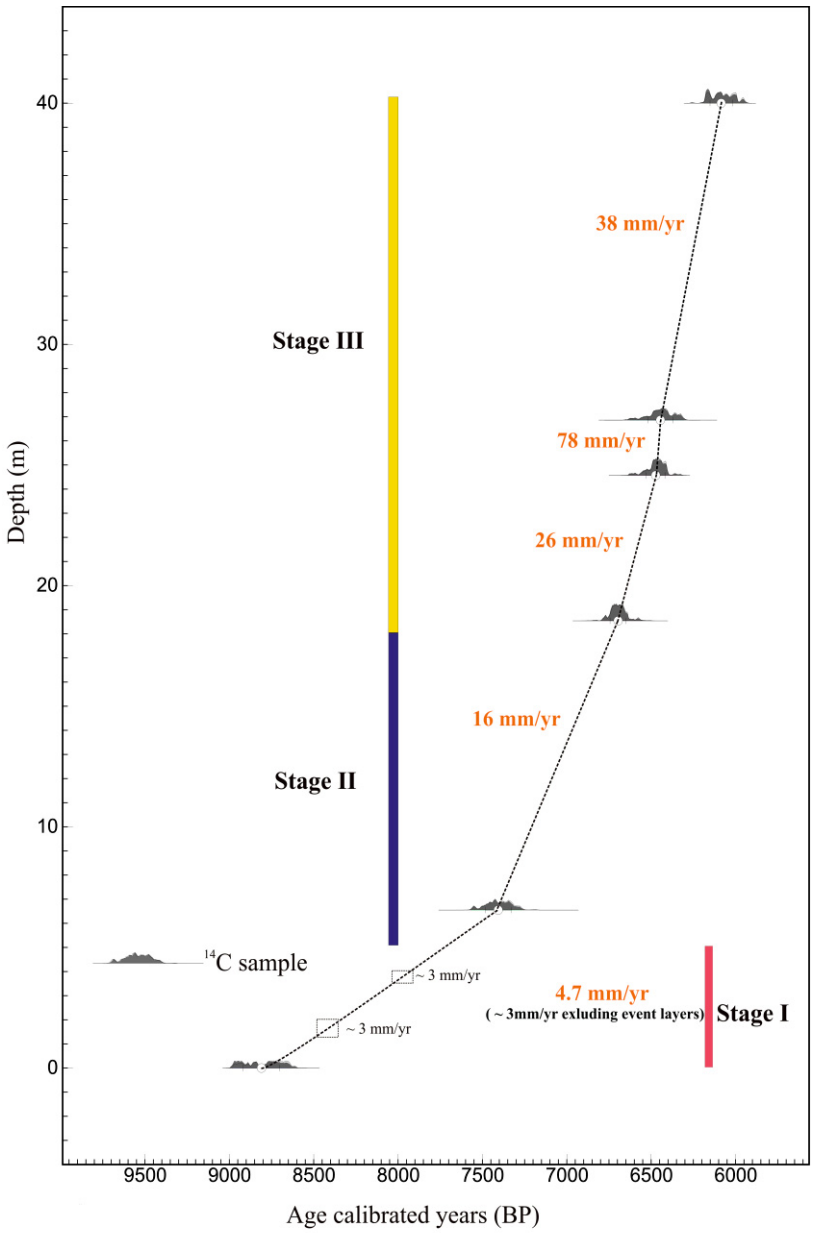

Fig. 3.3: *Age-depth plot based on the available ^{14}C dates from Atargu lake sediments. The calculated sedimentation rate shows a two fold increase between 18-41 m height of the lake sediment.*

3.4. Results

3.4.1. Modern sediments

Our observations and investigations on selected samples (M. Stebich, A. Bhattacharya, pers. comm.) indicated a complete absence of microfossils and scare, poorly preserved pollen.Previous work (Section 3.2.2) has shown that increased grain size and discharge rates are characteristic of stronger monsoon years (Sharma et al., 1991; Bookhagen et al., 2005).In this study we explore the potential of using mineralogical and geochemical indicators as environmental proxies.

The XRD investigations on the bulk modern surface sediments from the catchment area of Spiti River, upstream of Atargu, reveal that the main minerals in nearly all the samples are quartz, calcite, and illite. Minor minerals are albite, dolomite, clinochlore, muscovite, smectite, orthoclase and microcline (Fig. 3.4). The modern Spiti river sediment load shows largely the same mineralogical composition with high content of calcite (ca. 45%), quartz (18-32%) and illite/muscovite (9-22%). Minor minerals are dolomite, chlorite, albite and K-feldspars (2-6%each). Similar mineralogical percentages as in the Spiti River samples were determined for the Lingti and Shilla streams where the amount of calcite is about 55% and 46%, respectively. The right-bank tributaries Gyundi, Pin, and Rangrik nala show a slightly different pattern. In comparison to the Spiti sediment, the amount of calcite is significantly lower (Gyundi: 22%; Pin: 6%; Rangrik: 7%), whereas the amount of quartz (36, 33 and 49% respectively) and illite/muscovite (15, 33 and 37%) is higher (Fig. 3.4).

The quantitative XRF analyses of modern Spiti river bulk sediments shows high percentages of CaO (24-27 %) and SiO_2 (32-37 %). Similar results have also been observed from the left bank rivers with Shilla and Lingti showing high amount of CaO, 25% and 34% respectively. In contrast, the investigated right bank tributaries, Gyundi, Pin and Rangrik show lower percentages of CaO (14, 12 and 8% respectively) and very high percentages of SiO_2 (51, 61 and 71%). The results corroborate the semi-quantitative XRD analyses showing difference in contributions from left and right banks of the Spiti River.

Interestingly, the clay and coarser sand fraction collected from the Spiti river bed show different mineralogical proportions with higher calcite (45%) and quartz (32%) in the coarser fraction. In contrast, the clay fraction contains almost 15% less quartz, nearly the same percentage of calcite as compared to the modern sand, but more illite (24%) which is related to presence of shales in the catchment of left bank rivers.

We conclude that the mineralogy and geochemistry of modern sediments is governed by the petrology of the contributing catchment area and grain size of the sediment, and does not provide any direct palaeoenvironmental information.

3.4.2. Palaeolake sediments

The investigated outcrops near Atargu overlie Spiti bed load fluvial gravels, deposited prior to the damming of the river (Fig. 3.2b). A thin layer of slope debris deposited

subsequently is found on the top of most of the lake sediment outcrops. The investigated outcrops are located closer to the proximal part of the palaeolake (Fig. 3.2d) and consists mainly of alternating sand/silt to clay with thick coarse sand and gravel layers, whereas the sediments near the distal part (close to the landslide near Mane) comprise non laminated clay.

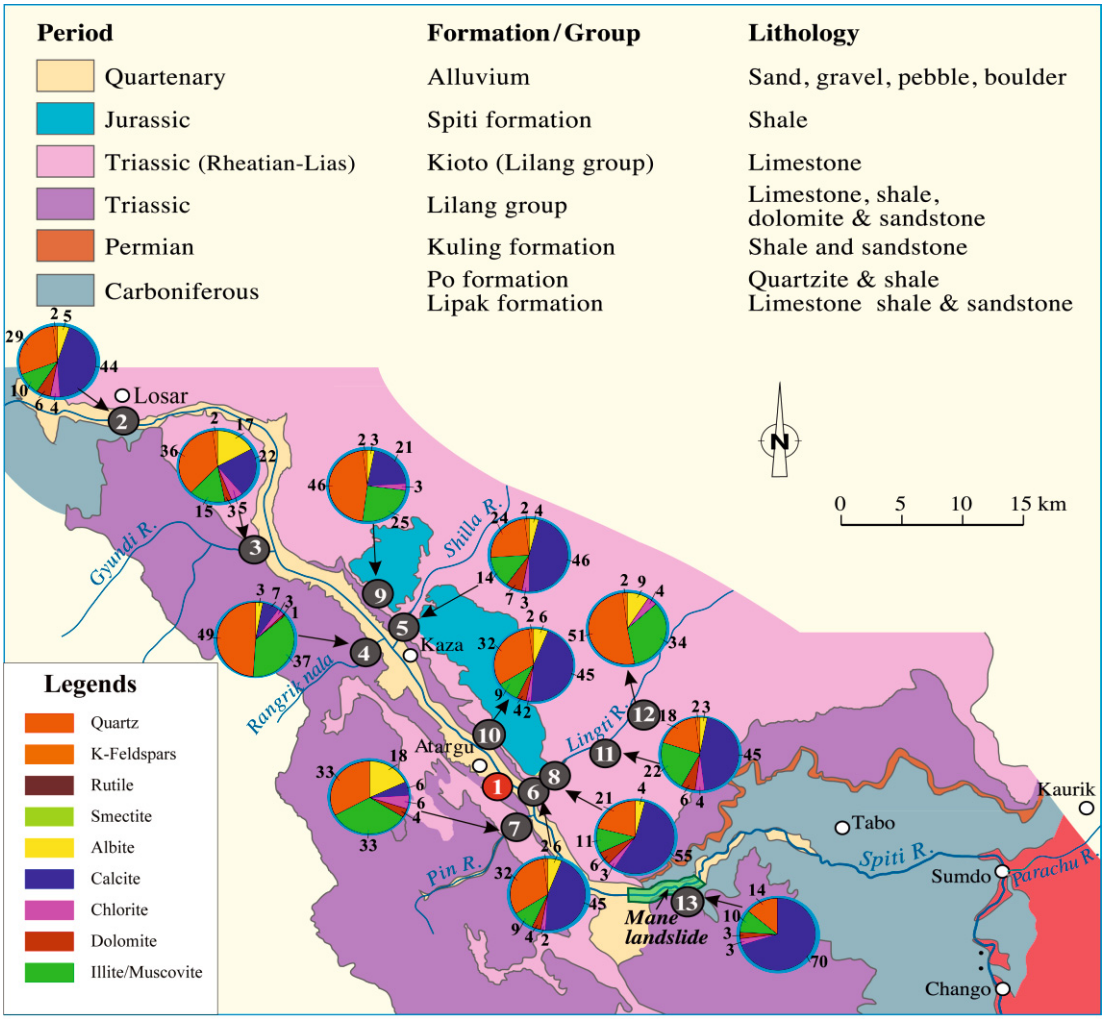

Fig. 3.4: *Semi-quantitative XRD results of the modern catchment area samples illustrated as pie charts (%): investigated palaeo outcrops (1); Spiti river near Losar (2); Gyundi river (3); Rangrik nala (4);Shilla river (5); Lingti river (6) (8) (11); Pin river (7);surface sediments near Kaza (9); Lidang (10); Rama(12); Mane landslide (13).*

Chronology

^{14}C dating: Our chronology of the Spiti palaeolake sediments is based on the ^{14}C dating of wood samples (8.7-6.1 cal ka, Bookhagen et al., 2005; Anoop et al., 2012).We have avoided dating bulk organic matter as the catchment area is dominated by limestone and there is possibility of hard water effect that can result in anomalously old dates (samples AT-7 and AT-8 in Table 3.2). Also, investigations on

luminescence dating (A. Murray, pers. comm.) reveal that the modern Spiti sediments have an apparent luminescence age of ≥2 ka. It remains a matter of speculation, and beyond the scope of this study, to determine if the residual luminescence amount has remained constant with time. In our view

the best way of obtaining a reliable chronology depends on the dating of well preserved terrestrial wood samples. The ^{14}C radiocarbon dates derived from our study (Table 3.2) are stratigraphically consistent and fit well with the previous ^{14}C age estimates from the region (Bookhagen et al., 2005).

Laminae counting: Thickness measurements on couplets were restricted to lower part of the lake sediments (0-6 m) where the sequence is well laminated. The calculated mean thickness for the couplets in these parts is ~3mm (Fig. 3.3). This agrees with the calculated mean sedimentation rate (excluding event layers e.g. sand, gravel) of ~3mm/yr for the lower part indicating the couplets to be clastic varves.

Table 3.2: AMS radiocarbon dates from the Mane palaeolake sediments.

No	Height (m) above base	Material	Lab number	Age (^{14}C BP)	Age (cal a BP) (1σ)
AT-1	40.9- 41[a]	wood fragment	n.a	5286 ± 35	6073 ± 66
AT-2	26.86 -26.88	wood fragment	Poz-33168	5650 ± 60	6436 ± 73
AT-3	24.57 -24.59	wood fragment	Poz-33167	5680 ± 40	6465 ± 53
AT-4	18.54 -18.55	wood fragment	Poz-33165	5870 ± 40	6691 ± 49
AT-5	6.55-6.57	wood fragment	Poz-33176	6490 ± 80	7397 ± 75
AT-6	0 - 0.1[a]	wood fragment	n.a	7926 ± 38	8781 ± 104
MA-1	12 (Top)	wood fragment	Poz-44128	5240 ± 40	6018 ± 74
MA-2	10.6	wood fragment	Poz-44127	5280± 60	6070 ± 82
MA-3	7.2	wood fragment	Poz-33173	5390 ± 40	6191 ± 72
AT-7	surface sample	modern root	Poz-22368	5790 ± 40	6588 ± 53
AT-8	10.8-11.2	bulk organic matter	Poz-22466	26260 ± 230	30905 ± 185

[a] denotes organic matter dates from previous work.

3.4.3. Lithostratigraphy

Our investigations of the lake outcrops reveal three dominant lithologies (Fig. 3.5), (i) laminated sediments (L), (ii) non laminated clays (NL), and (iii) event layers e.g., sand, dropstone, and gravel layers that occur preferentially in the previous two lithologies. Within the first two dominant lithologies (L and NL) we have identified different facies that are discussed in detail below. Soft deformation structures (fault grading stratigraphy, ball and pillow structures, contorted laminations, injection structures and diapiric flame intrusions) are also found within the lake sediments in

two zones (3-4.5 m and 6.5-7 m above the base) and are indicative of regional neotectonic activity (Anoop et al., 2012).

Laminated sediments (L):

Facies L_1: comprises of couplets, in which each couplet has a basal sublaminae of silt and sand (quartz and calcite dominated), and an upper silt/clay sub-laminae dominated by calcite and illite. Each couplet (2-4 mm thick) is separated from others by a sharp transition boundary (Fig. 3.6a). This microfacies indicates seasonality found in proglacial lakes (Leeman and Niessen, 1994) i.e. summer silt deposition (melting of glaciers) and winter (quiet-water) clay deposition. This facies is mostly found in the lower part (0-5m) of the lake sediments.

Facies L_2: These rythmites consist of a suite of multiple graded silt/sand sub-laminae (upto 6, each 5-20 mm thick) overlained by thick clay layer (Fig. 3.6b). The identified sublaminae show gradual transition boundaries. These rythmites are similar to those formed in a modern environment in a monsoon dominated high altitude region in Phewa tal, Nepal (Ross and Gilbert, 1999). We hypothesise that the L_2 sublaminae (graded sand/ silt) represent melt water/rainstorm summer events, and clay cap represents quiet winter event. These rythmites are mostly found in the upper part (18-41 m) of the lake sediments.

Facies L_3: This facies comprises of sequential deposition of sediments (Fig. 3.6c) with non laminated clay (A in Fig. 3.6c) overlain by graded sand/silt laminations characterised by sharp contacts (B in Fig. 3.6c). Above the graded laminations is cross laminated, fine to very fine sand with climbing ripple migration (C in Fig. 3.6c) and sharp (erosive) basal contacts. The cross laminated sand is finally overlain by interlaminated silts and mud layers (D in Fig. 3.6c). These characteristics appear in Bouma sequences (Leeder, 1999), suggesting intensified turbidity currents, as during periods of maximum discharge, (Gilbert, 1975; Sturm and Matter, 1978; Mulder et al., 1998). This facies is mostly found in the upper part (18-40 m, Fig. 3.5) of the lake sediments.

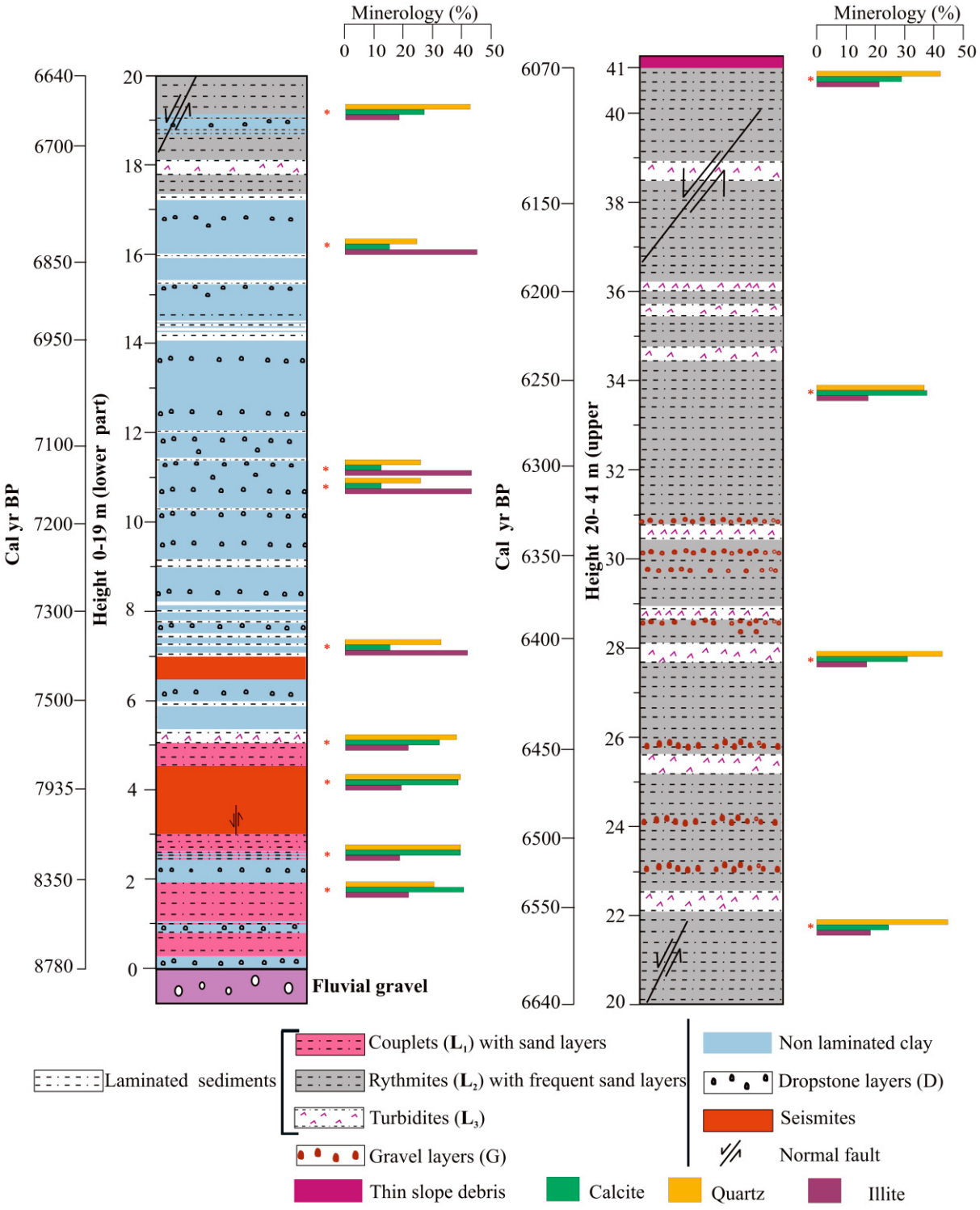

Fig. 3.5: *Detailed composite profile of 41 m thick Atargu sequence with identified lithofacies. Semi-quantitative XRD results on the selected outcrops samples are also shown. The geochemical variation noted within the outcrops is grain size dependent.*

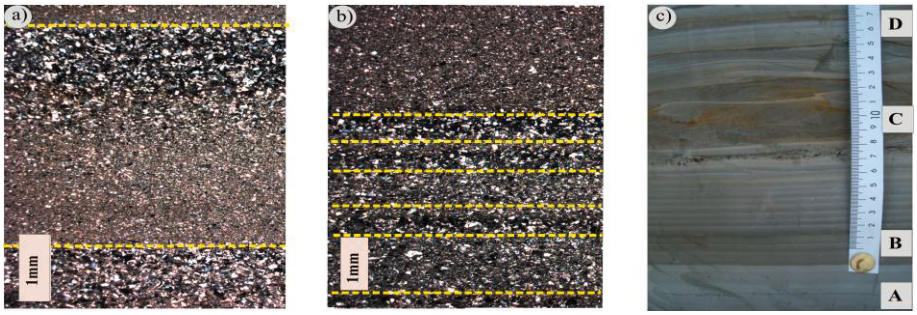

Fig. 3.6: *a) Thin section showing graded laminations with sharp gradational boundary; b) laminations with graded silt beds overlained by clay layer on the top; c) typical bouma sequence observed within the lake sediments; A) non-laminated clay; B) graded parallel laminations; C) cross laminated sand; D) laminated clay and silt.*

Non laminated clay (NL)

This section consists of homogenous fine clay with some intervening sub millimetre sand layers (Fig. 3.7a). The non laminated clay is mostly found in the lower part of the lake outcrops (below 18m) intervening between the dropstone layers. This lithology is indicative of low energy inflow and quiet sedimentation during which the fine sediment settles by suspension (Picard and High, 1972).

Fig. 3.7: *a) Dropstone layers within the lake sediment, note the bending of layers above and below dropstone layers ;b) non- laminated clay associated with dropstone layers indicative of quiet depositional environment in which particles settles mainly by suspension; c) laterally traceable dropstone layers (yellow dotted line) in clay matrix.*

Event layers

Sand layers (S): Poorly sorted sand layers, varying in thickness between 1mm to 10 cm, with sharp erosive upper and lower contacts, are found within the laminated sediments (Fig. 3.8a). Some of the sand layers display typical structures like current generated climbing ripple laminations, load cast structures, and pinch and swell structures. The sand layers with climbing ripple laminations are mostly associated with turbidity currents and are indicative of rapid deposition of an intrinsically brief and catastrophic nature (Fig. 3.8b, Walker, 1963; Allen, 1973). The load cast structure found are formed due to density heterogeneties and indicates fast sedimentation by high energy flows (Sen, 1980). We observe an abrupt increase in frequency of sand

layers within laminated sediments between (ca. 0-5m) and (ca. 18-41 m) height (Fig. 3.8c).

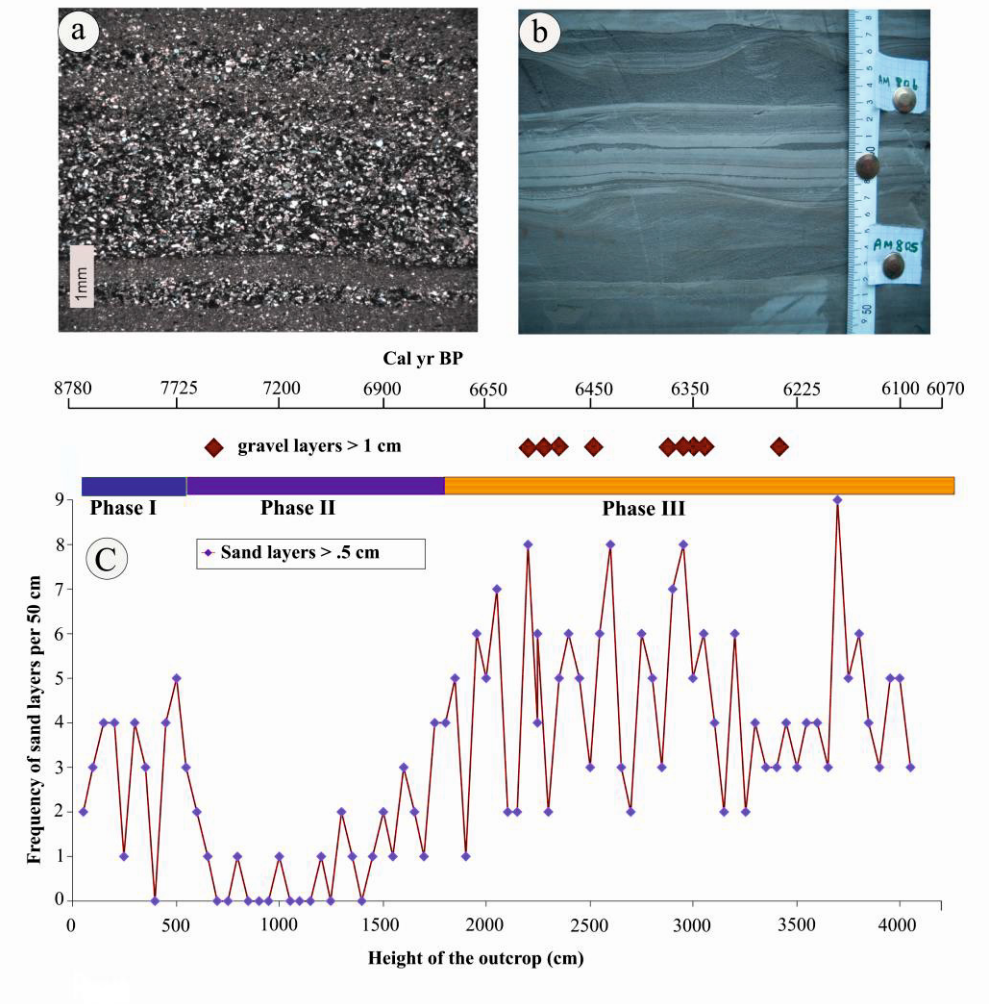

Fig. 3.8: *a) Thin section showing poorly graded sand layer; b) Cross ripple lamination found within the sand layer; c) Increase in the frequency of sand layers between 18-41m height of the outcrop.*

Gravel layers (G): The gravel layers occur between 22-34 m in the Atargu lacustrine profile. They are oxidised, poorly sorted, and have sizes ranging from sand to large boulders. They have a local origin as they cannot be traced over longer distances and appear to have formed as a product of colluvial processes that were deposited as debris cones or slope debris.

Dropstone layers (D): The dropstone layers are found at two intervals (0-3 m and 6-17 m above the base) within lake sediments. They are poorly sorted, mud supported and range from small pebble sized to big boulders (even greater than 20 cm) in size. They appear have settled gently (dropped from above, most likely from floating ice) on the laminated sediments that are deformed but not eroded. The stratum occurring

below the clast, and thus formed prior to the fall, is either bent downwards, penetrated or laterally rucked (Fig. 3.7b). The dropstone layers can be traced for longer distance within the outcrop eliminating the possibility of origin by local slope failure (Fig. 3.7c).

3.4.4. Geochemical analyses

The petrographic investigations and semi-quantitative XRF scanning of the selected palaeolake sediment blocks shows that the coarse grained layers are generally marked by sharp increase in the Si counts (Fig. 3.9). In contrast, the fine grained sublaminae and non laminated layers show higher Ca and K counts. The result is consistent with XRD data on modern sediments (Section 3.4.1) that show that coarser grain sizes are dominated by quartz whereas the finer fraction is marked by an increase in illite and calcite. This result has been further corroborated by the semi quantitative XRD investigations of distinct marker sand layers showing high percentages (30-40 %) of SiO_2 when compared to the clay layers (0-15 %).

Similarly, bulk XRD analyses from the different facies of the lake outcrop also indicated grain size dependency of mineralogical data: the lower (0-5m height) and upper part (18-41m) with more sand layers is dominated by quartz and calcite (80 % of the total sediment), whereas the middle stage (5-18m) comprises of dominant clay mineral (illite) with calcite and lower quartz amounts (Fig. 3.5). This difference can be attributed to the dominance of coarser grained event layers in the upper and lower part while the middle part encompasses mostly non laminated clay. Therefore, the geochemical variation within the lake sediment is grain size dependent and does not reveal any additional palaeoenvironmental information.

3.4.5. Palaeolake sediments within Mane landslide debris

These lake sediments (Fig. 3.2c) consist of 12m thick non- laminated dark brownish/buff coloured clay. The top of this sediment sequence was dated (sample MA-1 in Table 3.2) to 6020 cal yr BP. Since there are no visible lithological changes within this sequence we have used simple extrapolation to estimate a bottom age of ca. 6450 cal yr BP. The age of the Mane palaeolake sequence (6450- 6020 cal yr BP) indicates its deposition during the later stages of the lakes existence. The deposition of these sediments within the landslide debris is likely due to overflow from the lake upstream of the landslide debris.

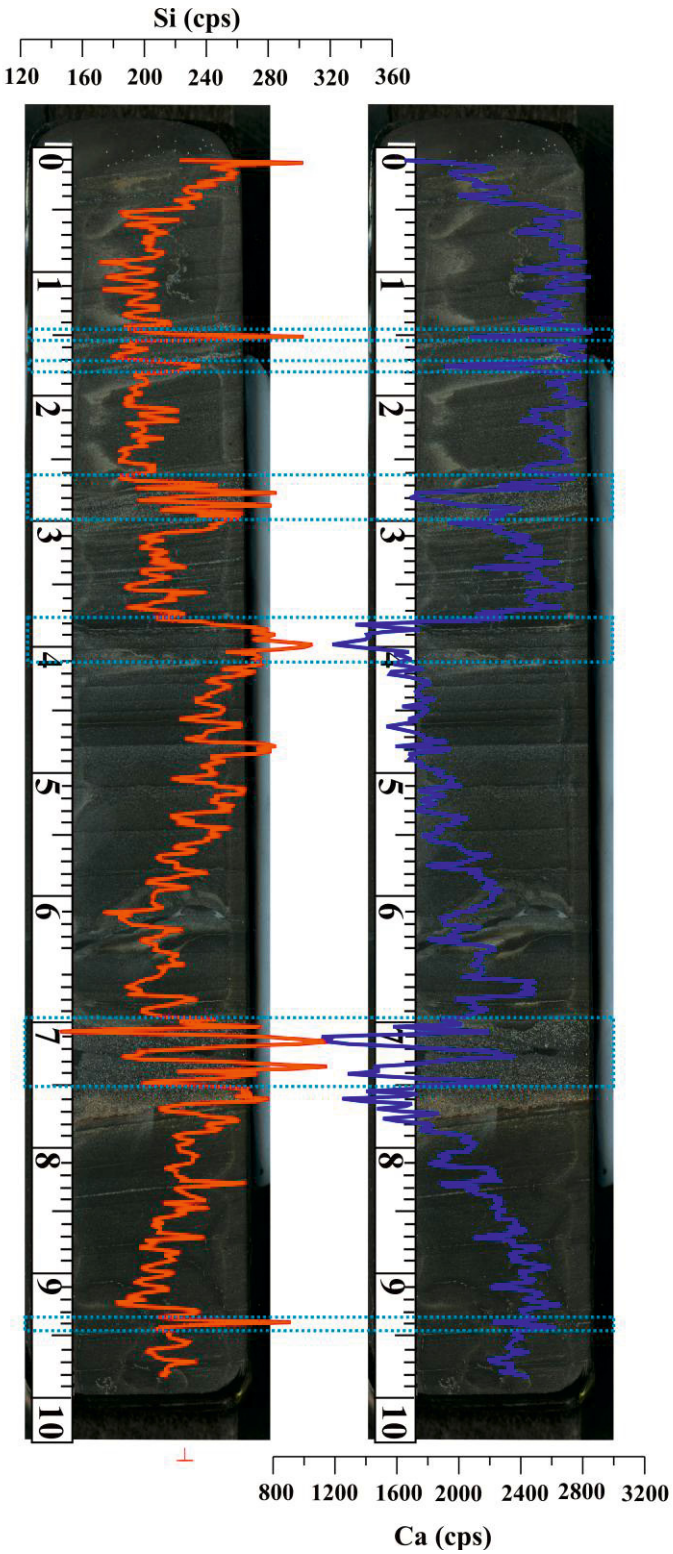

Fig. 3.9: *XRF counts for elements Si and Ca in palaeolake sediment blocks. Horizontal blue boxes indicate sand layers.*

3.5. Discussion

3.5.1. Lake evolution and inferred palaeoclimate

Based on the environmental conditions inferred from the lithology, we identify three stages during the lakes' existence: period of lake establishment (Stage I; 0-5m; shallow; 8.7-7.6 cal ka); deepwater lake with cooler climate conditions and weaker monsoon (Stage II; 5-18m; 7.6-6.8 cal ka) deepwater lake with high energy deposits; warm climate with increased monsoon influence (Stage III; 18-41m; 6.8-6.1 cal ka).

In the following interpretation we have considered dropstone layers as indicators of cooler temperatures; non-laminated clay layers as indicative of deposition under calm water conditions; sand and gravel layers, as well as rythmites and turbidites as indicative of intensified erosion during stronger ISM.

Stage I: Period of lake establishment (0-5m; 8.7-7.6 cal ka)

This interval was marked by the transition from fluvial environment to lacustrine facies. The frequent occurrence of sand layers, fluvial gravels, with intervening laminated sediments and clay (Fig. 3.5 and 3.8c) indicates a shallow lake level with proximity to the inflow. We infer this period to be the indicative of early stages of lake establishment. The rate of sedimentation in this zone is the lowest (4.7 mm/y, including the event layers) in the whole sequence (Fig. 3.3). Lithofacies are mostly dominated by couplets (L_1) characteristic of proglacial clastic varves. Interestingly, thin horizons of dropstone layers are found at different levels (8.7 and 8.4-8.2 cal ka) indicating short term cooler climate conditions.

Stage II: Cooler climate conditions with weaker monsoon (5-18m; 7.6-6.8 cal ka)

This stage is characterised by a nearly threefold increase (16 mm/y) in the sedimentation rate as compared to the first stage, a decrease in the overall grain size, and an absence of indicators of high energy inflow (e.g. sand and gravel) (Fig. 3.3). Sediments are dominated by non-laminated clays indicating deposition under quiet, deep water conditions. The frequent occurrence of dropstones between 9.5-12.5m (7.2-6.9 cal ka) is indicative of extended cooler conditions.

Stage III: Warm climate with increased monsoon influence (18-41m, 6.8-6.1 cal ka)

This stage is characterised by a dramatic increase in sedimentation rate - average is between 26-38 mm/y but rate as high as 72 mm/yr (including event layers) is noticed between 24-26 m height (Fig. 3.3). This part is dominated by rythmites with frequent

sand layers (S), rythmites (L_2), turbidites (L_3) and gravel layers (G) (Fig. 3.5 and 3.8c). Absence of dropstone layers indicates a shift from cooler to warmer conditions. The nearly threefold increase in the sedimentation rate, as compared to Stage II, indicates higher discharge of coarser sediments into the lake. An increase in coarser fraction in to the lake can be due to two possible scenarios; (i) lowering of lake level (proximity of the shore line); (ii) increased erosion from intensified monsoon. The overflow and deposition of lake sediments (ca. 6-6.4 cal ka) within the landslide debris would tend to support the second scenario. Additionally, the facies (e.g., turbidites) identified in this part (18-41 m) provide evidence for rapid deposition events, enhanced erosion and basin denudation associated with occurrences of rainstorms (extreme monsoon events**)** in this type of environmental setting (Sharma et al., 1991; Wulf et al., 2010).

3.5.2. Regional comparison of climate data

Our record from Spiti palaeolake sediments indicates two major climate periods: with weaker (7.6-6.8 cal ka) and enhanced monsoon (6.8-6 cal ka) with shorter cooler events at (8.7, 8.4-8.2 cal ka). We have undertaken a regional comparison of palaeoclimate records to obtain "snapshots" that can provide information about spatial extent of monsoon and westerlies during these periods. We also discuss the teleconnections that can cause such changes.

A strengthening of the ISM during the early Holocene resulting from enhanced summer insolation has been inferred from various proxy records (Gasse et al., 1996; Fleitmann et al., 2003; Gupta et al., 2003). However, recent studies, especially from the Himalayas and Tibetan plateau point towards a more complex regional pattern of precipitation changes during the early-mid Holocene (An et al., 2000; Prasad and Enzel, 2006; Chen et al., 2008). This variability can be interpreted in terms of spatiotemporal variation of South Asian monsoon in summer and the mid-latitude westerlies in winter in the Himalayan and Tibetan region. Due to this spatial inhomogeneity in the normal monsoon pattern, for comparison of our climate data we have focused largely on records (e.g., Demske et al., 2009) close to our study area and having a similar climate regime. To obtain "snapshots" of selected time slices, we have considered additional records from the wider Asian monsoon domain (Fig. 3.11).

A regional overview indicates that the dramatic intensification of the Asian summer monsoon began around 11.5 cal ka in response to the increase in the summer insolation (Morill et al., 2003).After an initial phase of strengthening (~11-9 cal ka), a

period of weaker monsoon and cooler climate is observed in the Himalayas and Tibetan Plateau during 9-8 cal ka (Van Campo and Gasse, 1993; Gasse et al., 1996; Yao et al., 1997; Demske et al., 2009) that is possibly correlatable with the well known "8.2 ka event" (O'Brien et al., 1995; Alley et al., 1997; Bond et al., 1997, Stager and Mayewski, 1997; Prasad et al., 2009). Several recent publications (e.g., Wang et al., 2002; Mischke and Zhang, 2010; Kotlia et al., 2010) have addressed the regional impact of the 8.2 cal ka event in the Himalayas. The dropstone layers found at ~8.7 and 8.4-8.2 cal ka within varved sediments (Stage I) indicate short periods of cooler climate. We propose that either (i) the 8.2 ka cold event began earlier and lasted longer in Himalayas, in agreement with recent studies that suggest that the 8.2 ka event is superimposed on a longer cooling event that began much earlier ca. 8.6 cal ka (Rohling and Pälike, 2005; Ellison et al., 2006), or (ii) the cooling at 8.7 cal ka in the Mane palaeolake record and other NW Himalayan sites (see below) is a regional climate signal.

The non-laminated clay and dropstones, with infrequent sand layers, observed during Stage II indicate cooler climate with weaker ISM in the Spiti valley between 7.6-6.8 cal ka. This inference is in agreement with a number of lake records from Tibetan and Himalayan plateau (Phadtare, 2000; Hong et al., 2003; Herzschuh et al., 2006; Demske et al., 2009; Mischke and Zhang, 2010). Coeval stronger westerlies have been observed in the palaeo records from the Himalayan region (Herzschuh, 2006, Demske et al., 2009) (Fig. 3.10b and c). Since westerlies bring precipitation in the form of snow in high altitudes, stronger westerlies would result in increased snow cover in Spiti region during this interval. This is further supported by dated moraines from the Spiti valley which yielded an age of 7.0±0.7 ka (Scherler et al., 2010). Regional comparison of glacier dynamics during the early Holocene from the Himalayan region also indicates advances/standstill during 8.2-7 ka (Appendix A_4). Sites farther south however, show moderate monsoon precipitation (Fleitmann et al. 2003; Prasad and Enzel; 2006) (Fig. 3.11e and f). The spatial precipitation pattern resembles that during "normal" ISM with decreasing moisture/precipitation to the north/north west.

The succeeding Stage III (ca. 6.8-6.1 cal ka) in the Spiti region shows a shift from cooler to warmer climate with intensified ISM, as evidenced by an increased frequency of occurrence of sand layers. Palynological evidence from the Tso kar basin (Demske et al., 2009) also provides evidence of the second Holocene humid phase

during 6.8–5 cal ka, related to resumed ISM (Fig. 3.10b). Warmer climate and increased precipitation during ca. 7.2–6.1 cal kais also reported from the monsoon dominated Garhwal Himalayas (Phadtare 2000, Fig. 3.10d). However, with the exception of Spiti, the other archives lack proxies for identifying abnormal monsoon years (extreme events). Interestingly the sites to the south show higher spatial climate variability; stalagmite data from Oman (Fleitmann et al., 2007), central (Quamar and Chauhan, 2012) and eastern India (Ponton et al., 2012) show a weaker monsoon, but lakes from NW India indicate increased westerly precipitation (Enzel et al., 1999; Prasad and Enzel, 2006).

3.5.3. Possible causes of changing seasonality during early- mid Holocene

From Stage II to Stage III there is an apparently abrupt (within decades) shift in seasonality to a stronger ISM and weaker westerlies in NW Himalayas. In central India there is a strengthening in ISM, weakening over the Arabian peninsula, but an increase in westerlies activity in NW India (Fig. 3.11). Although the regional overview of precipitation pattern (Fig. 3.11) bears some resemblance with the modern day "break monsoon" conditions in terms of positive rainfall anomalies over NW Himalayas (Krishnan et al., 2009), central India shows moister climate (Quamar and Chauhan, 2012) which does not fit into the overview. We note that this lake sediment record has few dates (5 for the whole Holocene) and the conclusions are based only on pollen data and need to be confirmed from additional sites/proxies in central India. Assuming that our inference of "break monsoon like" conditions, based on other sites, is correct then such conditions appears to have persisted for several centuries (6.8-6.1 cal ka) similar to that reported during the last millennium (Sinha et al., 2011). Stage III was coincidentally also characterised by lower solar insolation (Stuiver, 1998) although it is unclear if the switch is caused by a non-linear response to external forcing or internal forcing mechanisms. These ideas need to be confirmed by additional palaeodata and tested by palaeoclimate models to infer the triggering mechanism.

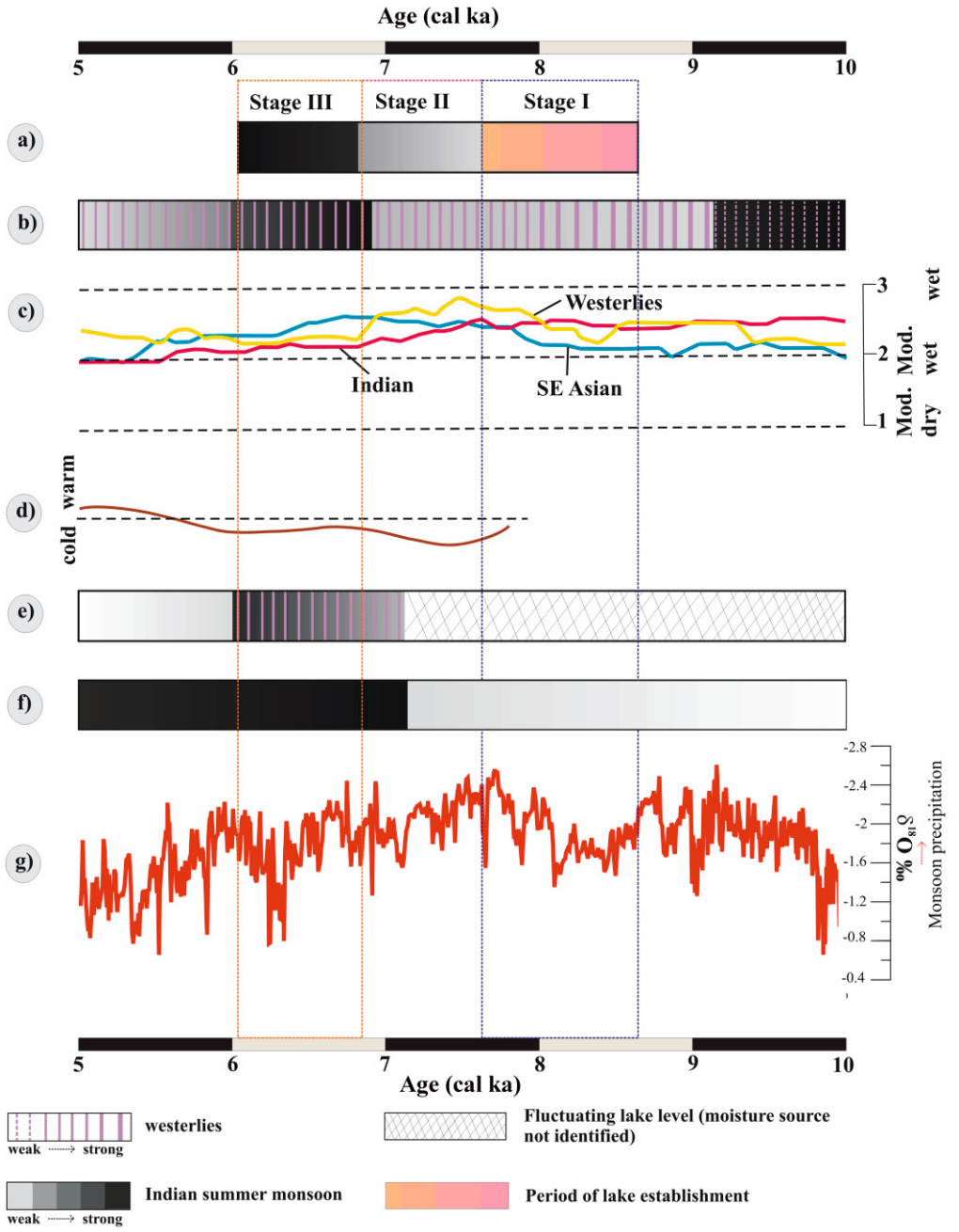

Fig.3.10: *Early-mid Holocene climate variability a) this study; b) pollen based climate information from Tso Kar lake, Ladakh, NW Himalayas (Demske et al., 2009); c)Holocene effective moisture over monsoonal Asia, inferred from the palaeoclimate records (Herzschuh, 2006); d) compilation of the climate variability inferred from NW Indian lakes (Prasad and Enzel et al., 2006); e) pollen based climate information from Din dad peat beds (Phadtare, 2000); f) pollen based climate information from Nitaya lake (Quamar and Chauhan, 2012); g) $\delta^{18}O$ stalagmite data from southern Oman (Fleitmann et al., 2003).*

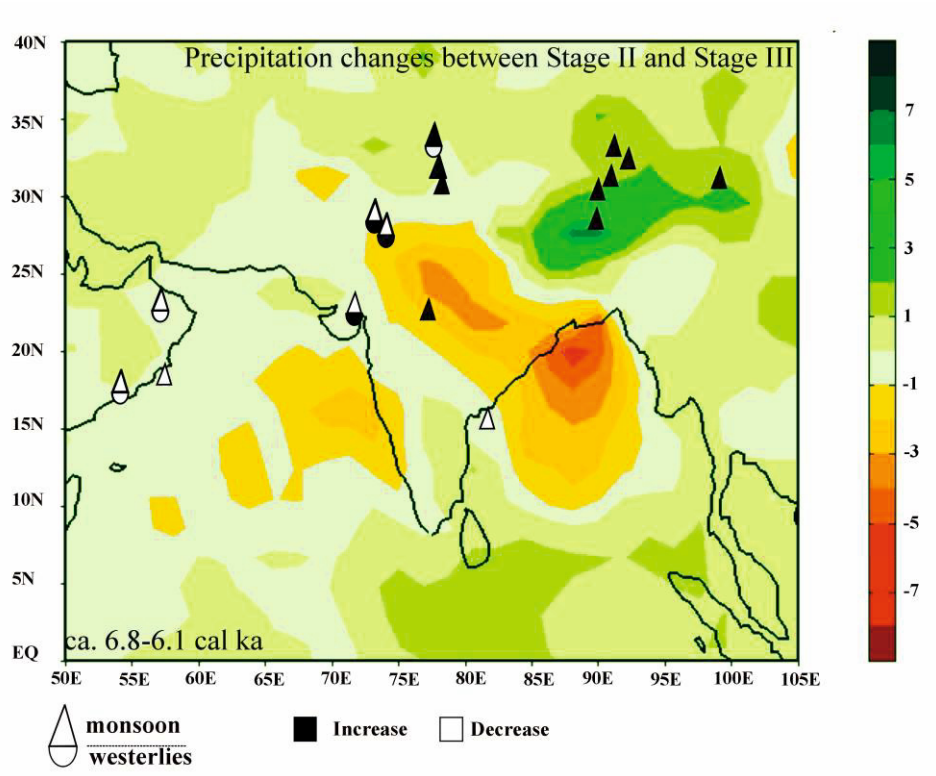

Fig. 3.11: *Spatial distribution of precipitation pattern from palaeorecords during 6.8-6.1 cal yr BP. The precipitation pattern has been superimposed on the modern spatial anomaly pattern estimated from NCEP re-analysis data during the break (b) monsoon.*

3.6. Conclusions

The investigation of palaeo lake sediments from upper Spiti valley reveals precipitation variability and changes in the moisture sources during the early-mid Holocene (8.7-6.1 cal ka). Based on the inferred environmental conditions from the lithology, we have identified three different stages: (i) Stage I (8.7-7.6 cal ka): period of lake establishment with colder intervals ca ~ 8.7 cal ka and between 8.4-8.2 cal ka; (ii) cooler climate conditions with stronger westerlies and weaker monsoon (7.6-6.8 cal ka), also marked by regional glacier advance; (iii) warm climate with intensified ISM and intensified erosion (18-41m, 6.8-6.1 cal ka, Stage III). The spatial precipitation pattern in stage II resembles "normal" ISM with decreasing moisture/precipitation to the north/north west. The switch between Stages II and III occurred over a few decades. Regional climate during Stage III (6.8-6.1 cal ka) indicates a W-E contrast in moisture regimes in northern India with stronger westerlies in NW Indian and intensified monsoon in NW Himalayas. This precipitation pattern shift is similar to that observed during the "break monsoon like" conditions.

3.7. Acknowledgements

The funding for this research was provided by the German Research Council (DFG, Deutsche Forschungs Gemeinschaft) graduate school GK-1364.We are grateful to T. Longpo, B. Lal and T. Cherring for their invaluable help during the field work and Silke Gärber for her help with laboratory analysis. We also thank A. Brauer, H. Wulf, D. Scherler, N. Basavaiah, K. Deenadayalan and R. Singh for constructive discussions, and B.S Kotlia for introducing us to this interesting region. Thanks are also due to P. K Mishra and P. Priya for their help with designing the figures.

Environmental implications of surface sediments from the monsoonal Lonar Lake, Central India

*N. Basavaiah[1], M. Wiesner[2], **A. Anoop**[3*], P. Menzel[2], K. Deenadayalan[1], A. Brauer[3], B. Gaye[2], R. Naumann[3], N. Riedel[4], M. Stebich[4], S. Prasad[3]*

[1]Indian Institute of Geomagnetism, Navi Mumbai, India.
[2]Universität Hamburg, Institute of Biogeochemistry and Marine Chemistry, Hamburg, Germany.
[3]German Research Center for Geosciences, Telegrafenberg, Potsdam, Germany.
[*] DFG Graduate School 1364, University of Potsdam, Germany.
[4]Research Station for Quaternary Palaeontology, Weimar, Germany

In review: Quaternary Research

Abstract

We report the results of our investigations into surface and catchment area sediments from the monsoonal Lonar lake, central India. Our results indicate that the distribution of the sedimentological and geochemical parameters within the lake is a function of lake depth and shape, proximity to inflowing streams, catchment slopes that influence the erosional processes, and the authigenic processes operating within the lake. The lake is stratified with an anoxic bottom layer below 4 m depth. The organic matter in the shore sediments is largely contributed by the catchment plants. Magnetic parameters indicate that the level of magnetic alteration may be used as a tracer to identify detrital inputs to the oxic/suboxic shallow water sediments against extensively altered ferrimagnetic iron oxides to paramagnetic ilmenite and iron sulfides in anoxic deep-section. Based on the spatial distribution of grain size and geochemistry, in conjunction with hydrological data, it is possible to identify the following parameters as palaeoenvironmental indicators (proxy): (i) Al as a proxy for surficial catchment erosion, (ii) carbonates as a proxy for drier conditions, (iii) Mn/Fe (low) as an indicator for anoxia, (iv) sedimentological parameters as indicators of major direction and energy of detrital transport.

Keywords

Isotopes, Lonar lake, Modern surface sediments, Monsoon, Palaeoenvironmental proxies

4.1. Introduction

The modern climate in India is dominated by the Indian Summer Monsoon (ISM). The winds in summer, blowing from the Arabian Sea towards the Indian subcontinent, bring large amounts of rainfall to the country and are the driving force behind the largely agriculture dependent economy. Recent studies (Goswami et al., 2006) point to an increase in the frequency and magnitude of extreme monsoon rainfall events over India against the backdrop of rising global surface temperatures. Model simulations (Rajendran et al., 2008) indicate spatially heterogeneous increase in monsoon rainfall by the end of this century. However, both these studies are based on instrumental records covering only a few decades. For perceiving trends, linkages, causal mechanisms of long term ISM variability, long-term high resolution palaeoclimate records, especially from the "core monsoon" regions of central India (Gadgil, 2003) are crucial.

There is evidence of climate variability from central India (Ely et al., 1996), but no long palaeoclimate data – this is linked to the fact that most of this region is covered by the Deccan basalts (Fig. 4.1a) and lacks natural lakes, with the exception of Lonar crater that was formed by meteorite impact (Milton et al., 1975). In 2008 a Indo-German team raised a ca. 10m long composite core from the Lonar lake as part of an international effort to reconstruct Holocene monsoon variability in central India. There are no palaeoshorelines visible in the basaltic crater though salt crusts found on the temples built during the past millennium within the crater clearly indicate lake level changes. Also, till date no studies on modern lake sediments, with the objective of proxy identification, a prerequisite for palaeoclimate reconstruction, are available from central India. In this study we report the results of our investigations to identify environmentally sensitive parameters/proxies from the surface sediments from the Lonar lake. Towards this end we have (i) investigated the geochemistry and sedimentology of modern sediments (clastics, organics, and evaporites), (ii) characterised the sources and mapped the surficial distribution of measured parameters, and (iii) undertaken statistical analyses to explore the interrelationships between the measured parameters and identify their implications for environmental reconstruction. As Lonar is a closed basin with largely uniform catchment area geology (Deccan basalts) the methods and results of this study have implications for developing proxies in other lakes in similar settings.

4.2. Study Site

4.2.1. Geology and Geomorphology

Lonar lake occupies the floor of an impact crater that formed on the ~ 65 Ma old basalt flows of the Deccan Traps (Fig. 4.1a, Frederiksson et al., 1973; Milton et al., 1975). The crater is a near-circular depression (Fig. 4.1b) with a rim-to-rim diameter of 1880 m and an average depth of around 135 m from the rim crest to the lake level. The slopes of the inner rim wall are quite steep averaging 30° in the west and southwest and 15°–18° in the east. The rim crest rises about 30 m above the surrounding plains, due to uplift of the target layers and deposition of impact breccia. The Quaternary deposits covering the basalts subaerially consist of gravel to boulder talus which accumulated below the upper sparsely vegetated slopes of the inner crater. Lakeward the talus grades into a densely forested belt of undifferentiated debris flow and slopewash deposits consisting of a mixture of sand, gravel, and silt with occasional cobbles (this study).

In addition to ephemeral runoff during the southwest-monsoon, inflow to the lake is by three perennial streams which issue from the cliffs of the deep gully in the northeast (Dhara and Sitanahani) and from the foot of the eastern crater wall (Ramgaya) (Fig. 4.1b). Tritium dating (our unpublished data) indicated a modern to sub-modern age for the groundwater. This is consistent with the local observations that a succession of weaker than normal monsoon years results in partial or complete drying up of the lake. At present these streams do not discharge directly into the lake but are diverted toward the agricultural areas in the northeast for irrigation.

A network of rills and gullies cuts the walls of the depression due to inward erosion of the centripetal drainage of the crater. Modest gullying is developed on the southeastern and northwestern peripheries while in the northeast a deeply incised channel occurs (Dhara canyon, Fig. 4.1b). In the northeast, the outflow from the Dhara canyon has built an alluvial fan into the lake that is used for agriculture (Fig. 4.1c). Downfan the grain size distribution changes from sandy gravel to silty sands and laterally passes into muddy sand flat which stretches from the fan head to the eastern edge of the lake. The flat has a maximum width of about 30 m and is characterised by patches of efflorescent crusts or intrasediment growth of trona and very thin, brittle black veneers of desiccation-cracked, residual algal-bacterial biomass washed onto the shore or left behind when the lake water receded (this study). In the

west and south, where the steep shorelines prevent formation of sand flats, debris flow and slopewash deposits extend to the lake banks.

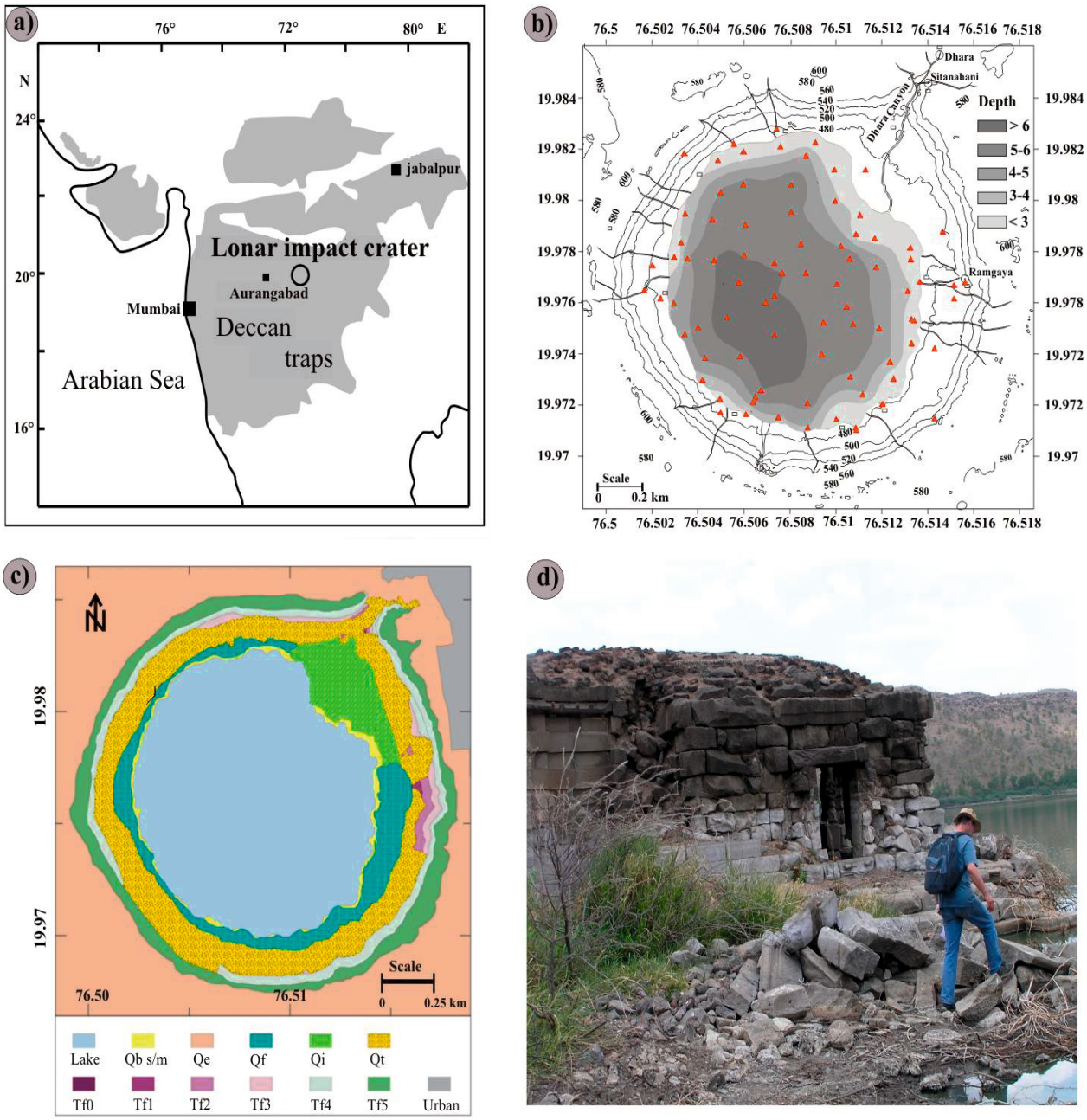

Fig. 4.1. *(a) Location of Lonar impact crater on the 65 Ma old Deccan Trap basalt (after Chakrabarti and Basu, 2006). (b) Bathymetry of Lonar lake and location of sampled points. (c) Geology of the Lonar crater (modified after Maloof et al., 2009). Q = Quaternary units, T = Tertiary units, Qb = beach, Qe = ejecta, Qf = forest, Qi = irrigated alluvial fan, Qt = talus. Tf0-Tf5 = basalt flows; (d) Precipitate of trona observed on a temple ruin at the eastern lake shore in 2008.*

4.2.2. Climate and Hydrology

In the Lonar region (central India), the wet and dry seasons of the monsoon system, along with the annual temperature fluctuations, produce three general climatic periods: (1) hot, wet weather from June to the end of September (southwest-monsoon) with an average rainfall of 680 mm and strong winds, (2) cool, dry weather from early October to February, and (3) hot, dry weather (though normally with high atmospheric humidity) from March to June. Temperatures during the pre-monsoon period are around 31°C, but may increase up to 45°C; southwest-monsoon and post-monsoon temperatures average 27°C and 23°C, respectively.

Data on the hydrochemistry of the feeder streams and on the thermohaline structure and circulation of the lake are sparse. Earlier accounts have reported that the spring waters are slightly alkaline (pH 7.5–10.5) and have HCO_3^-+CO_3^{2-}, Cl^- and Na^+ as the major ions. Ca, Mg, and SiO_2 are 1–2 orders of magnitude higher in the waters of the feeder springs than in the lake and the molar ratio of HCO_3^- to CO_3^{2-} is > 2 in the springs and < 2 in the lake - (Jhingran and Rao, 1958; Nandy and Deo, 1961; Venkatesh, 1967; Badve et al., 1993; Surakasi et al., 2007; Joshi et al., 2008). This groups Lonar lake into the Na-Cl-CO_3 subtype of saline lakes (Eugster and Hardie, 1978). The relatively high concentration of bicarbonate/carbonate and chlorine in the springs has been interpreted as indicating that the origin of the salts in the lake is due to the leaching from the country rock (Jhingran and Rao, 1958; Nandy and Deo, 1961).

Badve et al. (1993) and ECONET (1999) noted that the lake level changes have caused a massive tree die-off of mostly *Acacia nilotica* along the shore due to perpetual water logging. Furthermore, high lake level stands on top of the trend of rising lake waters are obvious from trona precipitates covering the walls of the shore temples (Fig. 4.1d) which are said to have been built in the 12th century (ECONET, 1999). At present the lake is hyposaline and had a maximum depth of ca. 6m (2008, this study); interseasonal lake level changes of up to 3m have been reported by Jha (2003). The lake has no outlet and underground springs feeding the lake have not been detected (Nandy and Deo, 1961).

The total phytoplankton biomass in the lake's epilimnion has been reported to vary widely between about 2000 to 300000 cells/ml (Satyanaraya and Chaudhari, 2007). Cyanophyceae dominate the algal assemblage (> 98%) followed by bacillariophyceae (largely pennate diatoms such as *Cymbella, Cocconeis, Nitzschia,* and *Navicula*) as well as

euglenophyceae and chlorophyceae (Badve et al., 1993; Malu, 2001; Satyanaraya and Chaudhari, 2007). Among the cyanophyceae the non-nitrogen-fixing, filamentous *Arthrothrix fusilini* (formerly *Spirulina platensis*) is the major species (Badve et al., 1993) which generates dense and locally surface-floating algal blooms. Also *Planktothrix agardhii* (formerly *Oscillatoria agardhii*) appears to dominate during some blooms. Zooplankton is dominated by rotifers (Malu, 2001). Higher trophic level organisms have not been reported except for the very rare occurrence of ostracods (*Cypris*) and gastropods (*Lymnaea*) (Badve et al., 1993); the lake is fishless. The microbial community other than cyanophyceae is highly diverse consisting of thermophilic, halophilic and alkalophilic bacteria which vary in numbers between 10^2 and 10^4 viable cells/ml (Joshi et al., 2005, 2007, 2008).

4.3. Materials and Methods

4.3.1. Collection of modern data and surface sediments

Hydrologic data of Lonar lake were obtained by a CTD sensor (EcoTec, YSI 6600V2-4-D) measuring temperature, pH value, salinity, and dissolved oxygen of the whole water column at 6 stations in February and May/June 2011. Meteorological data were acquired from the Indian Meteorological Department, Pune, and from the India Water Portal (http://indiawaterportal.org). Surface sediment samples from 68 locations covering the whole lake basin were collected in January 2007 and May 2008 using a Wildco Ponar type grab sampler with a maximum penetration depth of about 5–7 cm. Twenty eight samples were collected at different sites along the shoreline representing potential carbon sources such as soils, terrestrial plants and plankton to obtain information on the sources of the lake deposits (Fig. 4.1b).

4.3.2. Analytical methods

The analyses conducted on the sediments samples include total carbon, nitrogen, organic carbon, $^{13}C/^{12}C$, sulphur, lithogenics, grain size, abundance of major elements, and mineral magnetic parameters. The analytical methods for the different variables are described below.

Total carbon and nitrogen were measured on a Carlo Erba NA 1500 Elemental Analyzer; the standard deviation of the duplicate analyses was 0.15% for carbon and 0.005%

for nitrogen. Organic carbon analyses were performed on the same instrument after decarbonisation of the samples with 2N HCl^- the relative error of this method was ±5%. An empirical factor of 1.8 was used to convert organic carbon into total organic matter (Müller et al., 1986). Carbonate carbon was defined as the difference between total and organic carbon; the values were converted to calcite as this was the only carbonate phase detected in the surface sediments, both microscopically and by X-ray diffraction.

$^{13}C/^{12}C$ isotope ratios were determined using a Finnigan MAT 252 gas isotope mass spectrometer after high-temperature flash combustion in a Carlo Erba NA-2500 elemental analyzer at 1100°C. Values are expressed as $\delta^{13}C$ (‰) = $[(\delta_{sam} / \delta_{std}) - 1] \times 10^3$, where δ_{sam} = $^{13}C/^{12}C$ ratio of the sample, and δ_{std} = $^{13}C/^{12}C$ ratio of the reference standard PDB (PeeDee Formation Belemnite Limestone). Analytical precision was better than 0.1‰ based on replicate measurements of a reference standard; duplicate measurements of samples resulted in a mean deviation of 0.2 ‰. Total sulphur was analysed on a Woesthoff Casumat 8-Adge; the relative error was ± 5%.

The amount of lithogenic material was computed as the difference between the total sediment mass and the sum of carbonate, organic matter and amorphous silicate. Grain size of the lithogenic particles was measured on a Galai CIS-100 Laser Particle Sizer after stepwise removal of organic matter, carbonate and biogenic opal. Maximum clast and median grain sizes were calculated as ϕ_1 and ϕ_{50}, respectively; sorting was taken as $[(\phi_{84} - \phi_{16}) / 4] + [(\phi_{95} - \phi_5) / 6.6]$ (McManus, 1988). The standard deviation of the replicate analyses was ± 0.06 ϕ for the median diameter.

Quantitative abundance of the major elements (Si, Ca, Na, Al, Mn, Mg, Fe, Cl, and P) was determined by X-ray fluorescence spectroscopy (XRF). For this, 1 g powdered sample material was mixed together with 6 g Fluxama and 0.5 g nitrate ammonium and gradually heated and melted on 5 different burners. The resulting glass discs were analysed for quantitative chemical composition using PANalytical AXIOS Advanced analytical system. The water and CO_2 content were also calculated in order to determine the elemental percentages. X-ray diffraction technique was adopted for the determination of the minerals within the surface sediments. The analyses were performed using Siemens D-500 X-ray diffractometer (Cu kα radiation, 40 kV, 30 mA and graphite monochromator). Mineral composition within the surface sediments was additionally analysed with a Zeiss light microscope. The quantification of the different mineral phases was performed using the

MacDiff software following standard procedures (Chung, 1974). Replicate analyses indicated a precision of about ± 1% and in extreme cases, a precision of about 3%.

The measured magnetic parameters include magnetic susceptibility (χ) in a low AC magnetic field of 200 Am^{-1} and at a frequency of 976 Hz using an AGICO multi-function MFK1-FA, anhysteretic remanent magnetization (ARM) by superimposing a small 0.05 mT DC field onto a 100 mT peak alternating field, a stepwise acquisition of isothermal remanent magnetization (IRM) using a Molspin pulse magnetizer and hysteresis loops using a Molspin Nuvo vibrating sample magnetometer. ARM was expressed as χ_{ARM} after normalizing by the 50 μT direct bias field. The IRM obtained at 1 T was regarded as the saturation IRM (SIRM). All remanences were measured using a Molspin fluxgate magnetometer (noise level 2.5 x 10^{-5} Am^{-1}). Soft IRM (=SIRM – IRM_{-20mT}), Hard IRM (=SIRM – IRM_{-300mT}) and S-ratio (=IRM_{-300mT}/SIRM) were also calculated. The contributions of ferrimagnetic and paramagnetic minerals were obtained from the high field slope correction of hysteresis loops. The use of the mineral magnetic measurements as proxy parameters for climatic and environmental changes, is given in Basavaiah (2011) and Basavaiah and Khadkikar (2004).

4.3.3. Data analysis

Principal components analysis (PCA) was carried out to analyse the geochemical data by creating factors (new variables) which represent clusters of interrelated variables. PCA analysis is a multivariate method which can explain the major variations within the data set (Zhou et al., 2008). The analysis enables a reduction in data and description of complex system by means of small numbers of components (Loska and Wiechula, 2003; Wiechula et al., 2006). Each component is a weighted, linear combination of the original variables. PCA analysis was performed using XLSTAT, an add-in software package for Microsoft Excel (Addinsoft Corp.).

4.4. Results

4.4.1. CTD data

In contrast to 2008 when the water depth was 6m, the lake was shallower in 2011 with a maximum depth of about 5 m. The CTD measurements during February 2011 show that the water column was stratified comprising of a top oxygenated warm (~22°C) water layer,

ranging in thickness from 1.7–1.9 m in the shallow part and 1.9–2.3 m in the deeper part, with salinities between 8.0-8.2‰ and pH values of 10.3–10.4 (Fig. 4.2). The second (intermediate oxygen) layer extending down to about 4 m was characterised by strong oxygen depletion and slightly decreased temperatures (21.1–21.9°C). The salinities and pH values were almost in the same range as in the upper layer. At the five deeper stations a third layer was observed below 4 m. It was anoxic, had higher salinities (11.1–12.3‰), and lower pH values (9.5–9.8) compared to the water masses above. The temperature was slightly higher than in the intermediate water mass (21.5–21.9°C) (Fig. 4.2).

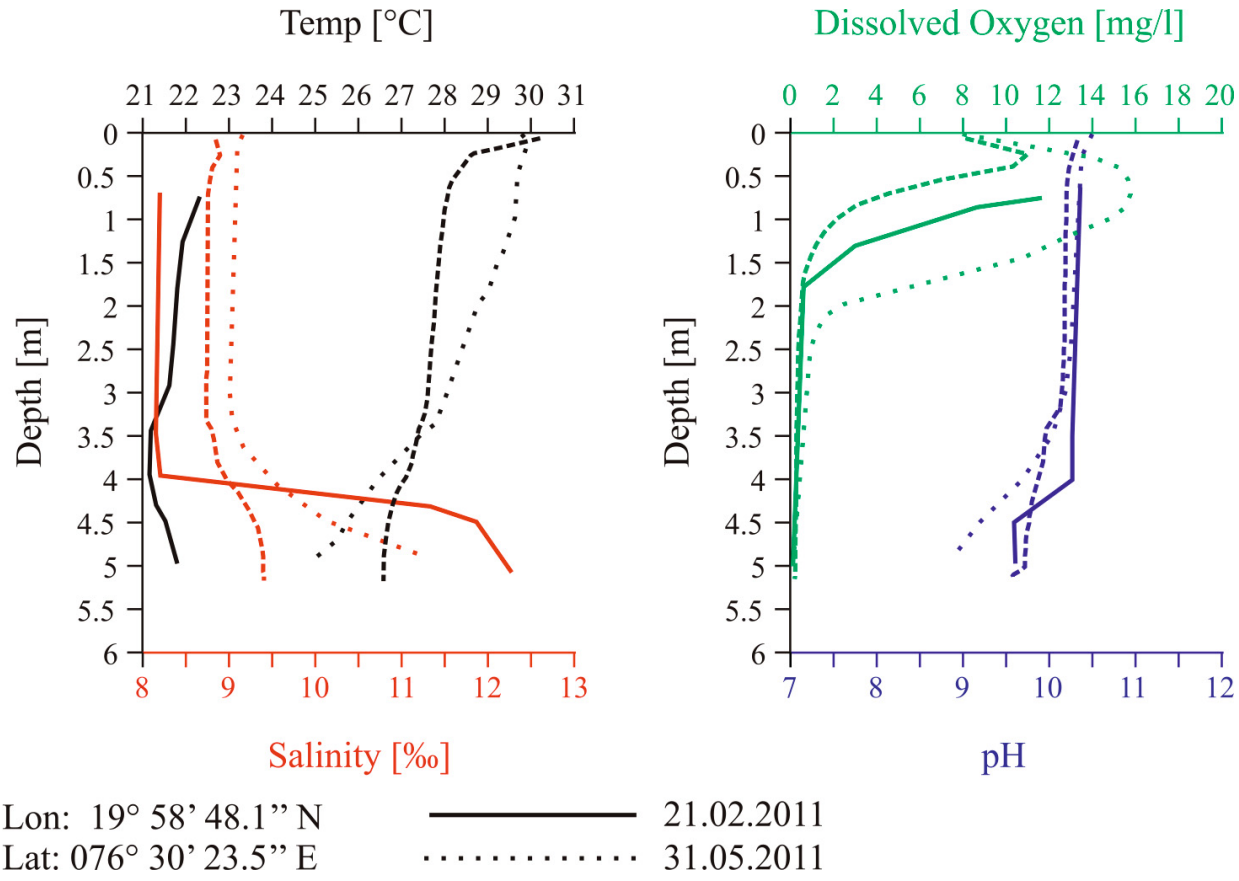

Fig. 4.2. *CTD water profiles from Lonar lake obtained in winter and late spring 2011. The lake is stratified and shows a halocline at about 4m depth. The upper layer can be divided into an oxygenated part (ca. 0-2m depth) and a sub- to anoxic part (ca. 2-4m depth).*

4.4.2. Sediment grain size

The predominant surface sediment type recovered within Lonar lake is soft to very soft homogenous mud with *in situ* colours ranging from greyish black (N 2) to olive-gray (5Y 4/2). Bottom fauna or bioturbational structures have not been observed. Fragments of higher plants (leaves and branches) were present in most of the samples, in particular from the northeastern part of the lake. Furthermore, unconsolidated clay pebbles (1–2 cm in diameter) were locally observed down to water depth of 4 m indicating alternating desiccation/cracking and erosion of mud on the lake banks during the hot dry and rainy seasons and rapid transport and rolling down by runoff. Lower lake level stands and evaporation are also indicated by the presence of whitish crusts of carbonate (< 2 mm) which were observed on top of the muds at depths between 1-4 m off the northern and eastern shore.

Lithogenic particles account for around 64% of the total sediment with the highest contributions occurring closer to the shore (65–75%) and lower values in the central part of the lake (50–55%) (Fig.4.3a). The average texture is 50.9 ± 11% sand, 48.9 ± 11% silt, and 0.2 ± 0.1% clay-sized particles which classifies the lithogenic fraction as silty sand (Shepard, 1954). Median grain sizes (Fig. 4.3b) of this fraction range from 4.5 to 2.5 φ (44–177 μm) with maximum clast sizes (Fig. 4.3c) attaining 0.6 to -0.4 φ (660–1320 μm).

4.4.3. Inorganic components

The minerals constituents identified within the sediment consist of both allochthonous and authigenic minerals. Allochthonous minerals include feldspars (albite and anorthite), zeolites and clay (smectite) minerals derived from the weathering of the catchment rocks. The authigenic mineral phase within the sediment comprises of carbonates (calcite) formed due to the processes within the lake. Interestingly, formation of carbonate efflorescent crusts with circular to elongate vugs containing crystals was noticed in year 1982 when the lake dried up completely. XRD analysis of these crusts (samples obtained from local villagers) revealed formation of monomineralic mineral, trona ($Na_3H(CO_3)_2 \cdot 2H_2O$) which precipitated directly from lake water as it became supersaturated because of evaporation. The precipitation of carbonate phase due to evaporative concentration can serve as a proxy for extremely dry conditions. However, microscopic and XRD studies detected calcite as the only carbonate phase found within the surface sediments.

In addition to the detrital and authigenic minerals, diagenetic (secondary) formation of halite is also detected in the surface sediments. Since the brine composition of the lake is of Na-Cl-CO_3 subtype, Na and Cl form the interstitial brine within the sediments. The Na measured in sediments is from the secondary halite that precipitates from the interstitial brine during the freeze-drying of the sediment samples for analytic measurements.

The major cation concentrations on the lake sediments shows the trend Fe > Ca > Al > Mg > Na. The spatial distribution of elements which represent the allochthonous fraction of lake sediments (e.g. Al) are not lake depth dependant but show high values towards the E and NW part of the lake (Fig. 4.4a). Interestingly, Ca distribution shows similar trend as detrital fraction (e.g. Al) with higher values in E and NW peripheries but is different in the deeper part of the lake (Fig. 4.4b). This is because the Ca concentration is contributed by $CaCO_3$ and also by other calcium bearing detrital minerals. Interestingly, the correlation coefficients between Ca with Al, and with $CaCO_3$ are -0.166 and 0.61 respectively (Appendix A_1) indicating that most of the Ca is derived from the carbonates. Since Ca is found only in stream inflow and not detected in lake waters (mss under preparation), we propose that Ca is rapidly precipitated in carbonate form during the seasonal summer evaporation. Therefore, Ca in sediments can, as a first approximation, be used as a proxy for amount of stream inflow.

Several elemental distributions are depth dependent. Sulphur and phosphorus concentrations increase with water depth (Figs. 4.4c and 4.4d); a similar relationship can be observed for Na (Fig. 4.4e). The calculated Mn/Fe ratio shows values decreasing from 0.018 to 0.014 towards the deeper part of the lake (Fig. 4.4f).

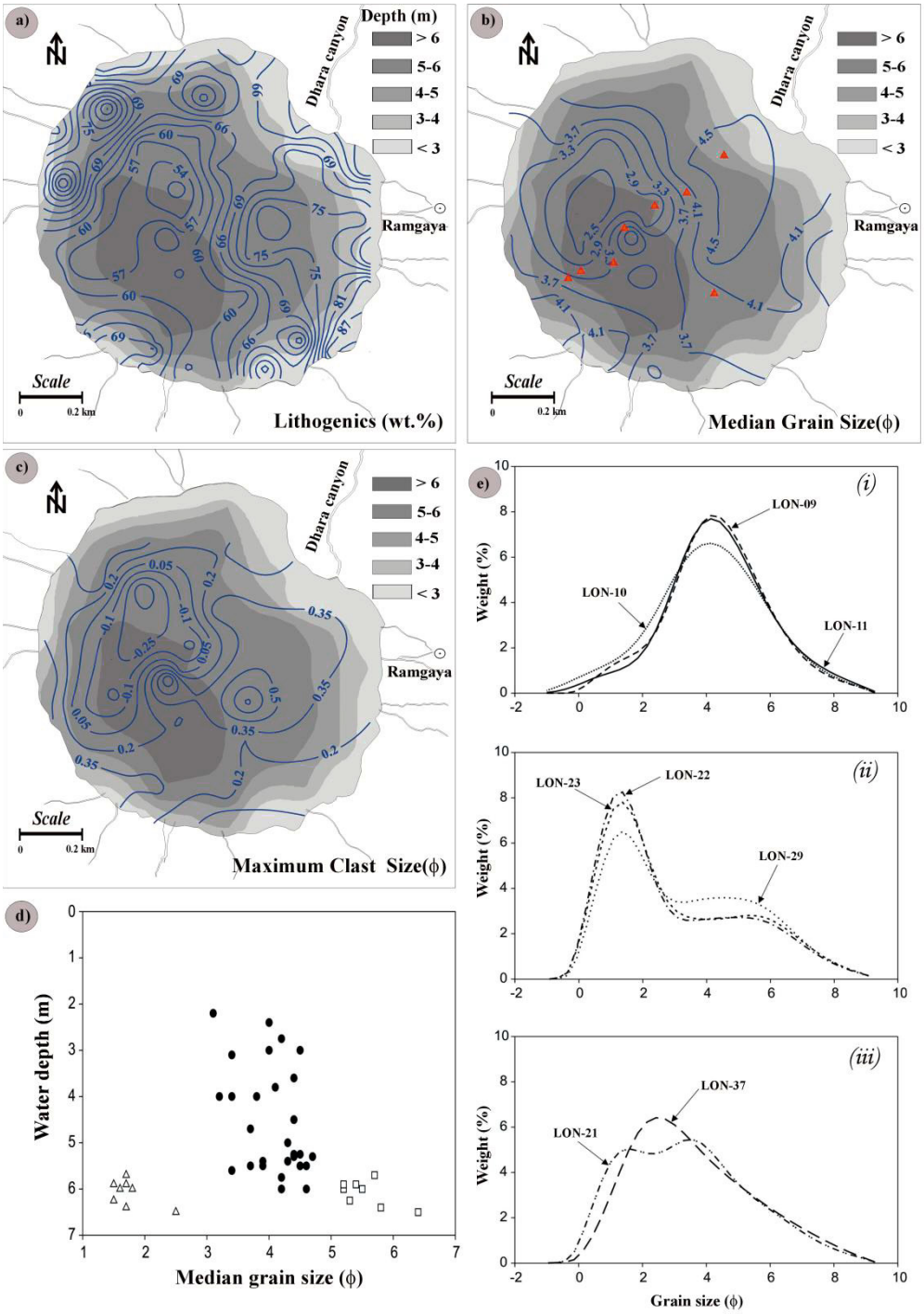

Fig. 4.3. *Distribution of a) lithogenics, b) median grain size, c) maximum clast size in surface sediments. (d) median grain size versus depth (filled circles showing unimodal grain size spectra, hollow triangles showing the coarse mode of bimodal grain size spectra, hollow squares showing the fine mode of bimodal grain size spectra. e) particle size spectra (i) unimodal grain size spectra from shallow stations in northeast Lonar lake, (ii) bimodal grain size spectra from stations in the centre of the lake, (iii) change from bimodal to unimodal grain size spectra towards the southwestern shore of the lake. See Fig. 4.3b for position of analysed sites.*

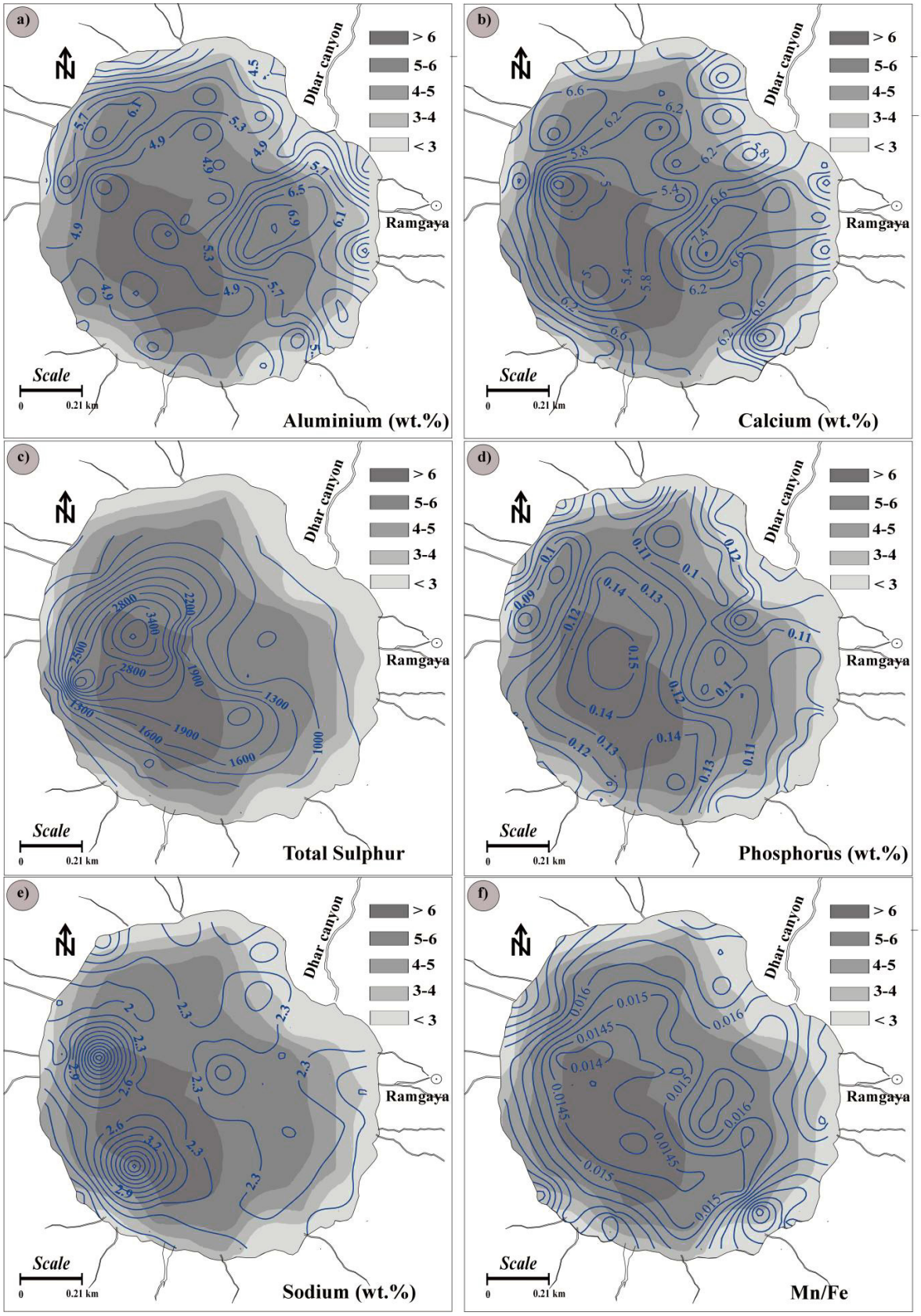

Fig.4. 4. *Major elemental concentrations in Lonar surface sediments.*

For interpreting the magnetic data we have divided the sediments into two groups: above 5m (shallow water, SW) and below 5m water depth (deep water, DW). Figs. 4.5a-d shows the spatial patterns within the lake with the maximum values for χ, S-ratio and SIRM/χ, tending to decrease away from the shore to deeper waters. The SIRM and percent of ferrimagnetic and paramagnetic minerals against water depth profiles are shown in Figs. 4.5e and 4.5f. Consistent with the inflows by the perennial streams from the north and east, the ESE-WNW trend is noted as the dominant magnetic trend of sedimentation at SWD, where relatively high values of χ, ARM, SIRM, S-ratios and SIRM/χ are observed (Figs. 4.5a-d). In SW, the magnetic mineralogy-dependent ratio SIRM/χ varies between 12 and 22 kAm^{-1} and the S-ratio values range between 0.98 to 1 (Figs. 4.5b and 4.5c). These values are consistent with a mixed assemblage containing magnetite and titanomagnetite (Peters and Thompson, 1998; Stoner and St-Onge, 2007). In DW, the χ values are extremely low, indicating fine-grained magnetic mineral phases as corroborated by relatively high χ_{ARM}/SIRM values. A decreased (increased) proportion of ferrimagnetic (paramagnetic) grains probably of diagenetic origin, is observed in DW (Figs. 4.5e and 4.5f), whereas S-ratio varies < 0.95, indicating hard phases of titanomagnetite and magnetite together with increase of paramagnetic grains (iron bearing clay minerals and pyrite) (Fig. 4.5f). According to Basavaiah (2011) and Basavaiah and Khadkikar, (2004), the very low magnitude of S-ratio variations suggests soils and sediments are derived from Deccan basalt, and the amount of magnetite in the samples depends on the degree of alteration of titanomagnetite. In summary, the distribution of magnetic mineralogy is bimodal, perhaps reflecting the presence of both primary (detrital) in shallow water deposits and secondary (diagenetic) minerals in deep-section.

4.4.4. Organic components

The amount of organic carbon (C_{org}) in the surface sediments varies between 0.16 and 6.28%, total nitrogen (N_{tot}) is in the range of 0.004 – 0.88%. Highest organic carbon values are found near the western shores (Fig. 4.6a). The C_{org}/N_{tot} (C/N) ratio of the surface sediment samples varies between 7.8 and 17.6. The peak values are present near the inflowing streams in the east and northeast, as well as in the west (Fig. 4.6b). The $\delta^{13}C$ values are between -23.1‰ and -16.2‰ with lowest values near the perennial streams in the east and highest values in the centre of the lake (Fig. 4.6c). Highest calculated organic matter content is found near the inflowing streams in the east (Fig. 4.6d).

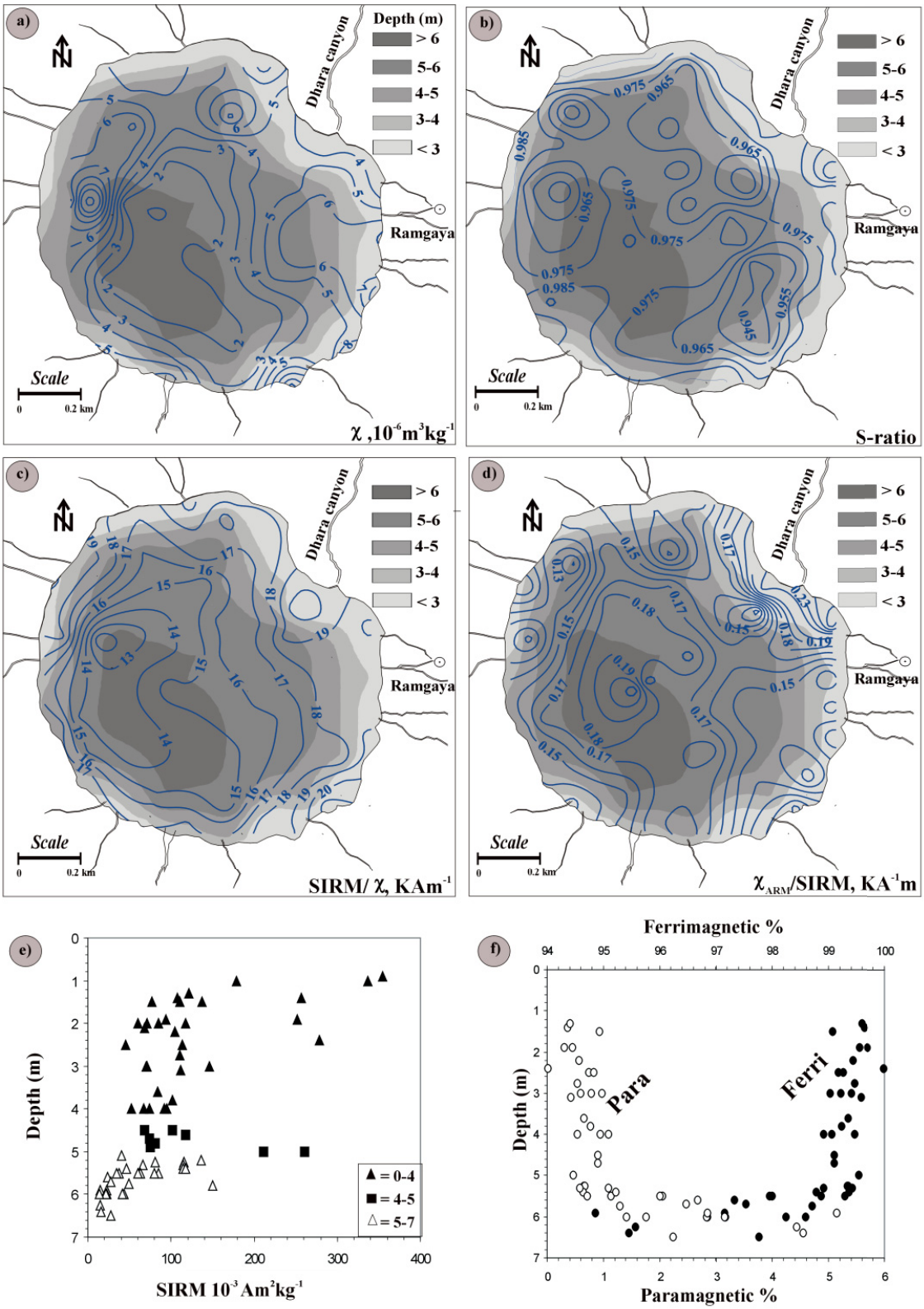

Fig. 4.5. *Spatial pattern of mineral magnetic parameters, a) magnetic susceptibility, b) S-ratio, c) SIRM/χ and d) χARM/SIRM. The variation of SIRM (e) and percentage of ferrimagnetic and paramagnetic (f) minerals against water depth.*

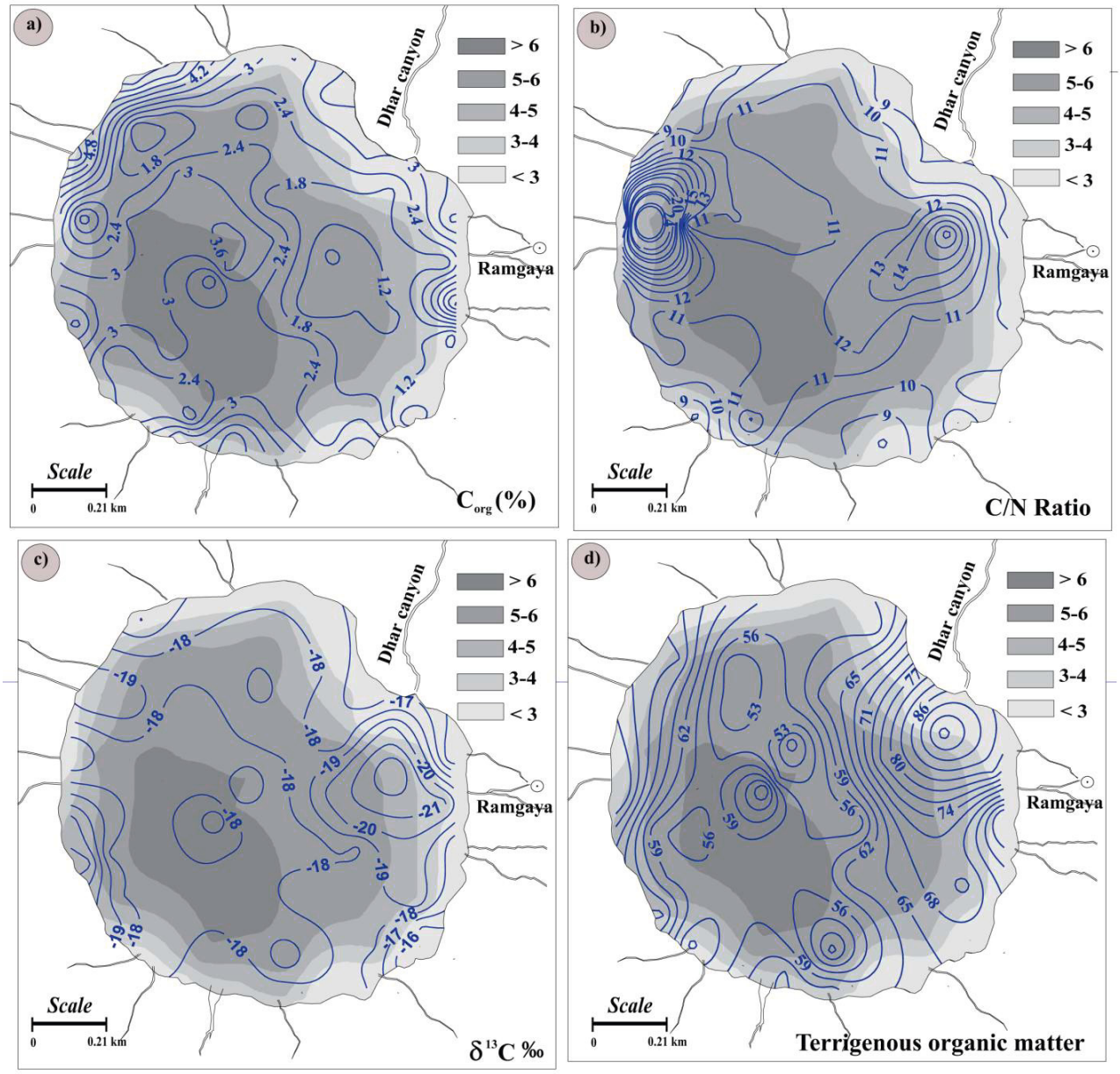

Fig. 4.6. *Distribution of phosphorus, Corg, C/N, δ13C, and terrigenous organic matter in Lonar lake sediments.*

4.5. Discussion

The distribution of the sedimentological and geochemical parameters within the Lonar lake is a function of lake depth and shape, proximity to inflowing streams, catchment slopes that influence the erosional processes, and the authigenic processes operating within the lake. The crater slopes are steepest in the west. The water depth is maximum in the southwest due to the direction of the meteor impact (Misra et al., 2010) - since the slope of the lake bed is determined by this impact direction, it is steepest in the southwest and west and less so in the northeast and east.

4.5.1. Hydrology

As there is no outflow from Lonar and only three minor groundwater fed streams, seasonal lake level changes are related to the regional climate patterns. During summer monsoon (June to September) the precipitation is very high and equals or even exceeds evapotranspiration. This leads to significant lake level rises for the period of summer monsoon accompanied by dilution imposed changes in chemical composition of the lake water (Badve et al., 1993). The stratification of Lonar lake indicates that dilution processes during the rainy season lower the salinity of the upper part of the water column generating a distinct stratification with highly saline bottom water. Throughout the rest of the year evapotranspiration is dominant. Within the dry season evaporation leads to increased salt concentration in the surface water and therefore weakens the stratification and supports complete overturn during spring to early summer. The salinities of bottom waters observed in February 2011 in this study are comparable to values of surface waters from April 2010 (S.Sarkar, Pers. Comm.). The relatively high temperatures of the February 2011 bottom water mass suggests that it may be fed by sinking surface waters becoming highly saline during the temperature and evaporation induced maximum prior to the SW monsoon. This leads to the assumption that deep mixing occurs once in a year or at least every couple of years while mixing of the upper and intermediate water layers observed within this study might take place in short intervals (daily-weekly-monthly). This groups Lonar lake into the warm monomictic lake type (Hutchinson and Löffler, 1956) with the overturn being induced by high salinity, and possibly aided by strong monsoon winds during this season.

As discussed earlier, the pH values of Lonar Lake water reported in the literature vary between 7.5-10.5. The pH values observed in this study (9.5–10.4) lie in the range mentioned above, and reveal seasonally driven differences between surface and deep water. The salinity related high pH of Lonar lake also causes a shift in the CO_2 (aq)-HCO_3^--CO_3^{2-} equilibrium towards HCO_3^- and CO_3^{2-} (Wetzel, 2001) diminishing the supply of carbon to plankton requiring CO_2(aq) for photosynthesis, and supporting the growth of plankton able to take up HCO_3^- as carbon source. In fact, the major phytoplankton species in Lonar Lake are *Arthrothrix fusilini* and *Planktothrix agardhii* (Badve et al., 1993) which are bicarbonate-using (Kaplan, 1981; Miller, 1990), non-nitrogen-fixing (Ciferri and Tiboni, 1985; Riddols, 1985) cyanophyceae.

4.5.2. Sediment grain size

In contrast to the classical model the coarsest sediments do not occur along the margins but in the central and western part of the lake. The particles size spectra (Fig. 4.3e) changes from unimodal distributions peaking at around 3–4.5 φ in the shallow portions in the northeast to bimodal, fine-tailed distributions in the lake centre with maxima at 1–2 and 5–6 φ; and further to the western and southwestern shoreline the patterns again become unimodal but coarse-grained with median values of 1.5 to 2.5 φ. However, when the fine mode median values of the bimodal distributions are plotted with those of the unimodal distributions, a trend of sediment fining with water depth is seen (Fig. 4.3d). We conclude that the lateral variations in grain size are due to two sources of the particles. In the northeast and east the broad and densely vegetated alluvial flats prevent the coarser grained particles from reaching the lake interior. In the west and southwest, the steeper cliffs, scarce vegetation, and limited alluvial area along the shore and steeper slope of the lake (Fig. 4.1b) provide the basis for high energy transport during seasonal flooding and down rushing of monsoon waters from the crater rim. This allows the coarse-grained material to be transported far into the lake. Further evidence that both near-shore and inner-lake particles have undergone short transport distances and rapid deposition is provided by the finding that the lithogenic particles are poorly to very poorly sorted (σ_1 = 1.56 – 2.29 φ; average = 1.86 φ).

4.5.3. Inorganic components

The spatial distribution patterns of geochemical elements in the Lonar lake can be attributed to the catchment erosion and the physical and chemical processes operating within the lake system: (i) the elements largely derived from detrital components (Al, Fig. 4.4a) do not show any distinct trend with depth but have relatively high values towards the shoreline. However, their high concentration towards the NW and eastern part can be attributed to the steeper crater slopes in the western part providing high energy transport of detrital material during seasonal monsoonal flooding, and to stream inflow in the eastern part; (ii) the Na and Cl form the interstitial brine within the lake sediments. Their increase with depth (Fig. 4.4e) indicates increased brine concentration towards the deeper part of the lake, attributable to less dilution in the deeper part due to their far distance from the perennial inflowing streams; (iii) sulphur contents within the sediment delineate (Fig. 4.4c) the water depth contours at the sampling sites with maxima below 4 m. In these anoxic sediments sulphur is probably enriched as sulphides. This supports the assumption that during most of the year that the deep (> 4 m

water depth) Lonar is almost permanently anoxic resulting in sulphate reduction in the upper centimetres of the sediments; (iv) the Mn/Fe ratio in lake sediments is commonly used as indicator for palaeo-redox conditions of the sediment-water interface at the time of deposition **(**Wersin et al., 1991). Low Mn/Fe ratios are mostly attributed to anoxic conditions. The negative correlation of Mn/Fe ratio with depth in the Lonar sediments indicates bottom anoxia in the Lonar lake (Fig. 4.4f). Correspondingly a high correlation (-0.8) also exists between sulphur and Mn/Fe; (v) the phosphorous in lake sediments could be adsorbed on clay minerals, iron and aluminium oxides, or the organic matter fraction. The strong positive correlation of P with organic matter and the negative correlation with Si, Fe, Al and Ca imply that phosphorous in Lonar lake sediments occurs largely as organic-P in authigenic organic matter (Appendix A_1). Therefore increase of phosphorus (Fig. 4.4d) can be attributed to enhanced productivity in the deeper part of the lake.

4.5.4. Magnetic parameters

In the sediments deposited at < 5 m water depth the magnetic assemblage of titanomagnetite, magnetite and hemoilmenite dominate with significant detrital input from the catchment, reflecting oxic-suboxic basin. The magnetic susceptibility is relatively lower in deep water sediments (ca. > 5 m), indicating the destruction of magnetic material and extra input of finer magnetic grain sizes under anoxic-sulfidic conditions – as discussed above the sulphur values are higher in deeper parts. Magnetic parameters can be used to identify the effects of processes such as allogenic, authigenesis and diagenesis into the Lonar lake.

4.5.5. Organic components

Lonar lake is highly eutrophic (hypertrophic) and covered with a thick algal mat during phytoplankton blooms (Badve et al., 1993). The sediments are, however, relatively low in total organic carbon (TOC) (0.1–6.3%; Ø = 2.6) compared to other eutrophic lakes which can have organic carbon contents between 4 and 8% in sediments (Choudhary et al., 2009; Meckler et al., 2004). This points to moderate to strong dilution by mineral matter. Increased soil erosion occurs during the ISM season when the monthly precipitation reaches 150–200 mm. The steep slopes of the inner rim support precipitation related erosion during the monsoon. Gullies and rills on the inner crater walls are evidences of seasonal erosive streams.

The TOC content in Lonar sediments is, generally, higher near the shoreline (Fig. 4.6a). Local nutrient sources around the lake, and macrophytes growing in the shallow parts, can

contribute to local productivity maxima. Macrophytes may also trap algal mats in near shore areas and augment the organic carbon sedimentation. C/N ratios can be used to identify, and through end-member mixing, may even be used to quantify organic matter sources. Algal mats and soil samples from the Lonar catchment have C/N ratios between 8 and 10 (Appendix A_2), typical for limnic plankton (Choudhary et al., 2009). Higher C/N ratios indicate input from land plants; two areas with such elevated C/N ratios are situated in the western part of the lake and off the Dhara river mouth (Fig. 4.6b). In the northeastern part of the lake the Dhara river most probably supplies this material whereas in the western part the source is not as obvious.

The maxima in C/N correspond with minima of $\delta^{13}C$ values of organic matter also indicate terrestrial input especially off the Dhara river. The reason for depleted $\delta^{13}C$ values of organic matter is the discrimination against ^{13}C during CO_2 uptake. This process is much stronger in C3 land plants such as the trees planted on the Dhara fan, than in C4 plants of which the majority are grasses (Farquhar, 1983). The C4 plants sampled in the Lonar catchment had $\delta^{13}C$ values around -13‰ whereas the C3 plants had a $\delta^{13}C$ average of -28‰. Macrophytes of the family *Cyperaceae* are common at Lonar and can be found in the shallow water almost all around the lake. During the 1980s reforestation projects were implemented by the forest department. In addition to native trees like *Acacia nilotica, Azadirachta indica, Dendrocalamus strictus* and *Tectona grandis* many non-indigenous species, for example *Eucalyptus* sp*., Delonix regia* and *Prosopis sp.* have been introduced to the Lonar Crater during this plantation (ECONET, 1999; Babar, 2010). The last, probably being introduced for its sodic soil restoration properties (Bhojvaid and Timmer, 1998), has overgrown vast areas near to the shoreline replacing other species (Babar, 2010). It's $\delta^{13}C$ of -27‰ is very close to the average of all C3 plants sampled in the catchment. Lonar soils incorporate both C3 and C4 plants and have a $\delta^{13}C$ average of -24‰. Lonar plankton being *Arthrospira spp.* has very enriched $\delta^{13}C$ values of -8‰ which is much higher than the $\delta^{13}C$ commonly found for *Arthrospira spp.* When CO_2 (aq) is limiting under conditions of strong eutrophication, the isotopic fractionation is reduced thereby enhancing planktonic $\delta^{13}C$ values (Hollander and McKenzie, 1991). The enriched values of Lonar Lake are, however, very uncommon as CO_2 (aq) is quickly replenished by exchange with the atmosphere, by decomposition of C_{org} and by the effort to stay in equilibrium with HCO_3^- and CO_3^{2-}. High $\delta^{13}C$ are rather related to the high pH of the lake water. Isotope fractionation between HCO_3^- and CO_2(aq) is strong (Deuser and Degens, 1967; Mook et al., 1974) with HCO_3^- being 8–12 ‰ heavier than CO_2.

Arthrospira spp., the dominant plankton in Lonar Lake, takes up HCO_3^- (Kaplan, 1981) which explains the enriched $\delta^{13}C$ in Lonar plankton.

Using a plankton end member of $\delta\ ^{13}C_{plankton}$ = -8 ‰ and the average $\delta\ ^{13}C$ of soils ($\delta\ ^{13}C_{soil}$ = -24‰) as the end member of terrestrial matter we calculated the relative contribution of terrigenous organic carbon according to the equation (Calder and Parker, 1968; Schultz and Calder, 1976):

$$TC_{terr}\ (\%) = \delta\ ^{13}C_{plankton} - \delta\ ^{13}C_{sample} / \delta\ ^{13}C_{plankton} - \delta\ ^{13}C_{soil} * 100 \quad (1)$$

with TC_{terr} (%) being the relative amount of land plant derived or soil organic carbon of total organic carbon in %.

This results in terrigenous contribution between 60-95% in Lonar sediments with maxima off the Dhara River and at some spots near the shore (Fig. 4.6d). We, however, believe that this is a high estimate as it may ignore plant fragments transported directly into the lake and having a more depleted $\delta^{13}C$ than soil.

4.5.6. Principal Component Analysis (PCA)

The Principal Component Analysis (PCA) of the Lonar surface sediments was performed to better examine the variance of a large set of intercorrelated variables. The data set used for analyses comprises various geo-chemical parameters derived from the fifty surface sediments. Principal component analysis extracted two principal components that account for 67.3 % of the variance from the 15 variables in the original data set.

The first axis (F1) explains 53.19 % of the total variance whereas the second PCA axis (F2) explains 13.94 % of the total variance (Fig. 4.7). The factor loadings of the measured parameters along the two axes are provided in Appendix A_3. The first axis (F1) shows high positive factor loadings for Si, Al, Ti, Fe, Mn, lithogenics and low positive values for Ca and Na. The high positive factors loadings on F1 axis represent the elements characteristic of the siliciclastic fraction (feldspars and clay fraction). The low positive value for Ca can be attributed to its possible dual sources. However, Na is contributed by the interstitial brines. The negative side of PCA axis F1 is marked by high loading of organic matter, $CaCO_3$, Mg, total carbon, phosphorous and intermediate values for $\delta^{13}C$. The negative loading therefore corresponds to the authigenic (carbonates) and organic fraction in the lake sediments. The intermediate negative loading value for $\delta^{13}C$ is due to their

contribution from two sources: authigenic and terrestrial. Interestingly, C/N values are significantly correlated with the lithogenics and are negatively correlated with the organic matter constituents and carbonate. This association is due to the enhanced contribution of terrestrial organic matter with high C/N ratios to sediments by terrestrial supply.

The second axis (F2) represents the dual source of calcium- detrital and authigenic precipitation with high and intermediate positive loadings for elemental concentration of Ca and $CaCO_3$ respectively. Thus F1 and F2 axis clearly separate the detrital fraction from the authigenic and organic component in the lake sediments (Fig. 4.7).

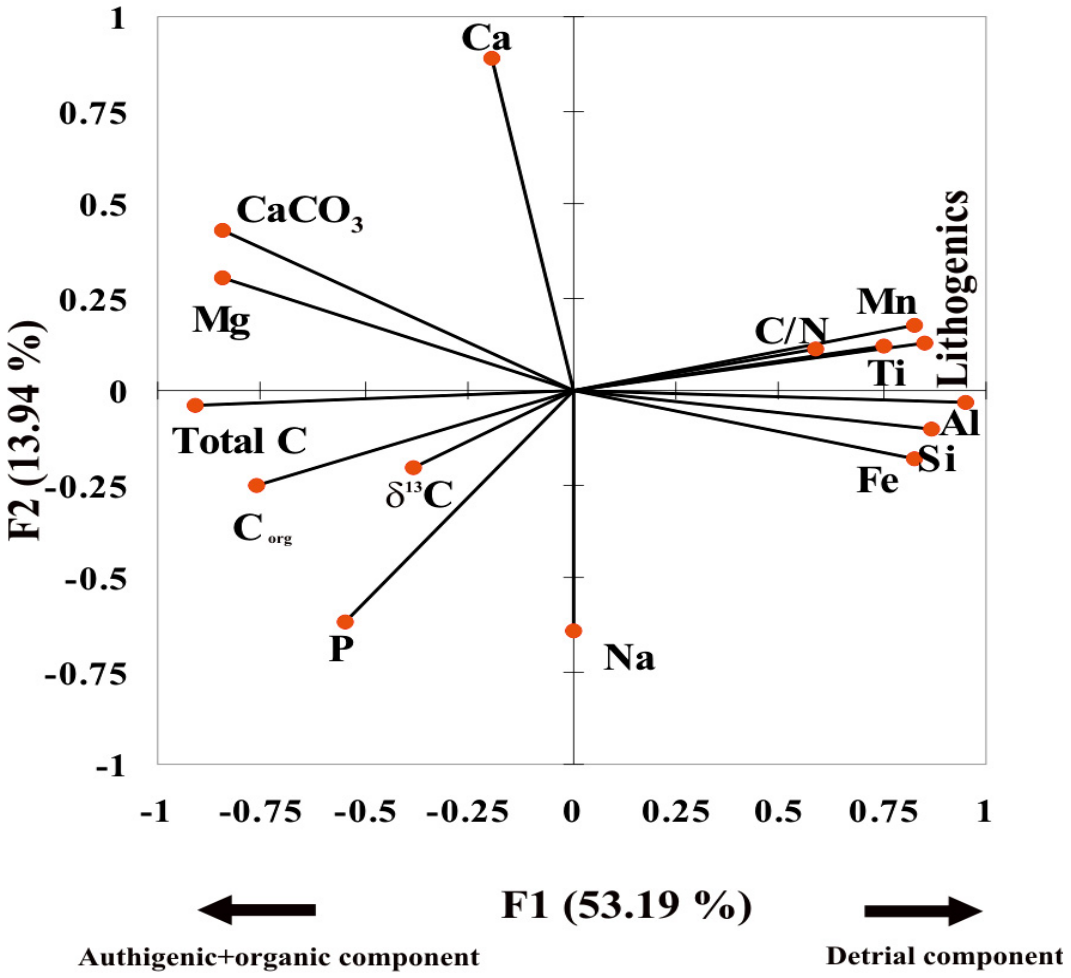

Fig. 4.7*. Biplot of F1 axis vs. F2 axis based on the principal component analysis of geo-chemical parameters from the Lonar surface sediments. A clear distinction can be seen between authigenic, detrital and organic fractions of the sediments.*

4.6. Conclusions

Summarising, the results of our investigations in Lonar lake indicate that

1. The Lonar lake shows strong fluctuations in water level with high levels during the SW monsoon. The lake is stratified with an anoxic bottom (below 4m water depth) layer.

2. C/N ratios and $\delta^{13}C$ values in lake sediments are in the range of plankton and soils from the Lonar lake and its catchment. Two end member mixing using $\delta^{13}C$ values show that between 60-95% of total organic matter is land derived. The lacustrine contribution is highest in the deepest part of the lake. Some planktons can also show highly enriched values of $\delta^{13}C$ of upto -8 ‰ related to high pH of lakes waters.

3. The level of magnetic alteration may be used as a tracer to identify detrital inputs to the oxic/suboxic shallow water sediments against extensively altered ferrimagnetic iron oxides to paramagnetic ilmentite and iron sulfides in anoxic deep-section.

4. Based on the spatial distribution of grain size and geochemistry, in conjunction with hydrological data, it is possible to identify the following parameters palaeoenvironmental indicators (proxies): (i) Al as a proxy for surficial catchment erosion, (ii) evaporitic carbonates (e.g., natron) can be used as a proxy for drier conditions; (iii) Mn/Fe (low) as an indicator for anoxia, (iv) Ca as a first approximate proxy for stream inflow, (v) mode and median values of particle size spectra can be used to trace the major direction and energy of transport.

Our results highlight the importance of understanding the modern processes operating in the lake system for developing proxies for palaeoenvironmental reconstruction. Especially, where the usual lake level change indicators (e.g., palaeoshorelines) are not visible, an understanding of the geochemistry and sedimentology can provide useful clues to past hydrological changes.

4.7. Acknowledgements

Funding for this study was provided by the Deutsche Forschungsgemeinshaft (DFG, Germany), Deutsches GeoForschungsZentrum Potsdam, Indian Institute of Geomagnetism, Mumbai and Universität Hamburg. The cooperation extended by the Forest and Wildlife Department of Maharashtra State, India made this study possible. We thank Mr. Praveen Kumar Mishra for his constructive comments on the manuscript at various stages.

Holocene climate variability: first results from Lonar lake, Central India

This Chapter is an edited version of the manuscript "Holocene Indian Summer Monsoon Variability: an overview of the HIMPAC project and first results from Lonar Lake, Central India" submitted to Quaternary Science Reviews. The work presented below is my contribution to the manuscript.

*S. Prasad, N. Basavaiah, M.R. Strecker, **A. Anoop**, R. Krishnan, P. Priya, G. C. Leckebusch, N. Riedel, P. Menzel, K. Deendayalan, P.K. Mishra, S. Sarkar, B. Bookhagen, A. Brauer, U. Cubasch, B. Gaye, B.N. Goswami, G.H. Haug, G. Helle, J. Kurths, A. Lücke, N. Marwan, N. Nowaczyk, B. Plessen, F. Riedel, D. Sachse, G. H. Schleser, M. Stebich, P. Tarasov, S. Weise, M. Wiesner, H. Wilkes, A.R. Yousuf and the HIMPAC team*

5.1 Sample collection and methodology

5.1.1 Coring, documentation and correlation

Three long cores and several short cores were raised from the Lonar lake in May-June 2008 using a floating platform and a UVITEC piston corer. The second core was raised with a 50 cm depth offset to cover gaps between sequential cores raised from the first borehole. Samples were collected in 1-2 m long plastic liners with an inner diameter of 9 cm. Additionally, several surface sediment samples were also collected using a grab sampler. Two long cores were opened in GFZ Potsdam in August-September. 2008. The cut surface of sediment cores was cleaned, photographed, and the lithology documented in detail.

5.1.2 Radiocarbon dating

We have collected terrestrial wood samples throughout the core to obtain a radiocarbon chronology (Table 5.1). We have also selectively dated the gaylussite crystals, bulk organic matter, and leaf fragment along with the wood fragments to ascertain the possibility of errors arising from reworked samples and/or any "hard water effect".

Table 5.1. *Radiocarbon dates on Lonar core sediments*

Sample	Depth (cm)	Lab no	Material	pMC*/14C date	Cal yr BP (1 σ)
L21	0	Poz-44133	Bulk	116.79±0.42*	-57
L20a	20	Poz-44142	Wood	143.51±0.0043*	-22±3
L20b		Poz 44143	Bulk	107.88±0.38	
L19	163.5	Poz 27189	Wood	564±30	587±42
L18		Poz 41602	Bulk	760±180	
L17	266	Poz 41605	Gaylussite	1105±30	968±40
L16	266.5	Poz 27190	wood	1105±30	1011±36
L15		Poz 41603	Bulk	1075±30	
L14	267.5	Poz 41604	wood	1100±30	1076±58
L13	383.5	Poz 41607	wood	1840±35	1769±84
L12	482	Poz 27236	wood	2315±35	2293±106
L11	511.5	Poz 44141	bulk	2680±35	2812±70
L10	612	Poz 44226	bulk	3470±35	3743±91
L9	778	Poz 27237	wood	4185±35	4703±94
L8	820	Poz 27191	wood	4600±60	5270±178
L7	870	Poz 41611	Wood	7420±40	8166±88
L6	870.5	Poz 27193	wood	7460±90	8355±114
L5	872	Poz 27194	wood	7410±100	8496±169
L4	882.5	Poz 27373	wood	8880±60	9915±175
L3	899	Poz 27253	wood	8990±80	10420±321
L2	902	Poz 27238	leaf	9740±50	10936±141
L1	904	Poz 27192	wood	9570±100	11081±178

5.2 Results

5.2.1. Development of composite lithology and depth

Correlation between cores from two boreholes was achieved using a combination of at least two of the three parameters: marker layers (Fig. 5.1a), magnetic susceptibility, and scanning XRF data. A continuous composite core of ca. 10m length is now available from the Lonar lake (Fig. 5.2a).

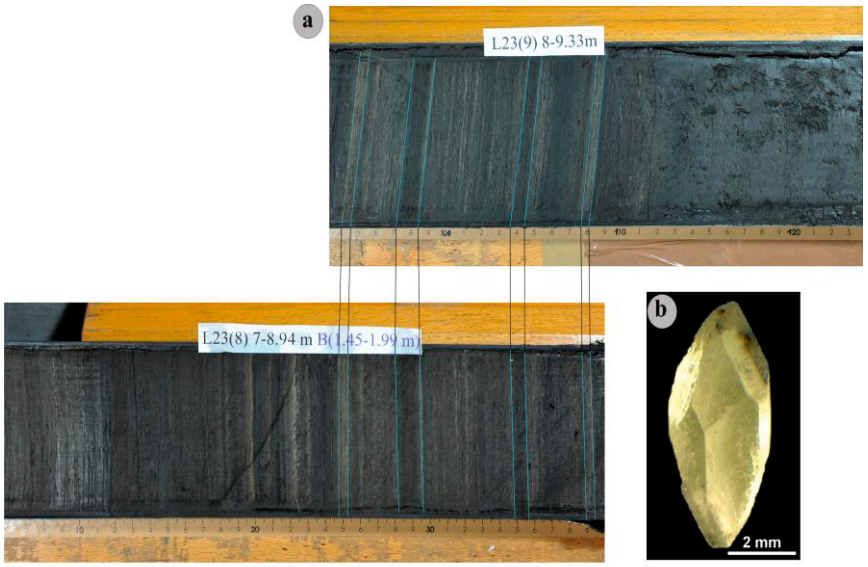

Fig. 5.1:*(a) Correlation between cores raised from parallel boreholes was achieved using prominent marker layers (laminated sediments, evaporite horizons, and other distinct lithological units); (b) Photograph of a gaylussite crystal.*

5.2.2. Chronology

The core chronology is based on AMS dating (Table 5.1 and Fig. 5.2b) of wood, leaf, gaylussite, and bulk material from the sediments. The radiocarbon dates on terrestrial fragments (wood, twigs and leaf) and a gaylussite crystal are in stratigraphic order indicating absence of reworking. Paired radiocarbon dates obtained on bulk sediments and terrestrial fragments at the same depth shows similar ages (within error bar) except for the single paired sample at 383.5 cm where the date on bulk material is significantly older. However, other single dates on bulk organic matter (shown as crosses in Fig. 5.2b) generally tend to be older (encircled crosses in Fig. 5.2b). Only two bulk organic matter dates between (511-612 cm) lie on the trend formed by the dates on terrestrial fragments. The magnitude of the "ageing" of bulk organics is not constant throughout the profile and ranges from ca. 450 to 1500 y BP. The apparent "older" ages for the bulk sediments could be caused by several factors, the most important being hardwater effect (Fontes et al., 1996; Björck and Wohlfarth, 2001). However, the absence of carbonate outcrops in the region eliminates the overestimation of bulk ^{14}C due to hardwater effect. Since Lonar lake shows high salinity, stratification, and high pH the apparent "ageing" could be most likely caused by lack of equilibration with atmosphere. In a hard water lake rich in bicarbonate ions, aquatic productivity will also

incorporate some "dead" carbon, resulting in older ages (Björck and Wohlfarth 2001; Wu et al., 2006). The coincidences of some of the older ages with zones of gaylussite crystals (high pH, stratification and salinity) also support such a scenario.

We have excluded the dates that are obvious outliers marked by circles in Fig. 5.2b. For the accepted dates shown in Table 5.1 the calibration was done using the OxCal programme (Bronk Ramsey, 2008) using the INTCAL04 and NH3 curves.

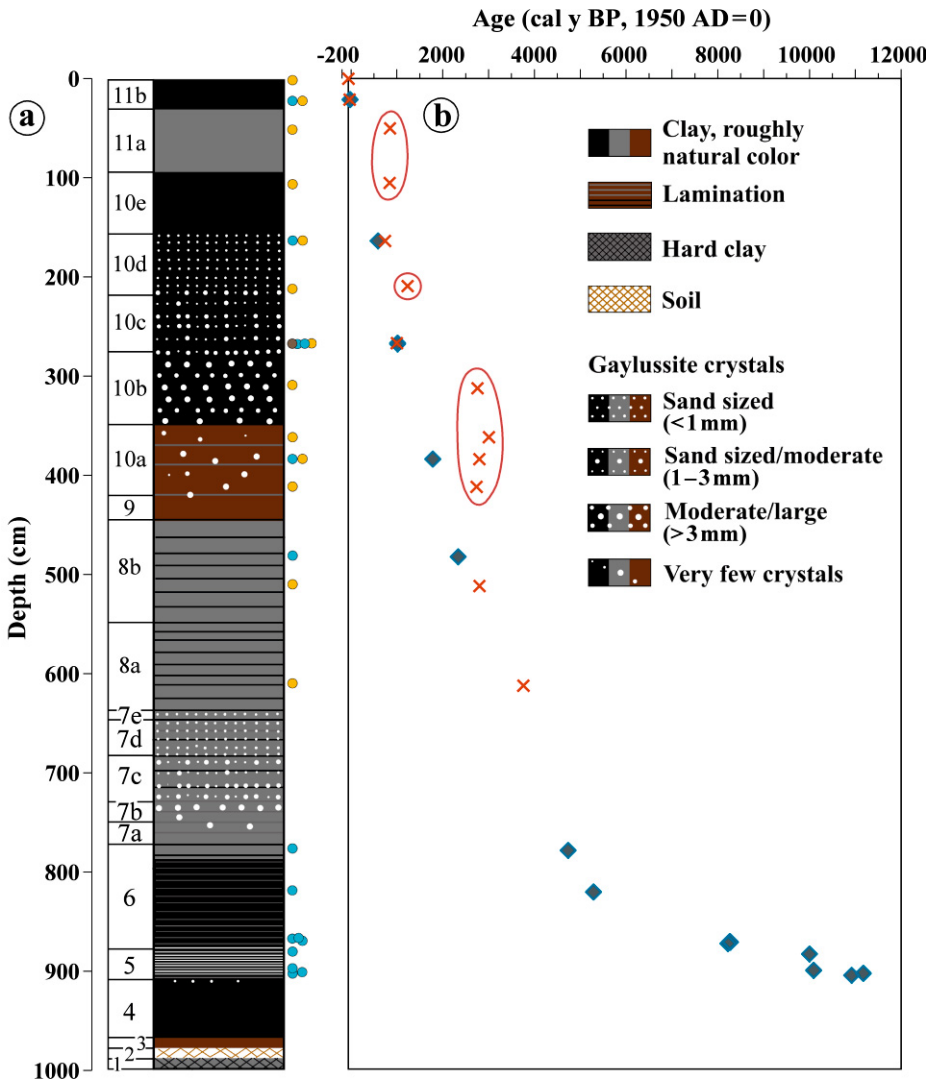

Fig. 5.2: *(a) Lonar litholog showing different lithounits (LT). Two prominent evaporate gaylussite horizons (LT7 and LT10) are also seen indicating drier conditions. Adjacent symbols indicate the position of dated samples: blue circles: terrestrial fragments, yellow circles (bulk organic matter, brown circles indicate dated gaylussite circles; b) Age versus depth plot of the Lonar core. All the ages obtained on terrestrial fragments (blue diamonds) are stratigraphically consistent. Dates on bulk organic matter (crosses) are generally older in the upper part. Outliers are encircled.*

5.2.3. Core description

The litholog of the Lonar core is shown in Fig. 5.2a. The core comprises largely of calcareous clay with laminations in the lower part and gaylussite (Na_2CO_3. $CaCO_3$. $5H_2O$) crystals (Fig. 5.1b) near the mid and upper part. Within the laminated section in lithounit 5, the darker laminae are composed of organic matter and the lighter laminae of clastics and authigenic calcite. The gaylussite crystals are generally with very few sediment inclusions. A detailed core description and lithounits (LT) is given below.

LT1: Hard calcareous clay (1004-988.5 cm).

LT 2: Soil (988.5-980 cm; older than 11.45 cal ka).

LT3: Black and light brown calcareous clay that shows indistinct bands (980-969.5 cm; 11.45-11.4 cal ka).

LT4: Dark grey homogenous clay with infrequent gaylussite (969.5-909.5 cm; 11.4-11.15 cal ka).

LT5: Clay with prominent light coloured laminations (sub mm to 11 mm thick). Thin section investigations reveal that this whole section is comprises of seasonality controlled sub-lamination: clay (monsoon erosion) with intercalations of organic (productivity) and calcareous (summer evaporation) layers. Several terrestrial wood fragments and one leaf is also found in this horizon indicating strong surficial inflow into the lake (909.5-877cm; 11.15-9 cal ka).

LT6: Dark grey/black calcareous laminated (sub mm to 11 mm thick) clay (877-759.5 cm; 9-4.66 cal ka).

LT7: Calcareous clay which can be divided into following subunits based on the amount of evaporitic gaylussite crystals: LT7a: Dark grey/black, laminated with very few medium (1-3 mm) to large (3-8 mm) sized gaylussite crystals (759.5-741 cm; 4.66-4.54 cal ka); LT7b: Dark grey/black, laminated with medium to large sized gaylussite crystals (741-736.5 cm; 4.54-4.51 cal ka); LT7c: Dark grey/black, laminated with small (< 1 mm) medium sized gaylussite crystals (736.5-688 cm; 4.51-4.06-cal ka); LT7d: Dark grey/black, laminated, with occasional brown/black couplets (1-2 mm thick), and small sized gaylussite crystals (688-

648.5 cm; 4.06-3.94 cal ka); LT7e: Dark grey, with frequent laminations (1-4 mm thick) and small size gaylussite crystals (648.5-642 cm; 3.94-3.89 cal ka).

LT8: Dark grey calcareous clay that can be divided into two subunits on the basis of frequency of lamination: LT8a: frequent laminations (1-4 mm thick) (642-550.5 cm; 3.89-3.10 cal ka); LT8b: moderate lamination (1-8mm thick) (550.5-446.5 cm; 3.10-2.19 cal ka).

LT9: Dark brown/grey calcareous clay with moderate lamination (1-2mm thick) (446.5-422.5 cm; 2.19-2.03 cal ka).

LT10: Clay which can be divided into 5 subunits based on size and amount of evaporitic gaylussite crystals: LT10a: Dark brown/grey calcareous clay with occasional lamination (1-2 mm thick) and very few large gaylussite crystals (422.5-349 cm; 2.03-1.55 cal ka); LT10b: homogenous black calcareous clay with few large gaylussite crystals (349-343.5 cm; 1.55-1.51 cal ka); LT10c: homogenous black calcareous clay with medium to large sized gaylussite crystals (343.5-281 cm; 1.51-1.11 cal ka); LT10d: homogenous black calcareous clay with small (to medium) sized gaylussite crystals (281-213 cm; 1.11-0.787 cal ka); LT10e: homogenous black calcareous clay with small sized gaylussite crystals (213-158 cm; 0.787-0.555 cal ka).

LT11: Calcareous clay that can is divided into 3 subunits based on carbonate content: LT11a: Homogenous, black, calcareous clay (158-94 cm; 0.555-0.287 cal y); LT11b: Dark grey clay (94-30 cm; 0.287-0.020 cal ka) with lower carbonate content compared to lithounits 1a and 1c; and LT11c: Black carbonate clay with high water content (30-0 cm; 0.020 cal ka to -58 (2008 AD) y BP).

Palaeoenvironmental implications of evaporative Gaylussite crystals from Lonar lake, Central India

***A. Anoop*[ab], *S. Prasad*[a*], *B. Plessen*[a], *N. Basavaiah*[c], *B. Gaye*[d], *R. Naumann*[a], *P. Menzel*[d], *S. Weise*[e], *A. Brauer*[a]**

[a]German Research Center for Geosciences (GFZ), Potsdam, Germany.
[b]DFG Graduate School 1364, University of Potsdam, Germany.
[c]Indian Institute of Geomagnetism, Navi Mumbai, India.
[d]Universität Hamburg, Institut für Biogeochemie und Meereschemie, Hamburg, Germany.
[e]UFZ Centre for Environmental Research, Dept. Catchment Hydrology, Halle, Germany

In review: Journal of Quaternary Sciences

Abstract

We have undertaken petrographic, mineralogical, geochemical and isotopic investigations on carbonate minerals found within a 10m long core from Lonar lake, central India, with the aim of evaluating their potential as palaeoenvironmental proxies. The core encompasses the entire Holocene and is the first such record from central India. While calcite and/or aragonite were found throughout the core, the mineral gaylussite was found only in two specific intervals (2030-555 cal a BP and 4660-3895 cal a BP). Hydrochemical and isotope data from inflowing streams and lake waters indicates that evaporitic processes play a dominant role in the precipitation of carbonates within this lake. Isotopic ($\delta^{18}O$ and $\delta^{13}C$) studies on the evaporative gaylussite crystals and residual bulk carbonates (calcite) from the long core show that evaporation is the major control on $\delta^{18}O$ enrichment in both minerals. However, $\delta^{13}C$ enrichment mechanisms are different with significant contribution from organic cycling processes in gaylussite, and biological productivity triggered enriched carbon in bulk carbonates.

Key words

Gaylussite, Isotopes, Lonar lake, Monsoon

6.1. Introduction

The mineralogy and geochemistry of lacustrine carbonates are widely used to infer palaeoenvironmental changes (Stuvier, 1970; Drummond et al., 1995; Leng and Marshall, 2004; Mangili et al., 2010). Fluctuations in the isotope composition ($\delta^{18}O$ and $\delta^{13}C$) of authigenic carbonate minerals can be used to infer long-term changes in the precipitation/evaporation (P/E) ratio, temperature, photosynthetic pathways, changes in seasonality, amount and tracks of precipitation (Leng et al., 2006; Spötl et al., 2010). The fundamental assumption underlying such investigations is the primary, unaltered nature of the carbonates as isotopic exchange with interstitial brines, re-precipitation, and/or re-crystallisation can result in the loss of primary signals (Pendall et al., 1994). In this study we present the results of our investigations on carbonates found in a ca. 10m long sediment core encompassing the Holocene (Prasad et al., submitted), raised from the Lonar lake in central India.

Lonar, an impact crater lake (Frederiksson et al., 1973; Milton et al., 1975; Maloof et al. 2009), is located in the core monsoon zone (CMZ) of central India. The available evidence indicates that Indian summer monsoon (ISM) remained the dominant precipitation source in this region during the Holocene (Prasad and Negendank, 2004). Central India is a climatically sensitive region as the interannual variability of the ISM in the CMZ is strongly correlated with the All India Rainfall (Rajeevan et al., 2010) and is impacted by various teleconnections (El Nino-Southern Oscillation, Indian Ocean Dipole, tropical mid-latitude interactions) (Krishnan, 2000; Gadgil, 2003; Ashok et al., 2004). Lonar lake offers the rare possibility of undertaking a long term regional palaeoclimate reconstruction as most of central India is covered by the Deccan basalts and lacks natural lakes. Investigations on Lonar sediment cores revealed abundant gaylussite crystals ($Na_2CO_3 \cdot CaCO_3 \cdot 5H_2O$) in some sections – the first such discovery from the Indian subcontinent. The objectives of the present study are to (i) examine the evidence for primary versus diagenetic origin of gaylussite crystals; (ii) investigate possible factors influencing the formation of carbonates in Lonar namely stream water chemistry and/or salinity induced by changes in P/E; (iii) evaluate the feasibility of using carbonate mineralogy and isotopic composition of gaylussite as an indicator of past hydrological changes; (iv) assess if isotopes of gaylussite offer any additional environmental information compared to isotope data from calcite and/or aragonite.

6.2. Study site

Lonar Lake is situated in the village Lonar, Buldhana district of Maharashtra State, India (19°58'N, 76°30'E; 600 m a.s.l) in Deccan flood basalts (Fig. 6.1a). Based on the geological studies, it is postulated that the lake was formed as a result of meteorite impact about ca. 50 ka BP (Frederiksson et al., 1973; Milton et al., 1975). The impact crater is a near-circular depression with a 1.8 km rim-to-rim diameter, and ~1.4 km of lithic breccias ejecta around the crater rim. The ejecta cover an area of ~ 6.7 km^2 and extend to a distance of ~ 700 m in all directions from the crater rim except to the west where it extends to a distance of more than 1 km (Misra et al., 2010). The crater has a raised rim of about 30 m from the surrounding plains due to uplift of the target layers and deposition of ejected debris and a depth of around 230-245 m from the rim crest to the crater floor (Fig. 6.1a) (La Touche and Christie, 1912; Fudali et al., 1980). The wall exhibits steep slopes with inner rim averaging 30° in the west and southwest and 15-18° in the east. A network of rills and gullies is formed on the walls of the crater due to intermittent runoff erosion. The Quaternary deposits found within the crater consist of gravel to boulder talus which accumulated below the upper sparsely vegetated slopes of the inner crater (Basavaiah et al., in review). Additionally, palaeosols, termed as 'red bole beds' formed by the weathering of lava flows are also reported within the inner crater (Naidu et al., 1990; Maloof et al., 2009).

6.3. Modern climate and hydrology

The modern-day rainfall in the Lonar region is mostly provided by the Arabian Sea branch of the southwest monsoon (Sengupta and Sarkar et al., 2006). The wet and dry seasons of the monsoon system, along with the annual temperature fluctuations, produce three general climatic periods: (i) hot, wet weather from June to the end of September (southwest-monsoon) with an average rainfall of 680 mm; (ii) cool and dry conditions from early October to February, and (iii) hot, dry weather (though normally with high atmospheric humidity) from March to June. Temperatures during the pre-monsoon period are around 31°C, but may increase up to 45°C; southwest-monsoon and post-monsoon temperatures average 27° and 23°C, respectively (Basavaiah et al., in review).

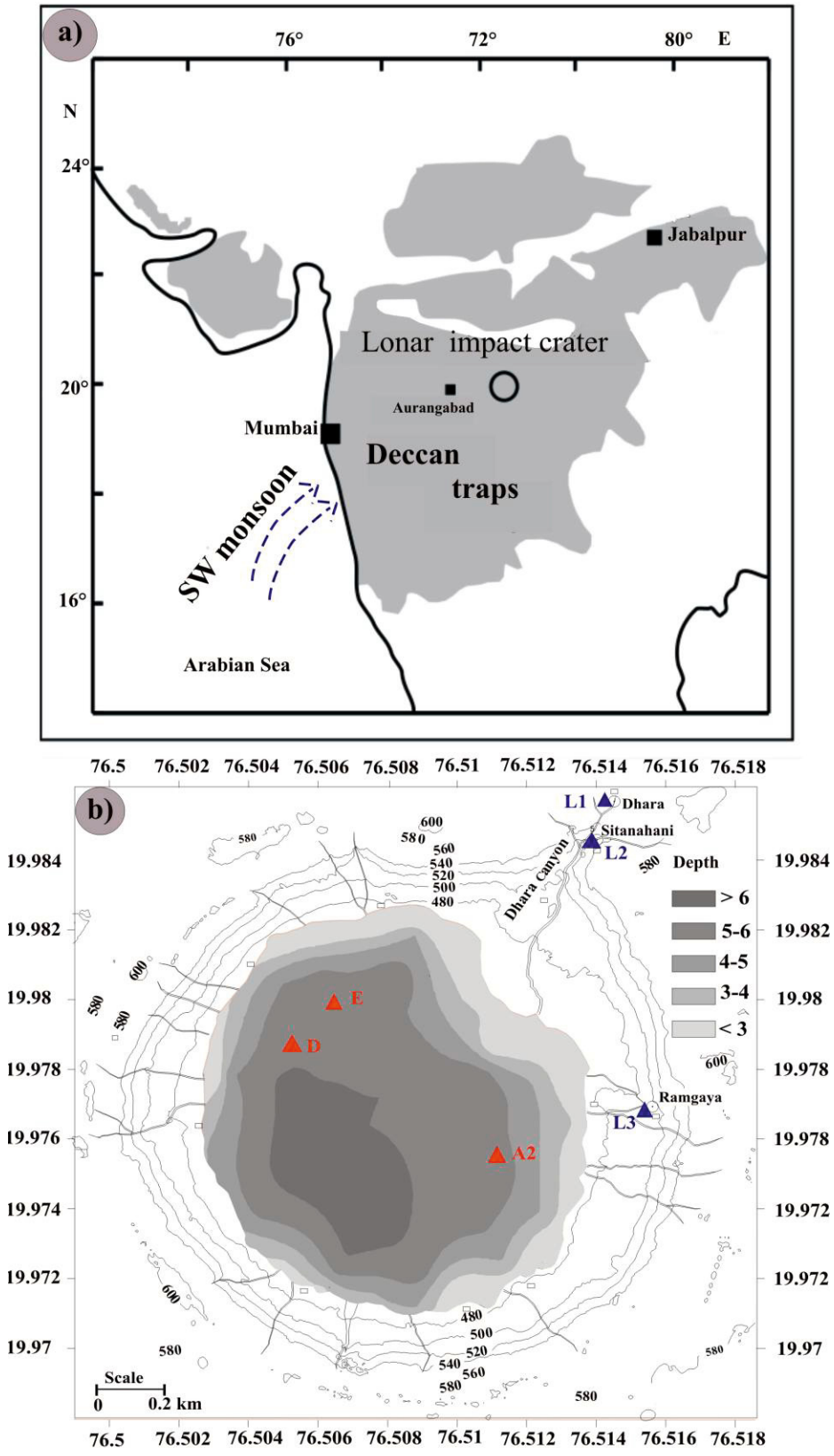

Fig. 6.1: *(a) Location of Lonar impact crater on the 65 Ma old Deccan Trap basalt (after Chakrabarti and Basu 2006). (b) Bathymetry of Lonar lake and location of sampled lake water (red triangle) and inflowing streams (blue triangle).*

Lonar Lake is a hyposaline (Jhingran and Rao, 1958; Nandy and Deo, 1961), alkaline lake (Joshi et al., 2008) with a maximum depth of less than 7 m. The lake is stratified throughout the year with anoxic bottom waters below 4 m depth. The upper oxic part shows salinities between 8.0- 8.2 ‰ and pH values of 10.3–10.4, whereas the anoxic bottom layer has relatively higher salinities (11.1–12.3 ‰), and lower pH values (9.5–9.8) (Basavaiah et al., in review). The lake is mostly fed by ephemeral runoff during the southwest-monsoon and three perennial streams which originate from a gully in the northeast (Dhara and Sitanahani) and from the foot of the eastern crater wall (Ramgaya) (Fig. 6.1b). The lake can be regarded as a superficially closed hydrological system owing to the absence of surface outlets. Since the ground water table is well above the lake surface, loss of lake water by seepage is not possible. The absence of outflowing streams results in seasonal lake level fluctuations in response to regional climate patterns. During the summer monsoon (June to September) precipitation is very high and equals or even exceeds evapotranspiration. This leads to significant lake level rises for the period of summer monsoon accompanied by dilution imposed changes in chemical composition of the lake water. Substantial decrease in salinity was observed in years with high precipitation (Badve et al., 1993). However, during dry seasons with low or absent precipitation, evaporation exceeds precipitation leading to increased salt concentration in the surface waters (Basavaiah et al., in review).

6.4. Methods

6.4.1. Sampling

In May-June 2008 we retrieved a 10m composite core from the Lonar lake at a water depth of 5.4 m using an UWITEC Sediment Piston corer. Lake water samples were collected from the oxic (ca. 50 cm) and anoxic bottom layer (ca. 400 cm) in February, 2011. The samples were filtered through WHATMAN cellulose acetate membrane filters (pore size: 0.45 µm), filled into pre-washed polyethylene bottles and stored in a refrigerator prior to analysis in the laboratory. For cation analysis, some drops of concentrated nitric acid were added to the filtered samples to lower the pH to 2-3.

6.4.2. Analytical procedure

X-ray diffraction (XRD) technique and thin sections studies were applied for the determination of the carbonate mineral assemblages within the core sediments. The XRD analyse were performed using a Bruker-axs D5000 analytical system with

measurements done at an angular range of 4-75°2θ with CuKα radiation. Additionally, quantitative determination of the chemical compositions of the gaylussite crystals was carried out using X-ray fluorescence (XRF) technique. For this, 1 g powdered sample material was mixed together with 6 g Fluxama and 0.5 g nitrate ammonium and gradually heated on 5 different burners. The resulting glass discs were analysed for chemical composition using PANalytical AXIOS Advanced analytical system.

Stable isotope analysis ($\delta^{13}C_{gy}$ and $\delta^{18}O_{gy}$) of the gaylussite crystals was performed at 1-4 cm (ca. 10-20 years) resolution. The crystals found within the sediments were mostly covered with mud and were cleaned with distilled water prior to the analysis. Since gaylussite crystals are known for their high solubility (Burkhardt et al., 2001), isotope analysis of same crystals (dry cleaned under microscope and washed) were carried out to find any changes in the isotope values due to cleaning with water. Additionally, crystals of varying size from the same layers were also analysed to test for size dependency on isotope composition. The results obtained show constant values for all the analysis.

For isotopic analysis, small parts (about 50 μg) of the cleaned gaylussite crystals were weighed into glass vials. The stable isotope measurements were determined using an automated carbonate extraction system (KIEL-IV) interfaced with a MAT253 IRMS (Isotope Ratio Mass Spectrometry) (Thermo Fisher-Scientific). Isotopic ratios relative to the VPDB (Vienna Peedee Belemnite) are calibrated to NBS19 (limestone) with a precision better than 0.03‰ for $\delta^{13}C$ and 0.06‰ for $\delta^{18}O$ measurements. No data are available on the fractionation factors of sodium bearing carbonates - therefore no quantitative estimates can be made with our data

The stable isotope ($\delta^{13}C_{bulk}$ and $\delta^{18}O_{bulk}$) compositions of bulk carbonates (calcite and/or aragonite) were determined in continuous flow mode using Finningan GasBenchII with a carbonate option coupled to a DELTAplusXL mass spectrometer. The visible gaylussite crystals were removed from the samples prior to analyses. From each sample, about ~400 μg were loaded into 10 ml Labco Exetainer vials. After automatically flushing with He, the carbonate samples were reacted in phosphoric acid (100 %) at 75°C for 60 min, following the analytical procedure described in Spötl and Vennemann (2003). The isotope compositions were given

relative to the VPDB standard in the conventional delta notation, and were calibrated against two international reference standards (NBS19 and NBS18). The standard deviation (1 sigma) for reference analyses was 0.06‰ for $\delta^{13}C$ and 0.08‰ for $\delta^{18}O$.

For total carbon and nitrogen determination, around 25 mg of sample material were loaded in tin capsules and combusted in the elemental analyzer. Total carbon and nitrogen content were calibrated against Acetanilide whereas for the nitrogen isotopic composition two ammonium sulphate standards (e.g. IAEA N-1 and N-2) were used. Replicate determinations show a standard deviation better than 0.2 % for C and N.

$\delta^{13}C_{org}$ of the bulk samples were performed using in-situ decalcified samples measured with elemental analyzer (NC2500 Carlo Erba) coupled via a ConFlowIII interface on a DELTA^{plus}XL mass spectrometer (ThermoFischer Scientific). Around 3 mg of sample was weighted into Ag-capsules, dropped with 20% HCl, heated for 3h at 75°C, and finally wrapped in to the Ag-capsules and measured as described above. The calibration was performed using elemental (Urea) and certified isotope standards (USGS24, IAEA_CH-7) and proven with an internal soil reference sample (Boden3). The reproducibility for replicate analyses is 0.2‰ for $\delta^{13}C_{org}$.

For analysis of stable isotopes of water ($\delta^{2}H_{H2O}$ and $\delta^{18}O_{H2O}$), few millilitres were filtered and filled into vials for automated analyses by cavity ring-down spectroscopy (Picarro L2120i with PAL autosampler and high-accuracy vaporizer). For every run the common data range is calibrated by two standards and additionally checked by a procedural standard. Analytical range of uncertainty is 0.25 ‰ ($\delta^{18}O_{H2O}$) and 0.8 ‰ ($\delta^{2}H_{H2O}$), respectively. In a ThermoFinnigan GasBench II the DIC from water samples is converted with orthophosphoric acid to CO_{2DIC}, which is flushed with a helium carrier to a Conflow III-DELTA Vplus mass spectrometer system determining its $\delta^{13}C_{DIC}$. Data are calibrated in an analogue manner as that of $\delta^{2}H_{DIC}$ and $\delta^{18}O$ and the analytical range of uncertainty for $\delta^{13}C_{DIC}$ is ±0.3 ‰.

6.4.3. Chronology

The chronology of the Lonar lake core sediments is derived from eighteen ^{14}C dates from wood, leaf, bulk organic material and gaylussite crystals (Prasad et al., sub.). Radiocarbon dating was carried out at Poznan radiocarbon laboratory, Poland. The obtained ^{14}C dates were calibrated using OxCal 4.1 software (Bronk Ramsay, 2008, 2009) with the IntCal 09 calibration curve (Reimer et al., 2009).

6.5. Results

6.5.1. Modern hydrochemical data

The hydrochemistry of Lonar lake water shows high values, varying between 3750 ± 330 and 3850 ± 370 mg/l, for Cl^- anions and Na^+ cations respectively (Table 6.1). An increase in Na and Cl ion concentrations is noticed towards the anoxic bottom waters. The Cl^- and Na^+ ion concentrations from the inflowing streams show low values of 59-97 and 32-73 mg/l respectively. Other major cation (K and Mg) in the lake water shows substantially lower values varying between 9-14 and 9-88 mg/l respectively. The Ca ion concentrations in the measured lake water samples are below the detection limit while the values from the inflowing streams vary between 42-72 mg/l.

Isotope data ($\delta^{18}O$, δD and $\delta^{13}C_{DIC}$) of lake waters and inflowing stream are listed in Table 6.1. The $\delta^{18}O$ and δD of the inflowing streams range from -2.1 to -3.1‰ and -15.4 to -21.4‰. However, the lake water samples show relatively enriched values for $\delta^{18}O$ and δD isotopes fluctuating between +4.2 to +5.5 ‰ and +14.7 to +21 ‰. Similarly $\delta^{13}C_{DIC}$ is enriched (+11 to +14.8 ‰) for the lake water samples and relatively depleted for the inflowing streams ranging between -9.9 to -12.6 ‰.

6.5.2. Carbonate precipitation

Samples from a thick efflorescent mineral crusts (collected from the local villagers) formed in the year 1982 when the lake completely dried up were investigated to understand the modern day mineral precipitation during extreme saline conditions. The crusts were dry and porous comprising of circular to elongate vugs, up to several mm wide, containing crystals (Fig. 6.2a). XRD analysis of these efflorescent crusts and the crystals revealed that they are not composed of equilibrium assemblages but dominated by one mineral trona ($Na_3H(CO3)_2 \cdot 2H_2O$). The stable isotope analyses performed on these trona crystals yielded values of 8.3‰, 8.5‰ for $\delta^{18}O$ and 7.4‰, 8‰ for $\delta^{13}C$. This thick crust was dissolved in the following monsoon season.

Table 6.1: *Hydrochemistry and isotope analysis of Lonar lake water and inflowing streams. Note that O-LW represents oxic lake water and A-LW denotes anoxic lake water.*

No.	Type	Lat. (N)	Long. (E)	Na (mg/l)	Cl (mg/l)	K (mg/l)	Mg (mg/l)	Ca (mg/l)	$\delta^{18}O$ (‰)	δD (‰)	$\delta^{13}C_{DIC}$ (‰)
A2	O-LW	19.976	76.511	3487	3423	9	31	n.a.	4.20	14.7	12.9
A2	A-LW	19.976	76.511	3776	3424	9	13	n.a.	4.30	15.3	12.0
D	O-LW	19.979	76.505	3795	3464	16	70	19	4.40	16.1	13.0
D	A-LW	19.979	76.505	3897	3494	10	74	n.a.	4.30	15.6	11.9
E	O-LW	19.980	76.507	3800	3996	12	88	n.a.	4.40	16.4	11.5
E	A-LW	19.980	76.507	4322	4079	15	12	n.a.	5.50	21.0	14.8
L1	Spring	19.986	76.514	58	97	2	59	72	-2.40	-15.4	-12.6
L2	Spring	19.985	76.514	45	24	1	36	30	-3.10	-21.3	-11.9
L3	Spring	19.977	76.515	73	59	1	47	43	-2.00	-13.0	-9.9

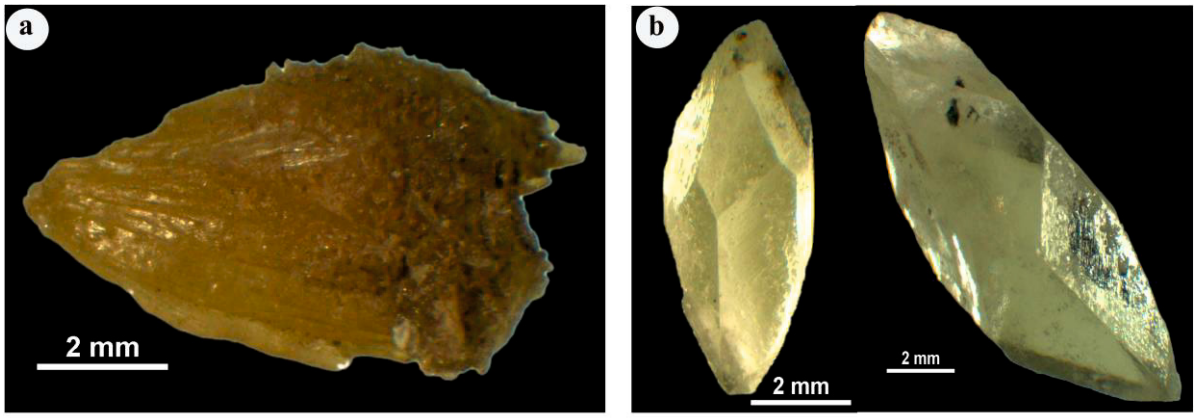

Fig. 6.2: *a) Trona precipitation in Lonar lake (modern environment) when the lake got completely dried up. b) Gaylussite crystals found within the lake sediments.*

6.5.3. Core sediments

Carbonate distribution

Detailed petrographical analysis combined with XRD analyses shows that the carbonate in the core consists of calcite and aragonite in mineral phase and gaylussite occurring as crystals (Fig. 6.2b). There is a noticeable difference in the vertical distribution of carbonate minerals within the core (Fig. 6.3a and 6.3b). Calcite is the major carbonate mineral found in the entire section of the core. Aragonite is restricted to the core interval between ca. 8.2-8.5 m (ca. 7250- 5360 cal a BP) whereas gaylussite crystals (Fig. 6.2b) are found in two distinct zones 1.58 -4.22 m (555-2030 cal a BP, upper zone) and 6.42-7.6 m (3895- 4660 cal a BP, lower zone) (Fig. 6.3a). Therefore, a sequential deposition of carbonate minerals is noticed within the core with precipitation of Ca-carbonates (aragonite/calcite) followed by coexistence of Ca-carbonates (calcite) and Na-Ca carbonates (gaylussite) and even exclusive occurrences of gaylussite crystals (Fig. 6.3b).

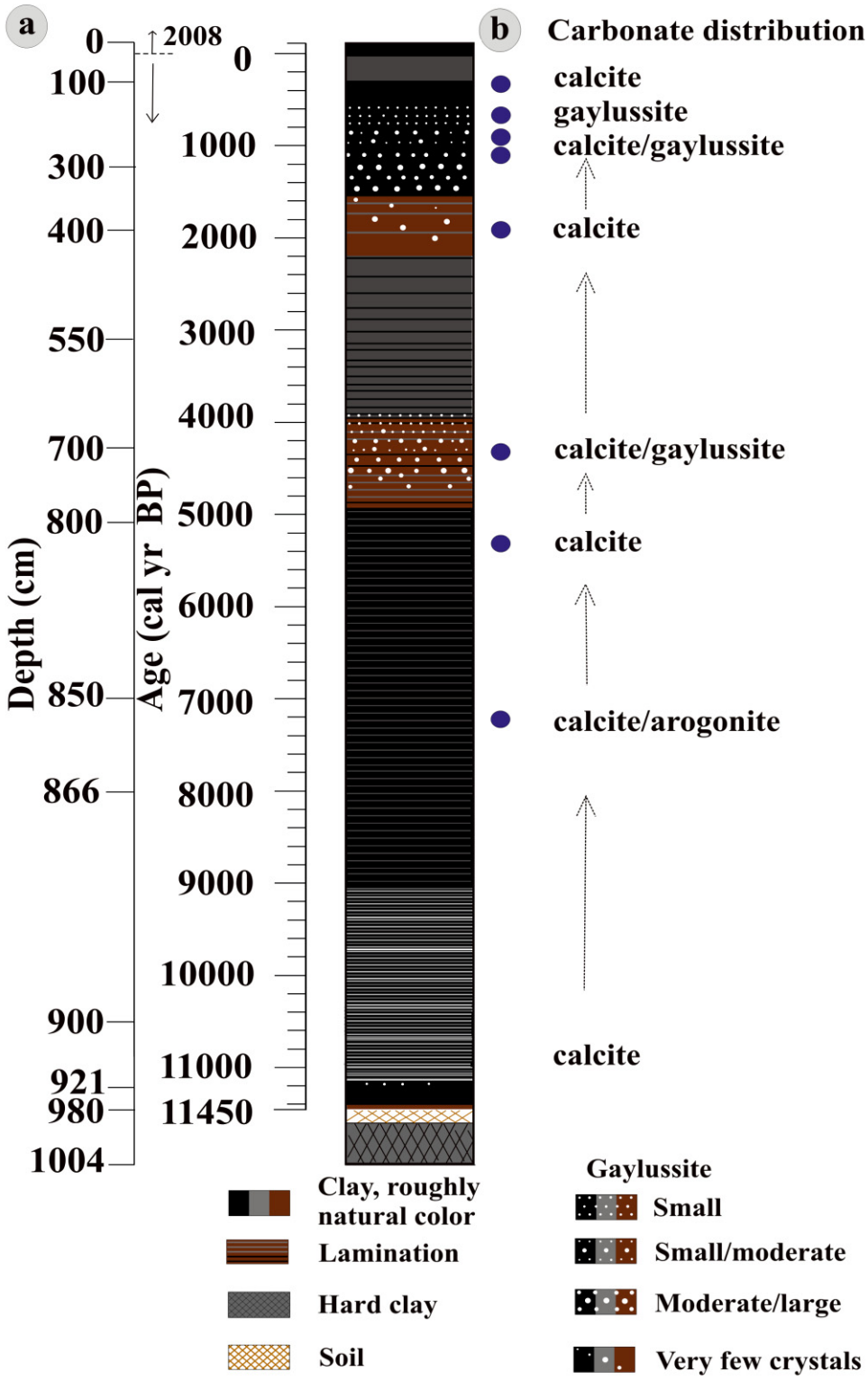

Fig.6. 3: *a) Lithology of the Lonar core. b) Carbonate distribution within the core sediments.*

6.5.4. Gaylussite crystals

Microfacies and mineralogy

The gaylussite bearing horizons are characterised by graded nature with the bigger ones at the base and a fining of the crystal size towards the top. They range in length from sub mm to 10 mm, with smaller crystals showing higher crystallanity (euhedral forms) when compared to the larger crystals. Most of the crystals appear parallel to the original sediment laminations. With a few exceptions, the crystals are mostly devoid of any mud inclusions. Quantitative chemical analyses of the gaylussite crystals reveal oxide percentages of CaO = 23.74%, Na_2O =25.58%, H_2O = 25.04%, and CO_3 = 26.85%. No other components are present above .01 wt %.

6.5.5. Isotope ($\delta^{18}O_{gy}$ and $\delta^{13}C_{gy}$) analysis of gaylussite crystals

Lower gaylussite sequence (G1: 3895- 4660 cal a BP)

The stable isotope analyses on the lower gaylussite sequences yielded enriched values for $\delta^{18}O_{gy}$ and $\delta^{13}C_{gy}$ ranging between +10 to +16‰ and +13 to +20‰. The isotopic value shows a progressive enrichment with decreasing age (Fig. 6.6). The most striking feature observed for the $\delta^{18}O_{gy}$ and $\delta^{13}C_{gy}$ isotopic values are their strong positive correlation (r =.89, significant at 99% confidence level) (Fig. 6.4a).

Upper gaylussite sequence (G2: 555-2030 cal a BP)

The upper gaylussite sequence also yielded enriched values of +8 to +18‰ and +9 to +15 ‰ for $\delta^{18}O_{gy}$ and $\delta^{13}C_{gy}$ respectively. A progressive enrichment in both isotopes is seen until ca. 1300 cal a BP. Subsequently while $\delta^{18}O_{gy}$ continues with its enrichment trend, $\delta^{13}C_{gy}$ shows a depleting trend (Fig. 6.6). The drop in the $\delta^{13}C_{gy}$ resulted in the formation of two distinct subzones within the upper gaylussite sequence (2030-1300 and 1300-550 cal a BP) with correlation coefficients of r =0.47 (significant at 95% confidence level) and -0.4 respectively (Fig. 6.4b).

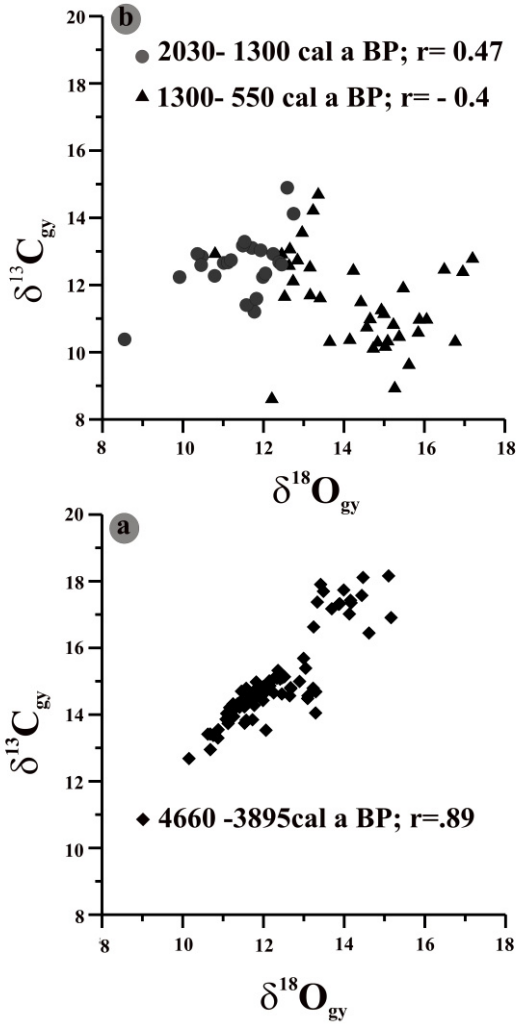

Fig. 6.4: *Covariance of $\delta^{13}C_{gy}$ and the $\delta^{18}O_{gy}$ isotope values from the lower (a) and upper (b) gaylussite sequence*

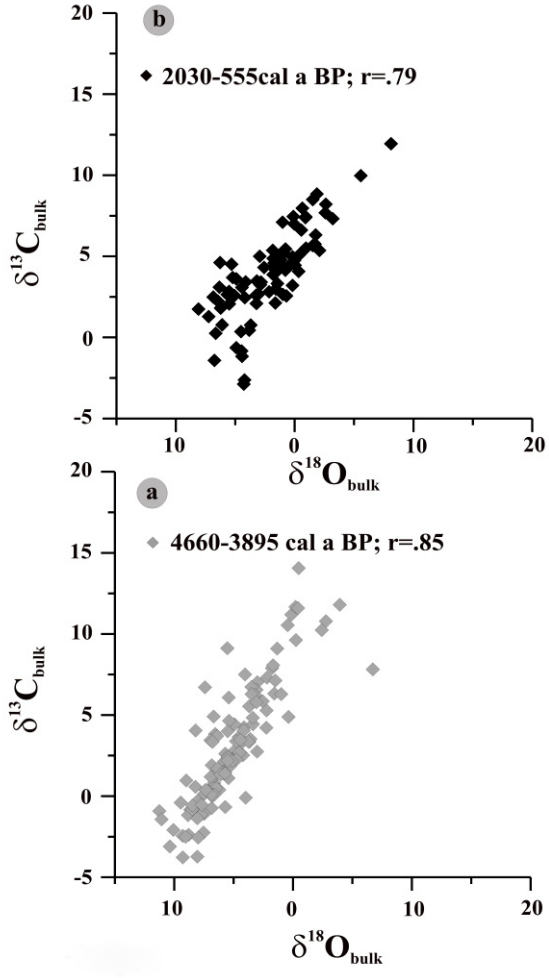

Fig. 6.5: *Covariance of $\delta^{13}C_{bulk}$ and the $\delta^{18}O_{bulk}$ isotope values from the lower (a) and upper (b) gaylussite zone*

.

Isotope data on bulk carbonates ($\delta^{18}O_{bulk}$ and $\delta^{13}C_{bulk}$)

The stable isotope composition of bulk carbonates (without visible gaylussite) in the G1 zone ranges from -11.3 to +6.7‰ for $\delta^{18}O_{bulk}$, and from -3.7 to +14‰ for $\delta^{13}C_{bulk}$. The $\delta^{18}O_{bulk}$ and $\delta^{13}C_{bulk}$ values show a strongly positive correlation coefficient of 0.85, comparable to the correlation coefficient of 0.88 for gaylussite (both significant at 99% confidence level) (Fig. 6.4a and 6.5a).

In the upper zone (G2) bulk carbonates ranges from -11.2 to +8.1 ‰ for $\delta^{18}O_{bulk}$, and -2 to +12‰ for $\delta^{13}C_{bulk}$. A strong positive correlation of 0.79 similar to the G1 zone is noted for the bulk carbonate values (Fig. 6.5b). However, unlike the lower zone a persistent enriched trend was noted for the $\delta^{18}O_{bulk}$ and $\delta^{13}C_{bulk}$ values around ca. 1400 cal a BP (Fig. 6.6).

Isotope and C/N data on bulk organics

$\delta^{13}C_{org}$ of the bulk sediment in the lower gaylussite (G1) zone shows values between -10.6 to -21‰ with a slight depleting trend. The C/N values (>20) are indicative of the dominant terrestrial vegetation contribution. In the upper gaylussite (G2) zone $\delta^{13}C_{org}$ varies between – 18.9‰ and -12.8‰. The values show no particular trend until ca. 1350 cal a BP when an enrichment trend (upto 5‰) is noticed for ca. 100y followed by an enriched stable value (Fig. 6.6). Similar is the case for C/N values showing a sudden persistent shift to aquatic dominated values (ca. 12) around 1300 cal a BP (Fig. 6.6).

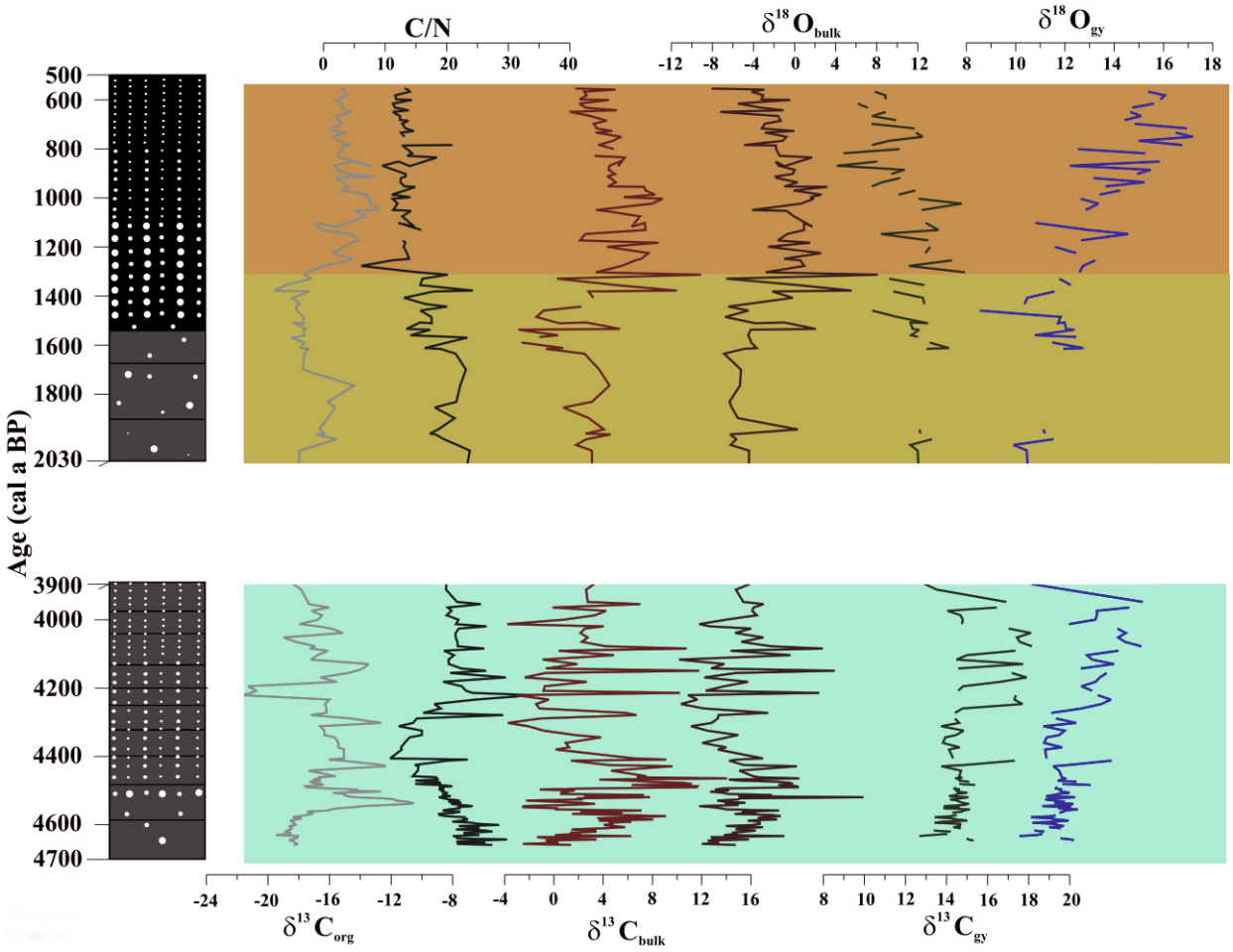

Fig. 6.6 *Isotope data on gaylussite crystals, bulk carbonates and organics ($\delta^{13}C_{org}$, C/N) from the gaylussite zones.*

6.6. Discussion

6.6.1. Evidence for primary versus diagenetic origin of gaylussite

Gaylussite may be of both authigenic and diagenetic origin (Eugster and Hardie, 1978; Renaut, 1986; Mees et al., 1991). The primary gaylussite mineral is mostly precipitated by the gradual evaporative concentration of the brine (Hardie and Eugster, 1970; Eugster and Hardie, 1978) at the sediment water interface (Bischoff, 1991) in contrast to calcite and aragonite that form in surface waters (McConnaughey, 1994; Leng and Marshall, 2004; Reddy and Hoch, 2011). Gaylussite usually succeeds the precipitation of calcite and is the first sodium carbonate mineral to be precipitated when saline, alkaline water is concentrated by evaporation (Fig. 6.7) (Rankama and Sahama, 1964; Renaut, 1986). Diagenetic formation of the gaylussite mineral by secondary processes occurs when alkaline brine rich in Na reacts with (i) primary calcite/ aragonite, (ii) waters containing Ca^{2+} and HCO_3^-, or (iii) calcite rich sediments (Eugster and Hardie, 1978).

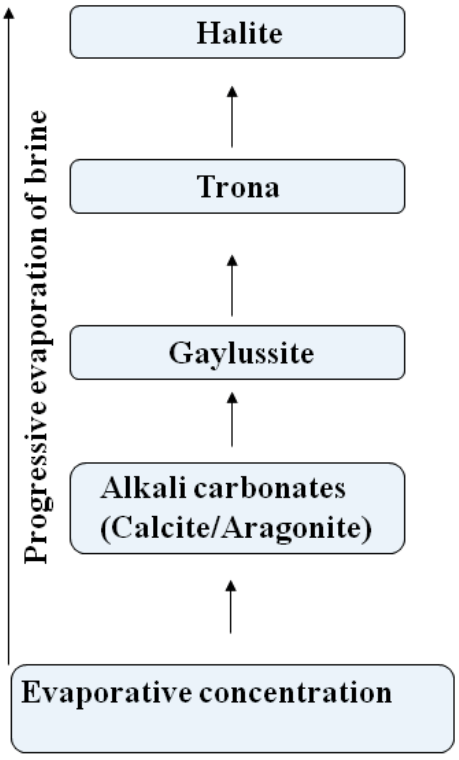

Fig. 6.7: *Sequential evaporative precipitation of minerals (modified after Hardie and Eugster, 1970; Eugster and Hardie, 1978)*

Gaylussite crystals in Lonar core sediments occur within distinct zones at 1.58-4.22m and 6.42-7.6m implying that they are formed when the water chemistry is conducive for their formation. The crystals are parallel to the original sediment lamination and, with a few exceptions, free from mud inclusions indicating a synsedimentary origin. The stratigraphic variation in the distribution of the carbonate minerals also provides useful insights into the formation of evaporitic minerals. The sequential precipitation of the Ca carbonates and Ca-Na carbonates (Fig. 6.3 and Fig. 6.7) indicates progressive brine evaporation in Lonar waters. According to the model of evaporite formation (Hardie and Eugster, 1970), when the brines reach saturation the first minerals to precipitate are the alkaline earth carbonates (calcite and aragonite). The precipitation of these minerals continues until either Ca^{2+} or CO_2^{3-} is exhausted. The selective removal of Ca induces a change in the ionic ratio of lake waters with a shift to a more Na rich brine and results in precipitation of gaylussite. Interestingly, the trona crusts formed during the 1982 dry phase are not preserved in the core sediments suggesting that dissolution of highly soluble evaporitic minerals also occurs in the basin.

We have also radiocarbon dated a single gaylussite crystal and a wood fragment from a depth of 266 cm, both of which yielded a similar age of 1015 ± 35 cal a BP excluding any post depositional alternation or diagenetic origin of the gaylussite.

6.6.2. Possible factors influencing the formation of carbonates in Lonar: stream water chemistry and/or evaporation induced salinity

A detailed understanding of the sources and chemistry of inflow into the Lonar lake is essential to infer the processes governing the evaporite formation. In addition to ephemeral runoff during the southwest monsoon, inflow into the lake is from three perennial streams (Dhara and Sitanahani in the northeast and Ramgaya in the east). Tritium dating indicated a modern to sub-modern age for the groundwater (Prasad et al., sub.). This is consistent with the local observations that a succession of weaker than normal monsoon years results in partial or complete drying of the lake. As the stream inflow is closely linked to the monsoon rainfall, the salinity changes can be assumed to be linked to input (inflow+precipitation)/evaporation (I/E). The isotopic data from the inflowing streams and lake waters corroborate this assumption. There is a considerable enrichment of heavier isotopes in lake waters ($\delta^{18}O$ = +4.2 to +5.5‰)

compared to the inflowing streams ($\delta^{18}O$= -2.1 to -3.1 ‰) suggesting evaporation from a closed system. A plot of $\delta^{18}O$ and δD isotope values along the Global Meteoric Water Line (GMWL) clearly supports the evaporative enrichment of lake water (Fig. 6.8). However, the enrichment of $\delta^{13}C_{DIC}$ (+12.9 to +14.8‰) can be induced both by loss of dissolved CO_2 due to strong evaporation, and phytoplankton photosynthesis (Lei et al., 2011). Since the present day Lonar lake is observed to support luxuriant bloom of phytoplankton (Joshi et al., 2008; own observations between 2008-2011), the $\delta^{13}C_{DIC}$ enrichment in the lake waters cannot be interpreted in terms of evaporation processes alone.

The chemistry of lake and inflowing waters clearly indicates that the contribution of Ca, Mg, and K is relatively low in both lake waters and the inflowing streams. The decrease in Ca^{2+} in lake water compared to the inflowing streams is due to the continuous removal of Ca^{2+} by authigenic carbonate precipitation. However, the several orders of magnitude enrichment of sodium and chlorides in lake waters relative to the inflowing streams suggests that evaporation processes mainly control the water chemistry and seasonal stratification. The vertical variation of these ions with depth, in combination with similar salinity (Basavaiah et al., in review) and isotopic trends, and bottom anoxia suggests evaporation induced stratification. In view of the minor contribution of Na (an essential ingredient of gaylussite) from the inflowing streams we conclude that the formation of gaylussite is controlled dominantly by salinity changes (I/E).

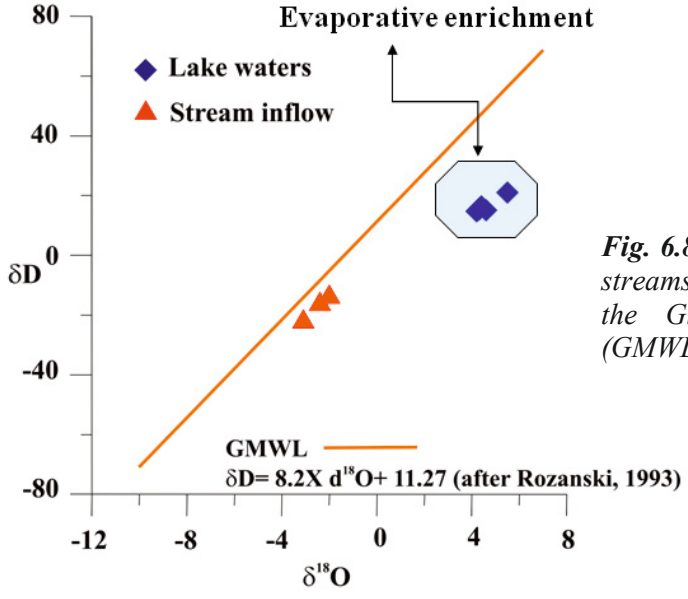

Fig. 6.8: *$\delta^{18}O$ and δD of the inflowing streams and lake water plotted along the Global Meteoric Water Line (GMWL).*

Modern precipitation of trona during extreme saline condition provides insights into the evaporative concentration processes resulting in the precipitation of carbonates. Trona usually succeeds the precipitation of gaylussite mineral (Eugster and Hardie, 1978; Fig. 6.7). Therefore, complete dehydration due to evaporation can result in the brines evolving into waters dominated by only a few major ions resulting in the formation of trona crust. The isotopically enriched values for the trona crystals (8.3‰, 8.5‰ for $\delta^{18}O$ and 7.4‰, 8‰ for $\delta^{13}C$) are typical of evaporitic deposits.

6.6.3. Factors governing the isotopic composition of carbonates and organic matter

The oxygen-isotopic composition of authigenic carbonate is controlled by (1) the isotopic composition of the water; (2) temperature at the time of precipitation; (3) potential evaporative enrichment; (4) inflow (Talbot, 1990; Valero-Garces et al., 1999; Leng et al., 2006). Therefore, the enrichment of $\boldsymbol{\delta}^{18}O$ isotope values cannot be interpreted as a function of simple evaporative concentration. However, in hydrologically closed lakes, especially in non-karstic catchments, the enriched values are most likely to reflect preferential evaporative loss of the ^{16}O (Leng and Marshall, 2004).

The carbon-isotopic composition of authigenic lacustrine carbonates are controlled by (1) biological processes such as (i) methanogenesis, which produces ^{13}C-rich carbon dioxide (CO_2) and ^{13}C-poor CH_4 during the bacterial fermentation of organic matter and (ii) photosynthesis, which selectively removes ^{12}C resulting in enrichment of ^{13}C in the dissolved CO_2 reservoir; (2) variations in $^{13}C/^{12}C$ values of the dissolved inorganic carbon; and (3) CO_2 exchange between water and atmosphere (Talbot, 1990; Valero-Garces et al., 1999). Additionally, $\delta^{13}C$ enrichment in carbonates could also occur from the evaporation induced loss of CO_2 from the brines (Stiller et al., 1985; Rosen et al., 1989; Mees et al., 1998).

Several factors can influence the long-term ^{13}C record of the organic component in lake sediments. The dominant factors are changes in organic productivity and pH of the water (Stuiver, 1975). Photosynthesis associated with organic productivity preferentially uses ^{12}C, leaving the DIC pool enriched in ^{13}C (Goreau 1977; Swart, 1983). Where dissolved CO_2 levels are low (<0.01 mol/l) photosynthetic organisms may be forced to change from CO_2 to HCO_3 based metabolism. In some aquatic plants this becomes significant above pH 6.3 and is probably of considerable importance above pH 8.5. Assimilation of HCO_3 can

produce organic matter that is relatively enriched in ^{13}C (Talbot, 1990; Meyers, 1997; Leng and Marshall, 2004). These effects are important in an alkaline water body like Lonar. The net result will be an increase of $\delta^{13}C$ of the organic matter and an elevated $\delta^{13}C$ in the DIC because of the preferential removal of the ^{12}C (Schelske and Hodell, 1991; Xu et al., 2006). Studies (Hollander et al., 1993; Stiller and Nissenbaum, 1999) have also revealed that the isotopic fractionation between CO_2 (aq) and phytoplankton is reduced during periods of high productivity associated with high growth rates. Therefore, enhanced aquatic productivity results in the relative enrichment of $\delta^{13}C_{org}$ of the lake sediments.

Lower gaylussite sequence (G1: 3895- 4660 cal a BP)

The isotopic data must be interpreted bearing in mind that the calcite and aragonite are formed in surface waters while gaylussite is formed at the sediment water interface. In the discussion below we explore the factors influencing the isotopic composition of bulk carbonates, gaylussite, and organic matter and their possible interlinkages.

Organic matter: The $\delta^{13}C_{org}$ value of organic matter is on average depleted by -31‰ compared to the $\delta^{13}C_{gy}$ of gaylussite crystals which is related to both the strong isotopic effect of carbon assimilation of up to -20‰ (Deuser et al., 1968) as well as to the addition of isotopically even more depleted land plants and organic matter from soils. C/N ratios above 25 indicate a strong input from land-plants (Meyers and Lallier-Verges, 1999). Even under the present highly eutrophic situation, between 50-90 % of the organic matter deposited in Lonar lake is derived from land plants (Basavaiah et al., in revision). Fluctuations in gaylussite carbon and oxygen isotopic ratios seem to be driven by evaporative cycles, whereas the difference between the $\delta^{13}C$ of organic carbon and $\delta^{13}C$ of gaylussite is driven by differences in the input of land plants.

Bulk carbonates: As most of the visible gaylussite crystals were separated before analyses, the bulk isotope signal is largely contributed by the calcite and/or aragonite. It has already been shown that $\delta^{18}O$ of aragonite is about 0.6% more positive than calcite formed under the same conditions (Land, 1980; Leng and Marshall, 2004). However, the high correlation (0.85) shown by the $\delta^{18}O_{bulk}$ and $\delta^{13}C_{bulk}$ in this zone indicates that, as in the case of gaylussite, the isotopic enrichment of the bulk carbonate is controlled by evaporation processes.

Gaylussite crystals: The $\delta^{13}C_{gy}$ and $\delta^{18}O_{gy}$ of gaylussite crystals in G1 sequence show strongly enriched values similar to the modern day carbonate (trona) precipitated during extreme saline conditions. The progressive enrichment of $\delta^{18}O_{gy}$ observed in gaylussite crystals can be attributed to lake waters that have undergone systematic evaporation (Craig and Gordon, 1965; Gibson et al., 1993) and imply that the deep waters in which gaylussite is formed are more saline than the surface waters. The high correlation between carbon and oxygen isotopes is characteristic of hydrologically closed lakes (Talbot, 1990; Li and Ku, 1997). We conclude that the co-varying enriched $\delta^{18}O_{gy}$ and $\delta^{13}C_{gy}$ in gaylussite are a result of evaporative processes that resulted in preferential loss of lighter isotopes.

Upper gaylussite sequence (G2: 555-2030 cal a BP)

Organic matter: The $\delta^{13}C_{org}$ and C/N values in the lower part (2030- 1350 cal a BP) in the G2 show similarity to the G1 indicating contribution derived from land plants. However, the sudden persistent shift in the enriched values for $\delta^{13}C_{org}$ and C/N in the upper part (2030- 1350 cal a BP) denotes dominance of aquatic productivity in the lake. This eutrophication about ca.1350 cal a BP is also supported by high values in nC17 biomarker typical for phytoplankton bloom (S.Sarkar, Personal comm.)

Bulk carbonates: The $\delta^{18}O_{bulk}$ and $\delta^{13}C_{bulk}$ with high correlation of 0.79 indicates, as in the lower part (G1), evaporation induced precipitation from a closed basin. However, the relative enrichment noticed in the bulk carbonates values around ca.1400 coincides with the period of eutrophication in the lake and is, therefore driven by high primary productivity in the lake.

Gaylussite: This section can be divided into two parts: the lower part (ca. 2000-1300 cal a BP) where the enriched $\delta^{18}O$ and $\delta^{13}C$ values of gaylussite crystals and their positive correlation (0.47 which is lower than 0.88 in G1) indicates evaporation and degassing are the major control on $\delta^{18}O$. However, organic productivity that operates in opposite direction on the DIC also plays a role in determining the $\delta^{13}C$ of gaylussite. A sudden drop of $\delta^{13}C_{gy}$ gaylussite was noticed at ca. 1300 cal a BP, though $\delta^{18}O_{gy}$ continues to show progressive enrichment. This relative depletion of $\delta^{13}C_{gy}$ of gaylussite crystals coincides with the enrichment of $\delta^{13}C_{org}$ of the bulk lake sediments, and a shift of C/N (ca. 12) indicating eutrophication in the lake.

However, high primary productivity in lakes should result in high $\delta^{13}C$ in the organic matter, bulk carbonates, and gaylussite crystals which is not seen in our data where $\delta^{13}C_{gy}$ showing a depleting trend. An explanation can be found when it is considered that the gaylussite, unlike calcite and aragonites, forms at the sediment water interface and, under persistent, well stratified conditions, could incorporate the ^{12}C released from respiration of previously sedimented organic carbon (Drummond et al., 1995; Hollander and Smith, 2001). Thus the sudden drop of the $\delta^{13}C$ gaylussite at ca. 1300 cal a BP suggests a biological influence and a decoupling of surface and deep waters as observed in stratified eutrophic lakes (Hollander and Smith, 2001).

6.6.4. Do isotopes of gaylussite offer any additional environmental information compared to isotope data from calcite and/or aragonite?

The environmental implications of occurrence of primary gaylussite, a palaeosalinity indicator are evident. In the case of Lonar lake sediments, the isotopic information obtained from gaylussite largely corroborates the inferences from bulk carbonates (calcite and/or aragonite). It is only in the upper gaylussite zone (G2) that the additional benefit of isotopic analyses of gaylussite becomes clear; here the $\delta^{13}C_{gy}$ persistent stratification in lake waters and occurrence of methanogenesis.

6.7. Conclusion

Detailed geochemical investigations were carried out on bulk carbonates, organic matter, and gaylussite crystals from the lacustrine sediments in Lonar lake, central India, during selected intervals (555-2030 cal a BP and 3895- 4660 cal a BP). Results from analysis of modern hydrochemistry and lake water isotopes ($\delta^{18}O$ and δD) show that Lonar lake responds to the balance between precipitation/evaporation (P/E) ratio. The sedimentological and mineralogical evidence from the core sediments indicates evaporation with a progressive enrichment of brine resulting in the precipitation of gaylussite crystals. The isotopic analysis ($\delta^{18}O_{gy}$ and $\delta^{13}C_{gy}$) on gaylussite crystals shows strong enrichment typical for evaporite deposits. The high covariance of $\delta^{18}O_{gy}$ and $\delta^{13}C_{gy}$ found in the lower part reveals evaporation effects and CO_2 degassing as controlling factors, whereas the lower covariance during ca. 555-2030 cal a BP reveals eutrophication of the lake

6.8. Acknowledgements

This project is being funded by the DeutscheForschungsGemeinschaft under the coordinated programme “Himalaya: Modern and Past Climates” (HIMPAC, FOR 1380). The Lonar coring and field expeditions have also received financial and logistic support from the Deutsches GFZ Potsdam, Indian Institute of Geomagnetism, and the Universität Potsdam. Water sample analyses and Tritium dating have been undertaken at the UFZ Helmholtz Centre for Environmental Research. Thanks are due to S. Pinkerneil and L. Czudowski for their help with preparing the samples.

7.1. Summary

My thesis comprises of five separate manuscripts dealing with the identification of climatically sensitive proxies and Holocene palaeoclimate reconstruction from the environmentally sensitive regions of upper Spiti valley, NW Himalaya and Lonar lake, Central India. Located in the tectonically active orogenic belt, the Mane palaeolake sediments from the Spiti valley also provided a unique opportunity for investigating the interplay between past climate and tectonic processes – this step is critical as tectonic activity in the upper catchment area can also result in intensified erosion making it difficult to decouple it from the monsoon erosional signal. The interpreted palaeoclimate data were then compared with other regional palaeo-records for a better understanding of the past climate dynamics and teleconnections. The key findings from my thesis are summarised below;

The lacustrine sediments in the upper Spiti valley were formed due to landslide damming of Spiti river during early-mid Holocene (8.7-6.1 cal yr BP). An integrated structural, morphometric and geomorphic analysis shows that several parts of the study area are structurally controlled and tectonically active. The modern and palaeolandslides occurred close to the active faults in the region. The effect of past-seismic shocks related to fault movements is recorded as deformational structures (seismites) and micro-faults within the lacustrine sediments. Seismites such as fault grading stratigraphy, ball and pillow structures, contorted laminations, injection structure and diapiric flame intrusions were identified at two intervals within the lake sediments. The normal faults with their strike showing near parallelism to the active Kaurik –Chango faults have also been identified within the lake sediments. Based on the identification of seismites and faults four episodes (ca. 7.8, 7.4, 6.5 and 6.1 cal ka) of neotectonic activity have been identified during the period of lake existence.

The paleoclimate reconstruction from Spiti valley was challenging as the clastic sediments do not contain organic proxies (organic matter, pollen, microfauna). The geochemistry of river sediment samples is related to the petrology of the catchment area and does not provide any direct palaeoenvironment information. However, the monitoring of modern sedimentary processes for past decades in the region (Sharma et al., 1991; Bookhagen et al., 2005; Wulf et al., 2010) revealed that during abnormal monsoon years, when monsoon penetrates far into the otherwise arid orogen, increased discharge accompanied by intensified erosion and enhanced mean basin denudation rates results in higher contribution of coarser sediments to the river load. This useful parameter provided the

vital clue for palaeoclimate reconstruction in the Spiti valley. Based on lithological and sedimentological characterisation of sediments three different environmental stages were identified (i) Stage I: period of lake establishment (8.7-7.6 cal yr BP) with intermittent cold intervals during ~ 8.7 cal ka and 8.4-8.2 cal ka; (ii) Stage II (7.6–6.8 cal yr BP) is characterised by cool quiet water conditions with sediments settling mainly by suspension, indicating a weakened Indian summer monsoon, and (iii) Stage III (6.8–6.1 cal yr BP) comprises of well laminated sediments with frequent sand layers, turbidites, and increase in sedimentation rate pointing towards stronger Indian summer monsoon activity. The regional comparison of precipitation pattern during this time slice (6.8–6.1 cal yr BP) suggests existence of "break monsoon like" conditions that can cause heavy precipitation over northern India and NW Himalayas.

In contrast to the Spiti valley, the investigation of modern limnological processes and sediments in the Lonar lake yielded several environmentally sensitive proxies. The lake shows stratification with an anoxic bottom (below 4m water depth) layer. Hydrological data, in conjunction with spatial distribution of grain size and geochemistry of the catchment and surface lake sediments, indicates (i) Al is a proxy for surficial catchment erosion; (ii) evaporitic carbonates (trona, gaylussite) are proxies for drier conditions; (iii) Mn/Fe (low) is an indicator for anoxia; (iv) mode and median values of particle size spectra can be used to trace the major direction and energy of transport. The modern geochemistry and isotopic investigations of lake water and inflowing streams indicate that the balance between evaporation and input water (E/I ratio) controls the lake water and carbonate isotopic ($\delta^{18}O$ and δD) composition. This data provides the framework for palaeoclimate reconstruction from a 10m long core retrieved from this lake. The core encompasses the entire Holocene and is the first well dated, high resolution archive from the core monsoon zone of central India. Detailed geochemical and mineralogical investigations on the core sediments reveal stratigraphic variations in the distribution of authigenic carbonate minerals. The presence of evaporitic gaylussite crystals in two distinct zones 1.58 -4.22 m (555-2030 cal yr BP, upper zone) and 6.42-7.6 m (3895- 4660 cal yr BP, lower zone) indicates two prominent intervals of drier climates. In addition to the palaeoenvironmental implications of occurrence of primary gaylussite, isotopic ($\delta^{18}O$ and $\delta^{13}C$) studies carried out on the gaylussite crystals furnish additional information on lake eutrophication, persistent stratification, and carbon recycling in the lake during last ca. 1200 years.

One major advantage of my work that focussed on lake sediments from two different climate zones is that it demonstrated the potential of regional "snapshots" of specific time slices (e.g., Fig. 11 in Chapter 3) in reconstructing the long term persistence of extremes (e.g., floods). While not the final word on this topic, this technique clearly demonstrates that the regional differences in climate can provide useful clues to causal mechanisms of climate change.

7.2. Future perspectives

Although my research focused only on two sites, the regional Holocene overview presented in Chapters 1, 2 and 3 clearly indicates a high complex pattern of precipitation changes in the vast Indian region. This is not surprising considering that there are three sources of precipitation with different forcing mechanisms: the ISM (Arabian Sea and the Bay of Bengal), the NE monsoon, and the winter westerlies (Mediterranean). The complex interactions between these determine the hydrological changes over the continent. Future investigations aimed at understanding the past climate need to address the following issues:

1. Characterisation of precipitation sources during different forcing mechanisms (e.g., ENSO, IOD, breaks), possibly by (water) isotopic transects.

2. Monitoring to determine regional climate sensitivity of proxies and development of transfer functions for quantification of palaeodata.

3. Generation of a wider network of high resolution palaeodata and hydrological changes.

4. Closer interaction with the (palaeo) modeling community to understand forcing mechanisms of climate change as has been done for the East Asian monsoon region (Polanski et al., 2012).

Appendix

Appendix A_1: Pearson correlation coefficient matrix for the measured geochemical parameters

Variables	Lithogenics	Si	Ti	Al	Fe	Mn	Mg	Ca	Na	P	Total C	C_{org}	$CaCO_3$	C/N	$\delta^{13}C$
Lithogenics	**1**	0.552	0.696	0.792	s0.573	0.711	-0.762	-0.031	0.036	-0.703	-0.806	-0.676	-0.739	0.284	-0.197
Si	0.552	**1**	0.604	0.900	0.857	0.753	-0.640	-0.234	-0.067	-0.245	-0.732	-0.578	-0.750	0.595	-0.403
Ti	0.696	0.604	**1**	0.649	0.564	0.690	-0.549	-0.071	-0.087	-0.489	-0.592	-0.464	-0.613	0.433	-0.228
Al	0.792	0.900	0.649	**1**	0.749	0.747	-0.828	-0.166	0.013	-0.466	-0.837	-0.682	-0.811	0.551	-0.436
Fe	0.573	0.857	0.564	0.749	**1**	0.872	-0.602	-0.357	-0.085	-0.230	-0.692	-0.518	-0.771	0.406	-0.243
Mn	0.711	0.753	0.690	0.747	0.872	**1**	-0.513	-0.053	-0.300	-0.522	-0.642	-0.501	-0.670	0.327	-0.283
Mg	-0.762	-0.640	-0.549	-0.828	-0.602	-0.513	**1**	0.377	-0.335	0.309	0.795	0.635	0.800	-0.515	0.330
Ca	-0.031	-0.234	-0.071	-0.166	-0.357	-0.053	0.377	**1**	-0.367	-0.379	0.098	-0.162	0.616	0.035	-0.070
Na	0.036	-0.067	-0.087	0.013	-0.085	-0.300	-0.335	-0.367	**1**	0.247	-0.103	-0.062	-0.146	0.055	0.215
P	-0.703	-0.245	-0.489	-0.466	-0.230	-0.522	0.309	-0.379	0.247	**1**	0.560	0.581	0.274	-0.277	0.176
Total C	-0.806	-0.732	-0.592	-0.837	-0.692	-0.642	0.795	0.098	-0.103	0.560	**1**	0.943	0.693	-0.502	0.194
C_{org}	-0.676	-0.578	-0.464	-0.682	-0.518	-0.501	0.635	-0.162	-0.062	0.581	0.943	**1**	0.413	-0.482	0.150
$CaCO_3$	-0.739	-0.750	-0.613	-0.811	-0.771	-0.670	0.800	0.616	-0.146	0.274	0.693	0.413	**1**	-0.329	0.204
C/N	0.284	0.595	0.433	0.551	0.406	0.327	-0.515	0.035	0.055	-0.277	-0.502	-0.482	-0.329	**1**	-0.531
$\delta^{13}C$	-0.197	-0.403	-0.228	-0.436	-0.243	-0.283	0.330	-0.070	0.215	0.176	0.194	0.150	0.204	-0.531	**1**

Appendix A_2: Organic carbon, total nitrogen and $\delta^{13}C$ of plankton, plants and soils from the Lonar crater.

Samples	C_{org} (wt. %)	N_{tot} (wt. %)	C_{org}/N_{tot}	$\delta^{13}C_{org}$ (‰)
Plankton	21.51	2.53	10.6	-8.46
Prosopis sp.	46.12	1.47	36.6	-27.02
Musa spp.	40.42	2.57	18.3	-26.33
Annona squamosa	44.08	2.49	20.7	-30.01
Justicia adhatoda	44.23	2.65	19.5	-28.77
Acacia nilotica	45.32	1.86	28.4	-29.73
Cassia auriculata	51.35	3.34	17.9	-29.58
Heteropogon spp.	40.25	0.84	55.9	-12.26
Cyperaceae	42.81	1.52	32.9	-28.20
Soil Lon-77	0.13	0.00	97.95	-19.22
Soil Lon-78	0.31	0.02	22.57	-24.91
Soil Lon-79	0.88	0.08	12.56	-24.12
Soil Lon-80	1.27	0.12	11.95	-24.52
Soil Lon-81	1.10	0.11	11.53	-26.69
Soil Lon-82	2.38	0.23	12.21	-24.32
Soil Lon-83	0.77	0.25	3.61	-23.87
Soil Lon-84	0.27	0.09	3.57	-24.28
Soil Lon-85	0.16	0.04	4.17	-18.27
Soil Lon-86	0.53	0.10	6.40	-24.96
Soil Lon-87	0.17	0.07	2.91	-18.13
Soil Lon-88	0.06	0.03	2.55	-20.92
Soil Lon-89	0.55	0.02	29.51	-23.40
Soil Lon-93	0.25	0.02	14.72	-18.28
Soil Lon-38V	1.25	0.12	12.2	-25.23
Soil RSV	1.24	0.11	13.2	-20.51
Soil Lon-41V	1.21	0.11	12.8	-25.98
Soil Lon-44V	1.34	0.35	4.5	-22.65
Soil Lon-45V	1.27	0.14	10.6	-23.39

Appendix A_3: Factor loadings for the geochemical parameters along F1 and F2 axis.

	F1	**F2**
Lithogenics	0.303	0.087
Si	0.308	-0.072
Ti	0.267	0.081
Al	0.336	-0.019
Fe	0.294	-0.126
Mn	0.293	0.120
Mg	-0.298	0.210
Ca	-0.067	0.617
Na	0.002	-0.443
P	-0.195	-0.430
Total C	-0.321	-0.030
C_{org}	-0.268	-0.174
$CaCO_3$	-0.298	0.294
C/N	0.208	0.074
$\delta^{13}C$	-0.136	-0.144

Appendix A_4: a) Map of South Asia showing locations of investigated sites; b) Glacier dynamics; 1) Khumbu Himal (Barnard et al., 2006), 2) Mount Everest (Owen et al., 2009), 3) Ganesh Himal (Gayer et al., 2006), 4) Annapurna, Nepal (Zech et al., 2009), 5) Upper Bhagirathi valley, Garhwal Himalaya (Barnard et al., 2004) 6) Nanga Parbat (Philips et al., 2000), 7) Muztag Ata and Kongur Shan (Seong et al., 2009). Red dotted line represent observed cold period in the Spiti valley.

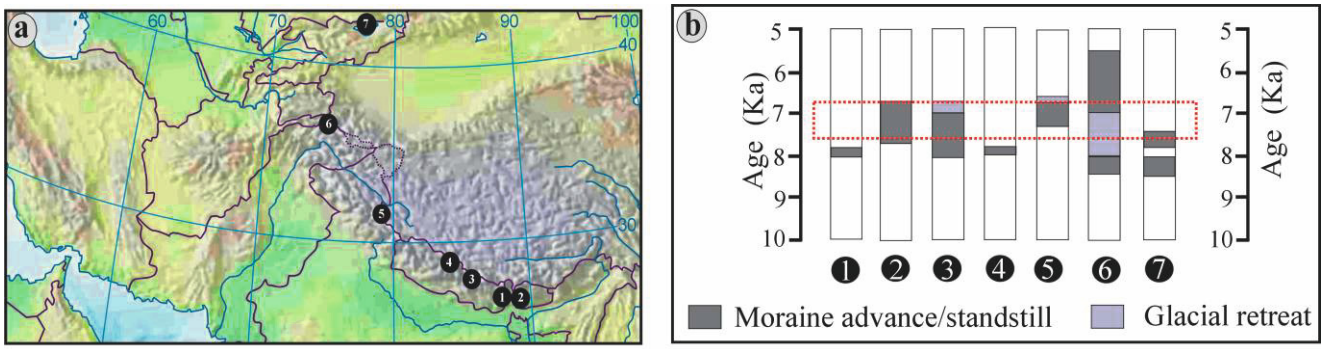

Bibliography

Abram, N. J., Gagan, M.K., Liu, Z., Hantoro, W.S, McCulloch, M.T, Suwargadi, B.W., 2007. Seasonal characteristics of the Indian Ocean Dipole during the Holocene epoch. Nature 445, 299–302.

Allen, J.R.L., 1973. A classification of climbing-ripple cross- lamination. Journal of Geological Society of London 129, 537–541.

Alley, R.B., Mayewski, P.A., Sowers, T., Stuiver, M., Taylor, K.C., Clark, P.U., 1997. Holocene climatic instability: A prominent, widespread event 8,200 years ago. Geology 25, 483-486.

An, Z., Porter, S.C., Kutzbach, J.E., Wu, X., Wang, S., Liu, X., Li, X., Zhou, W., 2000. Asynchronous Holocene optimum of the East Asian monsoon. Quaternary Science Reviews 19, 743–762.

Anoop, A., Prasad, S., Basavaiah, N., Brauer, A., Shahzad, F., Deenadayalan K., 2012. Tectonic versus climate influence on landscape evolution: a case study from the upper Spiti valley, NW Himalaya. Geomorphology 32-44, 145-146.

Ashok, K., Guan, Z., Saji, N.H., Yamagata, T., 2004. On the individual and combined influence of the ENSO and the Indian Ocean Dipole on the Indian Summer Monsoon. Journal of Climate 17, 3141–3154.

Baartman, J.E.M., Veldkamp, A., Schoorl, J.M., Wallinga, J., Cammeraat, L.H, 2011. Unravelling Late Pleistocene and Holocene landscape dynamics: The Upper Guadalentín Basin, SE Spain 9. Geomorphology 125, 172-185.

Babar, M.D., 2010. Geology, Microecological Environment and Conservation of Lonar Lake, Maharashtra, India. In: Sarkar, S., (ed.), Environmental Management. Sciyo Publications, Croatia, pp. 241-257.

Badve, R.M., Kumaran, K.P.N., Rajshekhar, C., 1993. Eutrophication of Lonar lake, Maharashtra. Current Science 65, 347-351.

Bagati, T. N., Thakur, V.C., 1993. Quaternary basins of Ladakh and Lahaul-Spiti in north western Himalaya. Current Science 64, 898-903.

Bamzai, A.S., Shukla, J., 1999. Relation between Eurasian Snow Cover, Snow Depth, and the Indian Summer Monsoon: An Observational Study. J. Climate 12, 3117–3132.

Barnard, P.L., Owen, L.A., Sharma, M.C., Finkel, R.C., 2001. Natural and human-induced landsliding in the Garhwal Himalaya of northern India. Geomorphology 40, 21–35.

Basavaiah, N., 2011. Experimental Geomagnetism, in Geomagnetism: Solid Earth and Upper Atmosphere Perspectives. Springer, Netherlands.

Basavaiah, N., Khadkikar, A.S., 2004. Environmental magnetism and its application towards palaeomonsoon reconstruction. Journal of Indian Geophysical Union 8, 1–14.

Behera, S.K., Krishnan, R., Yamagata, T., 1999. Unusual ocean-atmosphere conditions in the tropical Indian ocean during 1994. Geophys Res Lett., 26, 3001–3004.

Bhargava, O.N., 1990. Holocene tectonics south of the Indus Suture, Lahaul-Ladakh Himalaya, India: a consequence of Indian Plate motion. Tectonophysics 174, 315- 320.

Bhargava, O.N., Bassi, U.K., 1998. Geology of Spiti–Kinnaur Himachal Himalaya. Geological Survey of India Memoir 124, 1–210.

Bhattacharayya, A., Ranhotra, P.S., Shah, S.K., 2006. Temporal and spatial aspects of western Himalayan climate and their implication to monsoon dynamics. Journal of Geological Society of India 68, 507–515.

Bhattacharayya, A., Ranhotra, P.S., Gergan J.T., 2011. Vegetation vis-a-vis climate and glacier history during 12,400 to 5,400 BP from Dokriani valley, Garhwal Himalaya, India. Journal of Geological Society of India 77, 401–408.

Bhojvaid, P.P., Timmer, V.R., 1998. Soil dynamics in an age sequence of *Prosopis juliflora* planted for sodic soil restoration in India. Forest Ecology and Management 106, 181-193.

Bischoff, J.L., Herbst, D.B., Rosenbauer, R.J., 1991. Gaylussite formation at Mono Lake, California, USA. Geochim Cosmochim Acta 55, 1743–1747.

Björck, S., Wohlfarth, B., 2001. ^{14}C chronostratigraphictechniques in paleolimnology. In: Last, W.M., Smol, J.P. (Eds.), Tracking environ- mental change using lake sediments: basin analysis, coring, and chronological techniques 1, 205–245.

Blanford H.F., 1886. Rainfall of India. Mem. India Meteorol. Dep., 2, 217–448.

Bond, G., Showers, W., Cheseby, M., Lotti, R., P. Almasi, P., DeMenocal, P., Priore, P., Cullen, H., I. Hajdas I., Bonani, G., 1997. A pervasive millennial-scale cycle in North Atlantic Holocene and glacial climates. Science 278, 1257–1266.

Bookhagen, B., Burbank, D.W., 2010. Towards a complete Himalayan hydrological budget: The spatiotemporal distribution of snow melt and rainfall and their impact on river discharge. Journal of Geophysical Research-Earth Surface 115, 1-25.

Bookhagen, B., Thiede, R.C., Strecker, M.R., 2005. Late Quaternary intensified monsoon phases control landscape evolution in the northwest Himalaya. Geology 33, 149–152.

Bookhagen, B., Fleitmann, D., Nishiizumi, K., Strecker, M.R., Thiede, R.C., 2006. Holocene Monsoonal dynamics and fluvial terrace formation in the northwest Himalaya, India. Geology 34, 601-604.

Borgaonkar, H.P., Pant, G.B., Rupa Kumar, K., 1996. Ring-width variations in Cedrusdeodara and its climatic response over the western Himalaya. Int. J. Climatol. 16, 1409–1422.

Bronk Ramsey, C., 2001. Development of the radiocarbon calibration program OxCal. Radiocarbon 43, 355–363.

Bronk Ramsay, C., 2008. Deposition models for chronological records. Quaternary Science Reviews 27, 42–60.

Bronk Ramsey, C., 2009. Bayesian analysis of radiocarbon dates. Radiocarbon 51, 337–360.

Bryson, R.A., Swain, A.M., 1981. Holocene variations of monsoon rainfall in Rajasthan. Quat. Res. 16, 135 – 145.

Burkhardt, B., Israelson, C., Seaman, P., Stockmann, G., 2001. Ikaite tufa towers in Ikka Fjord, Southwest Greenland: their formation by mixing of seawater and alkaline spring water. J Sedimentary Res 71, 176–189.

Burbank, D. W., Anderson, R. S., 2000. Tectonic Geomorphology. Blackwell Scientific, Oxford.

Burns, S.J., Fleitmann, D., Mudelsee, M., Neff, U., Mangini, A., Matter, A., 2002. A 780-year annually resolved record of Indian Ocean monsoon variation in a speleothem from south Oman. Journal of Geophysical Research-Atmospheres 107, art. no. 4434.

Burns, S.J., Matter, A., Norbert, F., Mangini, A., 1998. Speleothem-based paleoclimate record from northern Oman. Geology 26, 499–502

Chakrabarti, R., Basu, A.R., 2006. Trace element and isotopic evidence for Archean basement in the Lonar crater impact breccia, Deccan volcanic province. Earth and Planetary Science Letters 247, 197–211.

Chakraborty, S., Bhattacharayya, S.K., Ranhotra, P.S., Bhattacharayya, A., Bhushan R., 2006. Palaeoclimatic scenario during Holocene around Sangla valley, Kinnaur, northeast Himalaya based on multiproxy records. Current Science 91, 777–782.

Charney, J. G., 1969. The intertropical convergence zone and the Hadley circulation of the atmosphere. Proc. WMO/IUCG Symp. Numer.Weather Predict. Jpn. Meteorol. Agency III: 73–79.

Chauhan M.S., Sharma, C., Rajagopalan G., 1997. Vegetation and climate during Late Holocene in Garhwal Himalaya. Palaeobotanist 46, 211–216.

Chauhan, M.S., Mazari, R.K., Rajagopalan, G., 2000. Vegetation and climate in upper Spiti region, Himachal Pradesh during late Holocene. Current Science 79, 373-377.

Chen, F., Yu, Z., M. Yanag, M., Ito, E., Wang, S., Madsen, D.B., Huang, X., Zhao, Y., Sato, T., Birks, J.B., Boomen, I., Chen, J., An, C., Wünnemann, B., 2008. Holocene moisture evolution in arid central Asia and its out-of-phase relationship with Asian monsoon history. Quaternary Sciences Review 27, 351–364.

Choudhary, P., Routh, J., Chakrapani, G.J., 2009. Comparison of bulk organic matter characteristics in sediments of three Kumaun Himalayan lakes. Current Science 97, 572-575.

Chung, F.H., 1974. Quantitative interpretation of X-ray diffraction patterns of mixtures: II. Adiabatic principles of X-ray diffraction analysis of mixtures. Journal of Applied Crystallography 7, 526-531.

Ciferri, O., Tiboni, O., 1985. The Biochemistry and Industrial Potential of Spirulina. Annual Review of Microbiology 39, 503-526.

Clemens, S., Prell, W., Murry, D., Shimmield, G., Weedon, G., 1991. Forcing mechanisms of the Indian Ocean monsoon. Nature 353, 720-726.

Cobb, K.M., Charles, C.D., Cheng, H., 2003. El Nino/Southern Oscillation and tropical Pacific climate during the last millennium. Nature 424, 271–276.

Cohen, J., Entekhabi, D., 2001. The influence of snow cover on Northern Hemisphere climate variability. Atmosphere–Ocean 39, 35–53.

Cox R.T., 1994. Analysis of drainage basin symmetry as a rapid technique to identify areas of possible quaternary tilt block tectonics: an example from the Mississippi embayment. Geological Society of America Bulletin 106, 571 – 581.

Cox, R.T., Van Arsdale, R.B., Harris, J.B., 2001. Identification of possible Quaternary deformation in the northeastern Mississippi Embayment using quantitative geomorphic analysis of drainage-basin asymmetry. Geological Society of America Bulletin 113, 615–624.

Craig, H., Gordon, L.I., 1965. Deuterium and oxygen-18 variations in the ocean and the marine atmosphere. In Proceedings of a Conference on Stable Isotopes in Oceanographic Studies and Paleotemperatures, Tongiorgi E, (eds). Spoleto, Italy; 9–130.

Cruz, R.V., Harasawa, H., Lal, M., Wu, S., Anokhin, Y., Punsalmaa, B., Honda, Y., Jafari, M., Li, C., Huu Ninh N., Asia, 2007. In: Climate change 2007: impacts, adaptation and vulnerability. In: Climate change 2007: impacts, adaptation and vulnerability. Contribution of Working Group II to the Fourth Assessment Report of the Intergovernmental Panel on Climate Change. ML Parry, OF Canziani, JP Palutikof, PJ van der Linden, CE Hanson. Eds. Cambridge: Cambridge University Press, pp. 469-506.

Dash, S.K., Singh, G.P., Shekhar, M.S., Vernekar, A.D., 2005. Response of the Indian summer monsoon circulation and rainfall to seasonal snow depth anomaly over Eurasia. Climate Dynamics 24, 1–10.

Delcaillau, B., Deffontaines, B., Floissac, L., Angelier, J., Deramond, J., Souquet, P., Chu, H.T., Lee, J.F., 1998. Morphotectonic evidence from lateral propagation of active frontal fold; Pakuashan anticline, foothills of Taiwan.Geomorphology 24, 263–290.

Demske, D., Tarasov, P.E., Wünnemann, B., Riedel, F., 2009. Late glacial and Holocene vegetation, Indian monsoon and westerly circulation in the Trans-Himalaya recorded in the lacustrine pollen sequence from Tso Kar, Ladakh, NW India. Palaeogeography, Palaeoclimatology, Palaeoecology 279, 172–185.

Deshmukh, S.K., Verekar, S.A., 2006. Keratinophilic fungi from the vicinity of meteorite crater soils of Lonar (India). Mycopathologia 162, 303-306.

Deuser, E.G., Degens, E.T., Guillard, R.R.L., 1968. Carbon isotope relationships between plankton and seawater. Geochimica et Cosmochimica Acta 32, 657–660.

Deuser, W.G., Degens, E.T., 1967. Carbon isotope fractionation in the system CO_2 (gas)-CO_2(aqueous)-HCO_3^-(aqueous). Nature 215, 1033-1035.

Dhar, O.N., Soman, M.K., Mulye, S.S., 1984. Rainfall over the southern slopes of the Himalayas and the adjoining plains during breaks in the monsoon. Journal of Climatology 4, 671-676.

Dickson, R. R., 1984. Eurasian snow cover versus Indian monsoon rainfall - An extension of the Hahn- Shukla results. J. Clim. Appl. Meteorol., 23, 171-173.

Dixit, S., Bera, S.K., 2012. Holocene climatic fluctuations from Lower Brahmaputra flood plain of Assam, northeast India J. Earth Syst. Sci., 121,135-147.

Dortch, J., Owen, L.A., Haneberg, W.C., Caffee, M.W., Dietsch, C., Kamp, D.U., 2009. Nature and timing of large-landslides in the Himalaya and Transhimalaya of northern India. Quaternary Science Reviews 28, 1037–1054.

Drummond, C.N., Patterson, W.P., Walker, J.C., 1995. Climate forcing of carbon-oxygen isotopic covariance in temperate-region marl lakes. Geology 23, 1031–1034.

ECONET, 1999. Rapid environmental assessment and the conservation and management plan for Lonar crater, Buldhana. Final Report, Maharashtra Tourism Development Corporation, Mumbai, pp 132.

Ellison, C. R. W., Chapman, M. R., Hall, I. R., 2006. Surface and deep ocean interactions during the cold climate event 8200 years ago. Science 312, 1929–1932.

Ely, L.L., Enzel, Y., Baker, V.R., Kale, V.S., Mishra, S., 1996. Changes in the magnitude and frequency of late Holocene monsoon floods on the Narmada River, central India. Geological Society American Bulletin 108, 1134–1148.

Enzel, Y., Ely, L.L., Mishra, S., Ramesh, R., Amit, R., Lazar, B., Rajaguru, S.N., Baker, V.R., Sandler, A., 1999. High-resolution Holocene environmental changes in the Thar Desert, northwestern India. Science 284, 125-128.

Eugster, H.P, Hardie, L.A., 1978. Saline lakes. In Lakes: Chemistry, Geology, Physics, Saline lakes, Lerman A (eds). Springer: New York; 237–293.

Farquhar, G.D., 1983. On the nature of carbon isotope discrimination in C4 species. Australian Journal of Plant Physiology 10,205–26.

Fleitmann, D., Burns, S.J., Neff, U., Mudelsee, M., Mangini, A., Matter, A., 2004. Palaeoclimatic interpretation of high-resolution oxygen isotope profiles derived from

annually laminated speleothems from Southern Oman. Quaternary Science Review 23, 935-945.

Fleitmann, D., Burns, S. J., Mudelsee, M., Neff, U., Kramers, J., Mangini, A., Matter A., 2003. Holocene forcing of the Indian monsoon recorded in a stalagmite from southern Oman. Science 300, 1737–1739.

Fontes, J.C., Gasse, F., Gibert, E., 1996. Holocene environmental changes in Bangong Co Basin (Western Tibet): Part 1. Chronology and stable isotopes of carbonates of a Holocene lacustrine core. Palaeogeography, Palaeoclimatology, Palaeoecology 120, 25–47.

Fredriksson, K., Dube, A., Milton, D.J., Balasundaram, M.S., 1973. Lonar Lake, India: An impact crater in basalt. Science 180, 862-864.

Fuchs, G., 1982. The Geology of the Pin Valley in Spiti, H. P., India. Jahrbuch der Geologischen Bundesanstalt Wien 124, 325–359.

Fuchs, M., Lang, A., 2009. Luminescence dating of hillslope deposits - a review. Geomorphology 109, 17-26.

Fudali, R.F., Milton, D.J., Fredriksson, K., Dube, A., 1980. Morphology of Lonar crater, India: Comparisons and implications. The Moon and the Planets 23, 439-515.

Gadgil S., 2007. The Indian Monsoon: Physics of the monsoon. Resonance 12, 4–20.

Gadgil, S., 2003. The Indian Monsoon and its Variability. Annual Review of Earth and Planetary Sciences 31, 429-467.

Garrote, J., Cox, R.T., Swann, C., Ellis, M., 2006.Tectonic geomorphology of the southeastern Mississippi Embayment in northern Mississippi, USA. Geological Society of America Bulletin 118, 1160 - 1170.

Gasse, F., Van Campo, E., 1994. Abrupt post-glacial climate events in West Asia and North Africa monsoon domains. Earth and Planetary Science Letters 126, 435-456.

Gasse, F., Fontes, J.Ch., Van Campo, E., Wei, K., 1996. Holocene environmental changes in Bangong Co basin (western Tibet). Part 4: discussions and conclusions Palaeogeography, Palaeoclimatology, Palaeoecology 120, 79–82

Ghosh, S., Das, D., Kao, S.C., Ganguly, A.R., 2011. Lack of uniform trends but increasing spatial variability in observed Indian rainfall extremes. Nature Climate Change 2, 86-91.

Gibson, J.J., Edwards, T.W.D., Bursey, G.G., Prowse, T.D., 1993. Estimating evaporation using stable isotopes: quantitative results and sensitivity analysis for two catchments in northern Canada. Nordic Hydrology 24, 79-94.

Gilbert, R., 1975. Sedimentation in Lillooet Lake, British Columbia. Canadian Journal of Earth Sciences 12, 1697–1711.

Goreau, T.J., 1977. Seasonal variations of trace metals and stable isotopes in coral skeleton: physiological and environmental controls. Proc 3rd Int Coral Reef Symp 2, 425-430.

Goswami, B. N., 2005. South Asian Summer Monsoon: An overview: in the global Monsoon System: Research and Forecast Edited by C.-P. Chang, Bin Wang, Ngar-Cheung Gabriel Lau, Chapter 5, pp 47.

Goswami, B.N., Vengugopal, V., Sengupta, D., Madhusoodanan, M.S, Xavier, P.K., 2006. Increasing trend of extreme rain events over India in a warming environment. Science 314, 1442-1445.

Gupta, A.K., Anderson, D.M., Overpeck, J.T., 2003. Abrupt changes in the Asian southwest monsoon during the Holocene and their links to the North Atlantic Ocean. Nature 421, 354–357.

Gupta, A.K., Das, M., Anderson D.M., 2005. Solar influence on the Indian summer monsoon during the Holocene. Geophys. Res. Lett., 32, L17703.

Hardie, L.A., Eugster, H.P., 1970. The evolution of closed-basin brines. In 50th Anniversary Symposia: Mineralogy and Petrology of the Upper Mantle; Sulfides; Mineralogy and Geochemistry of Non-Marine Evaporites, Morgan BA (eds). Min. Soc. Am Spec. Paper No. 3: 273–290.

Hayden H.H., 1904. The geology of Spiti with parts of Bushahr and Rupshu. Geological Survey of India Memoir 6, 1–121.

Herrmann, M., Lu, X.M., Berking, J., Schütt.B., Yao, T.D., Mosbrugger, V., 2010. Reconstructing Holocene vegetation and climate history of Nam Co area (Tibet), using pollen and other palynomorphs. Quaternary International 218: 45–57.

Herzschuh, U., 2006. Paleo-moisture evolution in monsoonal central Asia during the last 50,000 years. Quaternary Science Reviews 25, 163–178.

Herzschuh, U., Winter, K., Wünnemann, B., Li, S., 2006. A general cooling trend on the central Tibetan Plateau throughout the Holocene recorded by the Lake Zigetang pollen spectra. Quaternary International 154-155, 113–121.

Hintersberger, E., Thiede, R.C., Strecker, M.R., Hacker, B., 2010. E-W extension in the Northwestern Himalaya, NW India. GSA Bulletin 122, 1499-1515.

Holbrook, J., Schumm, S.A., 1999. Geomorphic and sedimentary response of rivers to tectonic deformation: a brief review and critique of a tool for recognising subtle epeirogenic deformation in modern and ancient settings. Tectonophysics 305, 287–306.

Hollander, D.J., Mckenzie, J.A., 1991. CO_2 control on carbon-isotope fractionation during aqueous photosynthesis: A paleo-pCO_2 barometer. Geology 19, 929-932.

Hollander, D.J., Smith, M.J., 2001. Microbially mediated carbon cycling as a control of the $\delta^{13}C$ of sedimentary carbon in eutrophic Lake Mendota (USA): new models for isotopic excursions in the sedimentary record. Geochim. Cosmochim. Acta 65, 4321–4337.

Hollander, D.J., Mckenzie, J.A., Hsu, K.J., Huc, A.Y., 1993. Application of an eutrophic lake model to the origin of ancient organic-carbon-rich sediments. Global Biogeochem.Cycles 7, 157–179.

Hong, Y.T., Hong, B., Lin, Q.H., Zhu, Y. X., Shibata, Y., Hirota, M., Uchida, M., Leng, X. T., Jiang, H.B., Xu, H., Wang, H. and Yi, L., 2003. Correlation between Indian Ocean summer monsoon and North Atlantic climate during the Holocene. Earth and Planetary Science Letters, 211, 371-380.

Hornung, T., Krystyn, L., Brandner, R., 2007. Tethys-wide mid-Carnian (Upper Triassic) carbonate productivity decline: evidence for the Alpine Reingraben Event from Spiti (Indian Himalaya)? Journal of Asian Earth Science 30, 285–302.

Hutchinson, G.E., Löffler, H., 1956. The thermal classification of lakes. Proceedings of the National Academy of Sciences of the United States of America 42, 84-86.

Jain, V., Sinha, R., 2005. Response of active tectonics on the alluvial Baghmati River, Himalayan foreland basin, eastern India. Geomorphology 70, 339-356.

Jha, M., 2003. A preliminary study of ecosystems and biodiversity in Lonar crater. Indian Forester 129, 1192-1200.

Jhingran, A.G., Rao, K.V., 1958. Lonar Lake and its Salinity. Records of the Geological Survey of India 85, 313-334.

Joseph, P.V., Srinivasan, J., 1999. Rossby waves in May and the Indian Summer Monsoon Rainfall. Tellus 51A, 854–864.

Joshi, A.A., Kanekar, P.P., Sarnaik, S., Kelkar, A.S., 2005. Bacterial diversity of Lonar lake ecosystem. In: Banmeru, P.K., Banmeru, S.K., Mishra, V.R. (eds.), Biodiversity of Lonar Crater. Anamaya, New Delhi, pp. 71-75.

Joshi, A.A., Kanekar, P.P., Kelkar, A.S., Sarnaik, S., Shouche, Y.S., Wani, A., 2007. Moderately halophilic, alkalitolerant *Halomas campisalis* MCM B-365 from Lonar Lake India. Journal of Basic Microbiology 47, 213-221.

Joshi, A.A., Kanekar, P.P., Kelkar, A.S., Shouche, Y.S., Vani, A.A., Borgave, S.B., Sarnaik, S., 2008. Cultivable bacterial diversity of alkaline Lonar lake, India. Microbial Ecology 55, 163-172.

Juyal, N., Pant, R.K., Basavaiah, N., Yadava, M.G., Saini, N.K., Singhvi, A.K., 2004. Climate and seismicity in the higher Central Himalaya during 20-10 ka: evidence from the Garbyang basin, Uttaranchal, India. Palaeogeography, Palaeoclimatology, Palaeoecology 213, 315-330.

Kanekar, P.P., Joshi, A.A., Kelkar, A.S., Borgave, S.B., Sarnaik, S.S., 2008. Alkaline Lonar lake, India – A treasure of alkaliphilic and halophilic bacteria. In: Sengupta, M. and Dalwani, R. (eds.): Proceedings of Taal2007: The 12th World Lake Conference, pp 1765-1774

Kaplan, A., 1981. Photoinhibition in Spirulina platensis: Response of Photosynthesis and HCO_3^- Uptake Capability to CO_2-Depleted Conditions. Journal of Experimental Botany 32, 669-677.

Kar, R., Ranhotra, P.S., Bhattacharyya, A., Sekar, B., 2002. Vegetation vis-à-vis climate and glacial fluctuations of the Gangotri glacier since the last 2000 years. Current Science 82, 347-351.

Khatri, K.N., Rai, K., Jain, A.K., Sinvhal, H., Gaur, V.K., Mithal, R.S., 1978. The Kinnaur earthquake, Himachal Pradesh India of 19 January, 1975. Tectonophysics 49, 1–21.

Kirby, E., Whipple, K.X., Tang, W., Chen, Z., 2003. Distribution of active rock uplift along the eastern margin of the Tibetan Plateau: inferences from bedrock channel longitudinal profiles. Journal of Geophysical Research 108, 2217.

Kotlia, B.S., Sanwal, J., Phartiyal, B., Joshi L.M., Trivedi, A., Sharma, C., 2010. Late Quaternary climatic changes in the eastern Kumaun Himalaya, India, as deduced from multi-proxy studies. Quaternary International 21344-55.

Kramer, A., Herzschuh, U., Mischke, S., Zhang, C.J., 2009. Holocene treeline shifts and monsoon variability in the Hengduan Mountains (southeastern Tibet Plateau) implications from palynological investigations. Palaeogeography, Palaeoclimatology, Palaeoecology 286, 23–41

Kripalani, R.H., Kulkarni, A., Singh, S. V., 1997. Association of the Indian summer monsoon with the Northern Hemisphere mid-latitude circulation. Int. J. Climatol., 17, 1055–1067.

Krishna Kumar, K., Rajagopalan, B., Cane, M.A., 1999. On the weakening relationship between the Indian monsoon and ENSO. Science 287, 2156–2159.

Krishnamurti T.N., Bhalme H.N., 1976. Oscillation of a monsoon system, Part I: observational aspects. J. Atmos. Sci., 33, 1937-1954.

Krishnan, R., Sugi, M., 2001. Baiu rainfall variability and associated monsoon teleconnections. Journal of Meteorological Society of Japan 79, 851-860.

Krishnan, R., Zhang, C., Sugi, M., 2000. Dynamics of breaks in the Indian summer monsoon. Journal of Atmospheric Sciences 57, 1354-1372.

Krishnan, R., Vinay Kumar, V., Sugi M., Yoshimura J., 2009. Internal feedbacks from monsoon-midlatitude interactions during droughts in the Indian summer monsoon. Journal of Atmospheric Sciences 66, 553-578.

Krishnan, R., Sundaram, S., Swapna, P., Kumar, V., Ayantika, D.C., Mujumdar, M., 2011. The crucial role of ocean-atmosphere coupling on the Indian monsoon anomalous response during dipole events. Climate Dynamics 37, 1-17.

Kucharski, F., Bracco, A., Yoo, J. H., Molteni, F., 2007. Low-frequency variability of the Indian monsoon-ENSO relationship and the tropical Atlantic: The "Weakening" of the 1980s and 1990s. Journal of Climate 20, 4255-4266.

Kuenen, P.H., 1958. Experiments in geology. Trans. Geol. Soc. Glasgow 23, 1–28.

Kumar, R., Bagati, T.N., Mazari, R. K., 1994. Uplifted Late Quaternary Debris Fan in the Upper Spiti Valley (H.P.) and its Environmental Significance. Journal of Geological Society of India 43,603 – 611.

Land, L.S., 1980. The isotopic and trace element geochemistry of dolomite: the state of the art. In Concepts and Models of Dolomitization Zenger, D.H., Dunham, J.B., Ethington, R.L., (eds). SEPM Spec. Publ., 28:87–110.

LaTouche, T.H.D., Christie, W.A.K., 1912. The Geology of the Lonar Lake. With a Note on the Lonar Soda Deposit by Christie W.A.K., Rec. Geol. Surv. India 36: 235-263.

Leeder, M., 1999.Sedimentology and Sedimentary Basins. From Turbulence to Tectonics. Oxford: Blackwell Science.

Leemann, A., Niessen, F., 1994. Varve formation and the climatic record in an Alpine proglacial lake: calibrating annually-laminated sediments against hydrological and meteorological data. Holocene 4, 1-8.

Lei, Y., Yao, T., Sheng, Y., Zhang, E., Wang, W., Li, J., 2011. Characteristics of $\delta\ ^{13}C_{DIC}$ in lakes on the Tibetan Plateau and its implications for the carbon cycle. Hydrological Processes 26, 535–543.

Leng, M.J., Marshall, J.D., 2004. Palaeoclimate interpretation of stable isotope data from lake sediment archives. Quaternary Science Reviews 23, 811–831.

Leng, M.J, Lamb, A.L., Heaton, T.H.E., Marshall, J.D., Wolfe, B.B., Jones, M.D., Holmes J.A., Arrowsmith, C., 2006. Isotopes in lake sediments. In Isotopes in Palaeoenvironmental Research, Leng, M. J., (eds). Springer, Dordrecht: The Netherlands; 147-184.

Li, H.C., Ku, T.L., 1997. δ13C – δ18O covariance as a paleohydrological indicator for closed basin lakes. Palaeogeography, Palaeoclimatology, Palaeoecology 133, 69-80.

Loska, K., Wiechula, D., 2003. Application of principal component analysis for the estimation of source of heavy metal contamination in surface sediments from the Rybnik Reservoir. Chemosphere 51,723–733.

Lowe, D.R., 1975.Water escape structures in coarse-grained sediments. Sedimentology 22, 157–204.

Lowe D.R., Lo Piccolo R.D., 1974. The characteristics and origins of dish and pillar structures. Journal of Sedimentary Research 44, 484–501.

Malik, N., Bookhagen, B., Marwan, N., Kurths, J., 2011. Analysis of spatial and temporal extreme monsoonal rainfall over South Asia using complex network. Climate Dynamics.

Maloof, A.C., Stewart, S.T., Weiss, B.P., Soule, S.A., Swanson-Hysell, N., Louzada, K.L., Poussart, P.M., Garrick-Bethell, I., 2009. Geology of Lonar Crater, India. GSA Bulletin 122, 109-126.

Malu, R.A., 2001. Phytoplankton diversity in Lonar lake. Environment and Ecology 19, 244-246.

Mamgain, A., Dash S.K., ParthSarthi, P., 2010. Characteristics of Eurasian snow depth with respect to Indian summer monsoon rainfall. Meteorology and Atmospheric science 110, 71-83.

Mangili, C., Plessen, B., Wolff, C., Brauer, A., 2010. Climatic implications of annual to decadal resolution stable isotope data from calcite varves of the Piànico interglacial lake record, Southern Alps. Global and Planetary Change 71, 168-174.

McConnaughey, T.A., LaBaugh, J.W., Rosenberry, D.O., Striegl, R.G., Reddy, M.M., Schuster, P.F., Carter, V., 1994. Carbon budget for a groundwater-fed lake: calcification supports summer photosynthesis. Limnol Oceanogr 39, 1319–1332.

McManus, J., 1988. Grain size determination and interpretation. In: Tucker, M.E. (ed.), Techniques in Sedimentology, Blackwell, Oxford pp. 63-85.

Meckler, A.N., Schubert, C.J., Cowie, G.L., Peiffer, S., Dittrich, M., 2004. New organic matter degradation proxies: Valid in lake systems? Limnology and Oceanography 49, 2023–2033.

Mees, F., Reyes, E., Keppens, E., 1998. Stable isotope chemistry of gaylussite and nahcolite from the deposits of the crater lake at Malha, northern Sudan. Chemical Geology 146, 87-98.

Mees, F., Verschuren, D., Nijs, R., Dumont, H., 1991. Holocene evolution of the crater lake at Malha, Northwest Sudan. Journal of Paleolimnology 5, 227–253.

Meyers, P.A., 1997. Organic geochemical proxies of palaeogeographic, paleolimnologic, and paleoclimatic processes. Org. Geochem. 27, 213–250.

Meyers, P.A., Lallier-Verges, E., 1999. Lacustrine sedimentary organic matter records of late Quaternary paleoclimates. J Paleolimnol 21, 345–372.

Miller, A.G. 1990. Inorganic carbon transport and accumulation in cyanobacteria. In: Codd, G.A., Dijkhuizen, L., Tabita, F.R., (eds.), Autotrophic microbiology and one-carbon metabolism. Kluwer Academic, Dordrecht, The Netherlands, pp. 25-53.

Milton, D.J., Dube, A., and Sengupta, S.S., 1975. Deposition of ejecta at Lonar crater. Meteoritics 10, 456-457.

Mischke, S., Zhang, C, 2010. Holocene cold events on the Tibetan Plateau. Global and Planetary Change 72, 155-163.

Misra, S., Arif, M.D., Basavaiah, N., Srivastava, P.K., Dube, A., 2010. Structural and anisotropy of magnetic susceptibility (AMS) evidence for oblique impact on terrestrial basalt flows: Lonar crater, India. GSA Bulletin 122, 563-574.

Mohindra, R., Bagati, T.N., 1996. Seismically induced soft-sediment deformation structures (seismites) around Sumdo in the lower Spiti valley (Tethys Himalaya). Sedimentary Geology 101, 69–83.

Mook, W.G., Brommerson, J.C., Staverman, W.H., 1974. Carbon isotope fractionation between dissolved bicarbonate and gaseous carbon dioxide. Earth and Planetary Science Letters 22, 169-176.

Moretti, M., Alfaro, P., Caselles, O., Canas, J.A., 1999. Modelling seismites with a digital shaking table. Tectonophysics 304, 369-383.

Morrill, C., Overpeck J.T., Cole, J.E., 2003. A synthesis of abrupt changes in the Asian summer monsoon since the last deglaciation. The Holocene 13, 465–476.

Morrill, C., Overpeck, J.T., Cole, J.E., Liu, K.B., Shen, C.M., Tang, L.Y., 2006. Holocene variations in the Asian monsoon inferred from the geochemistry of lake sediments in central Tibet. Quaternary Research 65, 232–243.

Müller, P.J., Suess, E., Ungerer, C.A., 1986. Amino acids and sugars of surface particulate and sediment trap material from waters of the Scotia Sea. Deep Sea Research 33, 819-838.

Mulder, T., Syvitski, J.P.M., Skene, K.I., 1998. Modelling of erosion and deposition by turbidity currents generated at river mouths. Journal of Sedimentary Research 68, 124-137.

Myrow, P. M., Thompson, K.R., Hughes, N.C., Paulsen, T.S., Sell, B.K., Parcha, S.K., 2006. Cambrian stratigraphy and depositional history of the northern Indian Himalaya, Spiti Valley, north-central India. Geological Society of America Bulletin 118, 491–510.

Naidu, A.S., Murali, A.V., Mowatt, T.C., 1990. Preliminary mineral analysis of the clay fraction of the red bole beds, Deccan Traps, India. Eos 71, 1713.

Nandy, N.C., Deo, V.B., 1961. Origin of the Lonar lake and its alkalinity. TISCO 8, 144-155.

Neff, U., Burns, S.J., Mangini, A., Mudelsee, M., Fleitmann, D., Matter, A., 2001. Strong coherence between solar variability and the monsoon in Oman between 9 and 6 ka ago. Nature 411, 290–293.

Obermeier, S.F., 1996. Using liquefaction-induced features for paleoseismic analysis Use of liquefaction-induced features for paleoseismic analysis — An overview of how seismic liquefaction features can be distinguished from other features and how their regional distribution and properties of source sediment can be used to infer the location and strength of Holocene paleo-earthquakes. Engineering Geology 44, 1-76.

O'Brien, S.R., Mayewski, P.A., Meeker, L.D., Meese, D.A., Twickler M.S., Whitlow, S.I., 1995. Complexity of Holocene climate as reconstructed from a Greenland ice core. Science 270, 1962–1964.

Overpeck J.T, Cole, J., 2007. Lessons from a distant monsoon. Nature 445, 270–271.

Overpeck J.T., Anderson, D.M., Trumbore S., Prell, W. L., 1996. The southwest monsoon over the last 18,000 years. Climate Dynamics 12, 213-225.

Owen, L.A., Gualtieri, L., Finkel, R.C., Caffee, M.W., Benn, D.I., Sharma, M.C., 2001. Cosmogenic radionuclide dating of glacial landforms in the Lahul Himalaya, northern India: defining the timing of late Quaternary glaciation. Journal of Quaternary Science 16, 555–563.

Owen, L.A., Kamp, U., Ghazanfar, U., Khattak, G.A., Harp, E.L., Keefer, D.K., Bauer, M.A., 2008. Landslides triggered by the 8 October 2005 Kashmir earthquake. Geomorphology 94, 1-9.

Pant G.B., Rupa Kumar, K., 1997. Climates of South Asia. John Wiley & Sons, Chichester, 320 pp.

Pendall, E.G., Harden, J.W., Trumbore, S.E., Chadwick, O.A., 1994. Isotopic approach to soil carbonate dynamics and implications for paleoclimatic interpretations. Quaternary Research 42, 60–71.

Perucca, L.P., Bracco, A.I., Moreiras, S.M., 2009. Determination of seismogenic structures and earthquake magnitud from seismites in the Acequion river, Precordillera Range, central-western Argentina. Journal of Iberian Geology 35, 5-18.

Peters, C., Thompson, R., 1998. Magnetic identification of selected natural iron oxides and sulphides. Journal of Magnetism and Magnetic Materials 183, 365-374.

Phadtare, N.R., 2000. Sharp decrease in summer monsoon strength 4000-3000 calyr B.P. in the Central Higher Himalaya of India based on pollen evidence from Alpine peat. Quaternary Research 53, 122-129.

Phartiyal, B., Kothyari, G C., 2012. Impact of neotectonics on drainage network evolution reconstructed from morphometric indices: case study from NW Indian Himalaya. Zeitschrift für Geomorphologie 56, 121 – 140.

Phartiyal, B., Sharma, A., Srivastava, P., Ray, Y., 2009. Chronology of relict lake deposits in the Spiti River, NW Trans Himalaya: Implications of Late Pleistocene–Holocene climate tectonic perturbations. Geomorphology 108, 264-272.

Picard, M.D., High L.R., 1972. Criteria for recognizing Lacustrine rocks. In: K.K. Rigby and W.K. Hambling, Editors, Recognition of Ancient Sedimentary rocks vol. 16, Society of Economic Geology, Paleontology and Mineralogy, pp. 108–145.

Ponton, C., Giosan, L., Eglinton, T.I., Fuller, D.Q., Johnson, J.E., Kumar, P., Collett T.S., 2012. Holocene aridification of India. Geophys. Res. Lett., 39, 1-6.

Prasad, S., Enzel, Y., 2006.Holocene palaeoclimates of India. Quaternary Research 66, 442-453.

Prasad, S., Gupta, S.K., 1999. Luminescence dating of a 54 m long core from Nal region, western India: Implications. Quaternary Science Reviews 18, 4195-1505.

Prasad, S., Negendank, J.F.W., 2004. Holocene palaeoclimate in the Saharo-Arabian Desert. In The Climate in Historical Times. Towards a Synthesis of Holocene Proxy Data and Climate Models, Fischer, H., Kumke, T., Lohmann, G., Flöser, G., Miller, H., von Storch, H., Negendank, J.F.W (eds.), Springer: Berlin; 209-228.

Prasad, S., Kusumgar, S., Gupta, S.K., 1997. A Mid – Late Holocene record of palaeoclimatic changes from Nal Sarovar: a palaeo-desert margin lake in Western India. Journal of Quaternary Science 12, 153-159.

Prasad, S., Witt, A., Kienel, U., Dulski, P., Bauer, E., Yancheva, G., 2009. The 8.2 ka event: evidence for seasonal differences and the rate of climate change in western Europe. Global and Planetary Changes 67, 218-226.

Quamar, M.F., Chauhan, M.S., 2012. Late Quaternary vegetation, climate as well as lake-level changes and human occupation from Nitaya area in Hoshangabad District, southwestern Madhya Pradesh (India), based on pollen evidence. Quaternary International 263, 104–113.

Rajeevan, M.S., Gadgil, S., Bhate, J., 2010. Active and break spells of the Indian summer monsoon. J. Earth Syst. Sci. 119, 229–247.

Rajendran, K., Kitoh, A., 2008. Indian summer monsoon in future climate projection by a super high resolution global model. Current Science 95, 1560-1569.

Rajendran, K., Kitoh, A., Mizuta, R., Sajani, S. and Nakazawa, T., 2008. High-resolution simulation of mean convection and its intraseasonal variability over the tropics in the MRI/JMA 20-km mesh AGCM. Journal of Climate 21, 3722-3739.

Ramaswamy, C., 1962. Breaks in the Indian summer monsoon as a phenomenon of interaction between the easterly and the subtropical westerly jet streams. Tellus 14A, 337–349.

Rankama, K., Sahama, T.G., 1964. Geochemistry. University of Chicago Press. Chicago.

Reddy, M.M., Hoch, A., 2011. Calcium Carbonate Nucleation in Alkaline Lake Surface Water, Pyramid Lake, Nevada, USA. Aquatic Geochemistry 18, 95-113.

Reimer, P. J., Baillie, M. G. L., Bard, E., Bayliss, A., Beck, J. W., Blackwell, P. G., Bronk Ramsey, C., Buck, C. E., Burr, G. S., Edwards, R. L., Friedrich, M., Grootes, P. M., Guilderson, T. P., Hajdas, I., Heaton, T. J., Hogg, A. G., Hughen, K. A., Kaiser, K. F., Kromer, B., McCormac, F. G., Manning, S. W., Reimer, R. W., Richards, D. A., Southon, J. R., Talamo, S., Turney, C. S. M., van der Plicht, J., Weyhenmeyer, C. E., 2009. IntCal09 and Marine09 radiocarbon age calibration curves, 0-50,000 years cal BP. Radiocarbon 51, 1111-1150.

Renaut RW, Tiercelin JJ, Owen RB. 1986. Mineral precipitation and diagenesis in the sediments of the Lake Bogoria basin, Kenya Rift Valley. In Sedimentation in the African Rifts, Frostick, L.E, Renaut, R.W., Reid, I, Tiercelin, J.J (eds), Spec. Publ. Geol. Soc. London 25; Blackwell Oxford; 159–175.

Riddols. A., 1985. Aspects of nitrogen fixation in Lough Neagh. II. Composition between *Aphanizomenon flos-aquae, Oscillatoria redekei* and *Oscillatoria agardhii*. Freshwater Biology 15, 299-306.

Ringrose, P.S., 1989. Paleoseismic (?) liquefaction events in late Quaternary lake sediment at Glen Roy, Scotland. Terra Nova 1, 57–62.

Rohling, E. J., Pälike H., 2005. Centennial-scale climate cooling with a sudden cold event around 8,200 years ago. Nature 434, 975–979.

Ropelewski, C.F., Halpert, M.S., 1987. Global and regional scale precipitation patterns associated with the El Nino/Southern Oscillation. Monthly Weather Review 115, 1606–1626.

Rosen, M.R., Miser, D.E., Starcher, M.A., Warren, J.K., 1989. Formation of dolomite in the Coorong region, South Australia. Geochim. Cosmochim. Acta 53, 661–669.

Ross J., Gilbert, R., 1999. Lacustrine sedimentation in a monsoon environment: the record from Phewa Tal, Middle Mountain region of Nepal. Geomorphology 27, 307–323.

Rozanski, K., Araguas-Araguas, L., Gonfiantini, R., 1993. Isotopic patterns in modern global precipitation. In Climate Change in Continental Isotopic Record Swart PK, Lohman, KL, McKenzie JA, Savin S (eds.), Geophysical Monograph 78, 1–37.

Saji, N.H., Goswami, B.N., Vinayachandran, P., Yamagata, T., 1999. A dipole mode in the tropical Indian ocean. Nature 401, 360–363.

Saraf, A.K., 2000. IRS-1C-PAN depicts Chamoli earthquake induced landslides in Garhwal Himalayas, India. Int. J. Remote Sensing 21, 2345–2352.

Satyanaraya, S., Chaudhari, P.R., 2007. Lonar Lake: A unique ecosystem rich in salinity tolerant phytoplankton community. 12th World Lake Conference, Oct 28 – Nov 2, 2007, Jaipur, Abstract No. SG5.

Schelske, C.L., Hodell, D.A., 1991. Recent changes in productivity and climate of Lake Ontario detected by isotope analysis of sediments. Limnol. Oceanogr. 36, 961–975.

Scherler, D., Bookhagen, B., Strecker M.R., 2010. Timing and extent of late Quaternary glaciations in the western Himalaya constrained by ^{10}Be moraine dating in Garhwal, India. Quaternary Science Reviews 29, 815–831.

Schoenbohm, L., Whipple, K., Burchfiel, B., Chen, L., 2004. Geomorphic constraints on surface uplift, exhumation, and plateau growth in the Red River region, Yunnan Province, China. Bulletin of the Geological Society of America 116, 895–909.

Schultz, D.J., Calder, J.A., 1976. Organic carbon 13C/12C variations in estuarine sediments. Geochimica et Cosmochimica Acta - Elsevier 40, 381-385.

Schulz, H., von Rad, U., Erlenkeuser, H., 1998. Correlation between Arabian Sea and Greenland climate oscillations of the past 110,000 years. Nature 393, 54-57.

Seilacher, A., 1969. Fault-graded beds interpreted as seismites. Sedimentology 13, 155–159.

Sen D.P., 1980. Bedform, facies and basin model of ancient glacial deposit: a study based on Talchir rocks (Up. Carboniferous) of Taratanr, Bihar, India. Palaeogeography Palaeoclimatology Palaeoecology 32, 45–67.

Sengupta, S., Sarkar, A., 2006. Stable isotope evidence of dual (Arabian and Bay of Bengal) vapour sources in monsoonal precipitation over north India. Earth Planet. Sci. Lett., 250, 511–521.

Shahzad, F., Gloaguen, R., 2011a. TecDEM: A MATLAB based toolbox for tectonic geomorphology, Part 1: Drainage network preprocessing and stream profile analysis. Computers and Geosciences 37, 250 – 260.

Shahzad, F., Gloaguen, R., 2011b. TecDEM: A MATLAB based toolbox for Tectonic Geomorphology, Part 2: Surface dynamics and basin analysis. Computers and Geosciences 37, 261 – 271.

Sharma C., 1992. Palaeoclimatic oscillation since last deglaciation in western Himalaya- A palynological assay. Palaeobotanist 40, 374–382.

Sharma, P.D., Goel, A.K., Minhas, R.S., 1991. Water and sediment yields into the Sutlej river from the high Himalaya. Mountain Research & Development 11, 87-100.

Shepard, F.P., 1954. Nomenclature based on sand-silt-clay ratios: Journal of Sedimentary Petrology 24,151-158.

Sikka, D.R., 1980. Some aspects of the large-scale fluctuations of summer monsoon rainfall over India in relation to fluctuations in the planetary and regional scale circulation parameters. Proc. Ind. Acad. Sci. Earth Planet. Sci., 89, 179-195.

Sims, J.D., 1973. Earthquake induced structures in sediments of Van Norman Lake, San Fernando, California. Science 182, 161–163.

Sims, J.D., 1975. Determining earthquake recurrence intervals from deformational structures in young lacustrine sediments. Tectonophysics 29, 141–152.

Singh, G., Joshi, R.D., Chopra, S.K., Singh A.B., 1974. Late Quaternary history of vegetation and climate of the Rajasthan desert, India. Philosophical Transactions of the Royal Society of London B 267, 467–501

Singh, G., Wasson, R.J., Agrawal, D.P., 1990. Vegetational and seasonal climatic changes since the last full glacial in the Thar Desert, northwestern India. Review of Palaeobotany and Palynology 64, 351–358.

Singh, P., Kumar, N., 1997. Effect of orography on precipitation in the western Himalayan region. Journal of Hydrology 199, 183-206.

Singh, S., Jain A.K., 2007. Liquefaction and fluidization of lacustrine deposits from Lahaul-Spiti and Ladakh Himalaya: Geological evidences of paleoseismicity along active fault zone. Sedimentary Geology 196, 47-57.

Singh, S., Sinha, P., Jain, A.K., Singh, V.N., Srivastava, L.S., 1975. Preliminary report on the January 19, 1975 Kinnaur Earthquake in Himachal Pradesh. Earthquake Eng. Stud. 75, 1–32.

Sinha, A., Cannariato, K.G., Stott, L.D., Li, H.C., You, C.F., Cheng, H., Edwards, R.L., Singh I.B., 2005. Variability of southwest Indian summer monsoon precipitation during the Bølling-Ållerød. Geology 33, 813–816.

Sinha, A., Stott, L., Berkelhammer, M., Cheng, H., Edwards, R. L., Buckley, B., Aldenderfer, M., Mudelsee M., 2011. A global context for megadroughts in monsoon Asia during the past millennium. *Quaternary Science Review30,* 47–62.

Sinha, A.K., 1989. Geology of higher central Himalaya. John Wiley and Sons, Chichester.

Sirocko, F., Sarnthein, M., Erlenkeuser, H., Lange, H., Arnold, M., Duplessy J.C., 1993. Century scale events in monsoonal climate over the past 24,000 years. Nature 364, 322–324.

Snyder, N., Whipple, K., Tucker, G., Merritts, D., 2000. Landscape response to tectonic forcing: digital elevation model analysis of stream profiles in the Mendocino triple junction region, Northern California. Bulletin of the Geological Society of America 112, 1250–1263.

Spötl, C., Vennemann, T.W., 2003. Continuous-flow IRMS analysis of carbonate minerals. Rapid Communications in Mass Spectrometry 17, 1004-1006.

Spötl, C., Nicolussi, K., Patzelt, G., Boch, R., 2010. Humid climate during deposition of sapropel 1 in the Mediterranean Sea: assessing the influence on the Alps. Global and Planetary Change 71, 242–248.

Stager, J.C., Mayewski, P.A., 1997. Abrupt early to mid Holocene climate transition registered at the Equator and the poles. Science 276, 1834-1836.

Staubwasser, M., Weiss, H., 2006. Holocene climate and cultural evolution in late prehistoric–early historic West Asia. Quaternary Research 66, 372-387.

Steck, A., 2003. Geology of the NW Indian Himalaya. Eclogae Geologicae Helvetiae 96, 147–196.

Stiller, M., Nissenbaum, A., 1999. A stable carbon isotope study of dissolved inorganic carbon in hardwater Lake Kinneret (Sea of Galilee). S. Afr. J. Sci. 95, 166–170.

Stiller, M., Rounick, J.S., Shasha, S., 1985. Extreme carbon-isotope enrichments in evaporating brines. Nature 316, 434–435

Stoner, J.S., St-Onge, G., 2007. Magnetic stratigraphy in paleoceanography: reversals, excursions, palaeointensity and secular variation, in Proxies in Late Cenozoic Paleoceanography, C., Hillaire-Marcel, and A. de Vernal., (Eds.) Proxies in. Late. Cenozoic. Paleoceanography, Elsevier pp. 99-137.

Stuiver, M., 1970. Oxygen and carbon isotope ratios of freshwater carbonates as climatic indicators. J. Geophys. Res. 75, 5247–5257.

Stuiver, M., 1975. Climate versus changes in ^{13}C content of the organic component of lake sediments during the late Quaternary. Quaternary Research 5, 251- 262.

Stuiver, M., Reimer, P.J., Bard, E., Beck, J.W., Burr, G.S., Hughen, K.A., Kromer, B., McCormac, G., van der Plicht, J., Spurk, M., 1998. IntCal98 radiocarbon age calibration, 24,000–0 cal BP. Radiocarbon 40, 1041–83.

Sturm, M., Matter, A., 1978. Turbidites and varves in Lake Brienz (Switzerland): deposition of clastic detritus by density currents. Special Publications of the International Association of Sedimentologists 2, 147–168.

Sundaram S., Krishnan, R., Dey A., Swapna P., 2010. Dynamics of intensification of the boreal summer monsoon flow during IOD events. Meteorology and Atmospheric Physics 107, 1-15.

Surakasi, V.P., Wani, A.A., Shouche, Y.S., Ranade, D.R. 2007. Phylogenetic analysis of methanogenic enrichment cultures obtained from Lonar lake in India: Isolation of *Methanocalculus* sp. and *Methanoculleus* sp. Microbial Ecology 54, 697-704.

Swain, A.M., Kutzbach, J.E., Hastenrath, S., 1983. Estimates of Holocene precipitation for Rajasthan, India, based on pollen and lake-level data. Quat. Res. 19, 1 – 17.

Swart P.K., 1983. Carbon and oxygen isotope fractionation in scleractinian corals: a review. Earth-Sci Rev 19, 51–80.

Talbot, M.R., 1990. A review of the palaeohydrological interpretation of carbon and oxygen isotopic ratios in primary lacustrine carbonates. Chemical Geology (Isotope Geoscience Section) 80, 261-279.

Thakker, C.D., Ranade, D.R., 2002. An alkalophilic *Methanosarcina* isolated from Lonar crater. Current Science 82, 445-458.

Thiede, R. C., Arrowsmith, J. R., Bookhagen, B., McWilliams, M. O., Sobel, E. R., Strecker, M. R., 2006. Dome formation and extension in the Tethyan Himalaya, Leo Pargil, NW-India. Bulletin of the Geological Society of America118, 635–650.

Thompson, L.G., Yao, T., Mosley-Thompson, E., Davis, M.E., Henderson, K.A., Lin, P.N., 2000. High-Resolution Millennial Record of the South Asian Monsoon from Himalayan Ice Cores. Science 289, 1916-1919.

Trivedi, A., Chauhan, M.S., 2009. Holocene vegetation and Climate Fluctuations in northwest Himalaya, based on Pollen Evidence from Surinsar Lake, Jammu region, India. Journal Geological Society of India 74, 402-412.

Ummenhofer, C. C., Sengupta, A., Li, Y., Taschetto, A.S., England, M.H., 2011. Multi-decadal modulation of the El Nino-Indian monsoon relationship by Indian Ocean variability. Environmental Research Letters 6, 1-8.

Upadhyay, R., 2003. Earthquake-induced soft-sediment deformation in the lower Shyok river valley, northern Ladakh, India. Journal of Asian Earth Science 21, 413–421.

Valero-Garcés, B.L., Delgado-Huertas, A., Ratto, N., Navas, A., 1999. Large ^{13}C enrichment in primary carbonates from Andean Altiplano lakes, northwest Argentina. Earth and Planetary Science Letters 171, 236–266.

Van Campo, E., Duplessey, J.C., RossignolStrick, M., 1982. Climatic conditions deduced from a 150-kyr oxygen isotope–pollen record from the Arabian Sea. Nature 296, 56–59.

Van Campo, E., Gasse, F., 1993. Pollen- and diatom-inferred climatic and hydrological changes in Sumxi Co basin (western Tibet) since 13,000 yr. BP. Quaternary Research 39, 300–313.

Vannay, J.C., Sharp, Z.D., Grasemann, B., 1999. Himalayan inverted metamorphism constrained by oxygen isotope thermometry. Contributions to Mineralogy and Petrology 137, 90–101.

Venkatesh, V., 1967. The Lonar crater- some geochemical data. Journal Geological Society of India 8, 29-37.

Walker, R.G., 1963. Distinctive types of ripple-drift cross-lamination. Sedimentology 2, 173-188.

Wang, N.L., Yao, T.D., Thompson, L.G., Henderson, K.A., Davis, M.E. 2002. Evidence for cold events in the early Holocene from the Guliya ice core, Tibetan Plateau, China. Chinese Science Bulletin 47, 1422–27.

Wang, P., Zhang, B., Qiu, W., Wang, J., 2011. Soft-sediment deformation structures from the Diexi paleo-dammed lakes in the upper reaches of the Minjiang River, east Tibet. Journal of Asian Earth Sciences 40, 865-872.

Wang, Y., Liu, X., Herzschuh, U., 2010. Asynchronous evolution of the Indian and East Asian Summer Monsoon indicated by Holocene moisture patterns in monsoonal central Asia. Earth-Science Reviews 103, 135-153.

Wasson, R.J., Smith, G.I., Agrawal D.P., 1984. Late Quaternary sediments, minerals, and inferred geochemical history of Didwana lake, Thar desert India. Palaeogeography, Palaeoclimatology, Palaeoecology 46, 345–372.

Webster, P. J., Magaña, V., Palmer, T. N., Shukla, J., R. Tomas, A., Yanai, M., Yasunari, T., 1998. Monsoons: Processes, predictability and prospects for prediction, Journal of Geophysical Research 103, 14,451–14,510.

Webster, P.J., Moore, A.M., Loschnigg, J.P., Leben, R.R., 1999. Coupled ocean–atmosphere dynamics in the Indian Ocean during 1997–98. Nature 401, 356–360.

Weidinger, J.T., Korup, O., 2009. Frictionite as evidence for a large Late Quaternary rockslide near Kanchenjunga, Sikkim Himalayas, and India— Implications for extreme events in mountain relief destruction. Geomorphology 103, 57-65.

Wersin, P., Höhener, P., Giovanoli, R., Stumm, W., 1991. Early diagenetic influences on iron transformations in a freshwater lake sediment. Chemical Geology 90, 233-252.

Wetzel, R., 2001. Limnology, Lake and River Ecosystems. Third Edition, Academic Press.

Wiechula, D., Fischer, A., Kwapuliñski, J., Loska, K., Fischer, T., Kurpas, P., 2006. Multivariate statistical analysis of metal concentrations in teeth of residents of Silesian region, southern Poland. Archives of Environmental Contamination and Toxicology 51,314–320.

Wu, Y., Lücke, A., Zhangdong, J., Sumin, W., Schleser, G.H., Battarbee, R.W., Weilan, X., 2006. Holocene climate development on the central Tibetan Plateau: a sedimentary

record from Cuoe Lake. Palaeogeography, Palaeoclimatology, Palaeoecology 234, 328-340.

Wünnemann, B., Demske, D., Tarasov, P., Kotlia, B.S., Reinhardt, C., Bloemendal, J., Diekmann, B., Hartmann, K., Krois, J., Riedel, F., Arya, N., 2010. Hydrological evolution during the last 15 kyr in the TsoKar lake basin (Ladakh, India), derived from geomorphological, sedimentological and palynological records. Quaternary Science Reviews 29, 1138-1155.

Wulf, H., Bookhagen, B., Scherler, D., 2010. Seasonal precipitation gradients and their impact on fluvial sediment flux in the Northwest Himalaya. Geomorphology 118, 13-21.

Xu, H., Ai, L., Tan, L., An, Z., 2006. Stable isotopes in bulk carbonates and organic matter in recent sediments of Lake Qinghai and their climatic implications. Chemical Geology 235, 262-275.

Yadava, M.G., Ramesh, R., Pant G.B., 2004. Past monsoon rainfall variations in peninsular India recorded in a 331-year-old speleothem. The Holocene 14, 517–524.

Yamagata, T., Behera, S.K., Luo, J.J., Masson, S., Jury, M.R., Rao, S.A., 2004. The coupled ocean-atmosphere variability in the tropical Indian Ocean. Geophys Monogr., 147, 189–211.

Yao, T., Thompson, L., Si, Y., 1997. The climatic variation since the Last Interglaciation recorded in the Guliya ice core. Science in China (Series D). 40, 662-668.

Zhou, J., Ma, D.S., Pan, J., Nie, W.M., Wu, K., 2008. Application of multivariate statistical approach to identify heavy metal sources in sediment and waters: a case study in Yangzhong, China. Environmental Geology 54, 373–380.

Zhu, L.P., Zhen, X.L., Wang, J.B., Lu, H.Y., Xie, M.P., Kitagawa, H., Göran Possnert, G., 2009. A ~30,000-year record of environmental changes inferred from Lake Chen Co, Southern Tibet. Journal of Paleolimnology 42, 343-358.

Appendix:

Barnard, P.L., Owen, L.A., and R.C. Finkel, R.C., 2004. Style and timing of glacial and paraglacial sedimentation in a monsoonal influenced high Himalayan environment, the upper Bhagirathi Valley, Garhwal Himalaya. Sedimentary Geology 165,199–221.

Barnard P.L., Owen L.A., Finkel R.C., 2006. Quaternary fans and terraces in the Khumbu Himal south of Mount Everest: their characteristics, age and formation. Journal of Geological Society of London 163, 383–399.

Gayer E., Lave, J., Pik, R., France-Lanord, C., 2006. Monsoonal forcing of Holocene glacier fluctuations in Ganesh Himal (Central Nepal) constrained by cosmogenic 3He exposure ages of garnets. Earth and Planetary Science Letters 252, 275–28

Owen, L.A., Robinson, R., Benn, D.I., Finkel, R.C., Davis, N.K., Yi, C., Putkonen, J., Li, D., Murray, A.S., 2009. Quaternary glaciation of Mount Everest, Quaternary Science Reviews 28, 1412–1433.

Phillips, W.M., Sloan, V.F., J.F. Shroder Jr, J.F., Sharma, P., Clarke M.L., Rendell, H.M., 2000. Asynchronous glaciation at Nanga Parbat, northwestern Himalaya mountains, Pakistan. Geology 28, 431–434.

Seong, Y.B., L.A. Owen, L. A., Yi, C., Finkel, R.C., 2009. Quaternary glaciation of Muztag Ata and Kongur Shan: evidence for glacier response to rapid climate changes throughout the Late Glacial and Holocene in westernmost Tibet. GSA Bulletin 121, 348–365.

Zech, R., Zech, M., Kubik, P.W., Kharki, K., Zech, W., 2009. Deglaciation and land- scape history around Annapurna, Nepal, based on ^{10}Be surface exposure dating. Quaternary Science Reviews 28, 1106–1118.

List of Publications

- **Anoop, A**., Prasad, S., Basavaiah, N., Brauer, A., Shahzad, F., Deenadayalan K., 2012. Tectonic versus climate influence on landscape evolution: a case study from the upper Spiti valley, NW Himalaya. *Geomorphology*, 145-146, 32-44.
- Basavaiah, N., Wiesner, M., **Anoop, A.**, Menzel, P., Riedel, N., Gaye, B., Brauer, A., Stebich, M., Prasad, S., 2012. Environmental implications of surface sediments from the monsoonal Lonar Lake, Central India. *Quaternary Research* (under revision).
- **Anoop, A.**, Prasad S., Plessen B., Naumann R., Menzel P., Basavaiah N., Weise S., Gaye, B., Brauer A., 2012. Palaeoenvironmental implications of evaporative Gaylussite crystals from Lonar lake, Central India. *Journal of Quaternary Science* (in review).
- Prasad, S., Basavaiah, N., Strecker, M.R., **Anoop A**., et al., 2012. Holocene Indian Summer Monsoon variability: an overview and first results from the Lonar lake, central India. *Quaternary Science Reviews* (in review).
- **Anoop, A**., Prasad, S., Krishnan, R., Gärber, S., Naumann, R., Dulski, P., 2012. Extreme events and spatiotemporal changes in precipitation patterns in NW Himalayas during the early-mid Holocene. *Quaternary Research* (in review).

Extended Abstract

- S. Prasad, A. Brauer, S. Gärber, N. Basavaiah, B.S. Kotlia, **Anoop A**., 2008. Holocene climate variability in the Himalayan region: preliminary results from lake sediments in the Spiti valley, India. *Himalayan Geology* 29 (73-75).